



ASES SOLAR 2021

Empowering a Sustainable Future

Hybrid Conference

August 3-6, 2021

Boulder, CO

**Official Conference
Proceedings**



AMERICAN
SOLAR
ENERGY SOCIETY

American Solar Energy Society National Solar Conference 2021 Proceedings

Edited by

Robert Foster, Paulette Middleton, Henry Vandermark, James Stalker, Gilbert Michaud, Remi Akinwonmi, Julian Wang, Debbie Coleman, Nathan Edmunds, John Burke, Abraham Ellis, Dara Bortman, Paul Ndione, David Ginley, Elaine Hebert, Dale Miller, Carly Cipolla and Carly Rixham
SOLAR 2021 National Organizing Committee & ASES Technical Division Leaders

Dale Miller

Chair, SOLAR 2021 National Solar Conference

Copyright © 2021 by the American Solar Energy Society

American Solar Energy Society

2525 Arapahoe Ave, Ste E4-253
Boulder, CO 80302

Email: info@ases.org

Web: www.ases.org

ISBN: 978-3-982 0408-6-8

All rights reserved. No part of the publication may be reproduced, transmitted, in any form or by any means, electronic, mechanical, photocopying, recording or otherwise, without permission of the publisher, except in the case of brief quotations embodied in critical articles and review or where prior rights are preserved.

Produced by

International Solar Energy Society
Wiesentalstr 50
79115 Freiburg
Germany

Tel: + 49 761 45906 – 0

Fax: + 49 761 45906 – 99

Email: hq@ises.org

Web: www.ises.org

Notice

Neither the International Solar Energy Society and the American Solar Energy Society, nor any one of the supporters or sponsors of the American Solar Energy Society National Solar Conference 2021 (SOLAR 2021) makes any warranty, express or implied, or accepts legal liability or responsibility for the accuracy, completeness or usefulness of any information, apparatus, product or process disclosed, or represents that its use would not infringe privately on rights of others. The contents of articles express the opinion of the authors and are not necessarily endorsed by the International Solar Energy Society, American Solar Energy Society or by any of the supporters or sponsors of SOLAR 2021. The International Solar Energy Society and the American Solar Energy Society do not necessarily condone the politics, political affiliation and opinions of the authors or their sponsors.

Scientific Program

Introduction

Introduction

Miller, D. 1

Solar2021

True Sustainability With Low Embodied Energy <i>Clemens, J.</i>	7
Community Solar Food Drying in Afghanistan <i>Foster, R., Fazli, F.</i>	19
A review on Solar Thermal System Design, Integration, and Techno-economic Modeling for Industrial Heating and Cooling Processes <i>Hiben, Y., Kahsay, M.B., Lauwaert, J.</i>	31
Infinite-NTU Modeling for Studying Charging Cycle of Packed-Bed Solar Thermal Energy Storage <i>Hiben, Y.</i>	43
Credit for Reducing Sunshine <i>Komerath, N.M., Deepak, R., Deepak, A.</i>	52
Nonimaging Optics and Constructal Design Towards Optimal Solar Cookers <i>Rincón-Mejía, E., Rincón, A.G., Rincón-Rubio, V.</i>	64
Optimizing the Operational Parameters of an Electrochemical Purification Cell for Corrosion Mitigation in CSP Plants During Operation <i>Rippy, K., Howard, E., Vidal, J., Witteman, L.</i>	76
Reuse of Solar Photovoltaic Systems for Social and Economic Benefit <i>Stromberg, R.</i>	81
Influence of Diffuse and Ground-Reflected Irradiance on the Spectral Modeling of Solar Reference Cells <i>Vignola, F., Andreas, A., Gotseff, P., Habte, A., Kessler, R., Mavromatakis, F., Peterson, J., Sengupta, M., Snider, S.</i>	93
A Study of Reflector-Enhanced Bifacial PV <i>Wilk, R., Dobosz, M., Rueter, M.</i>	103

Introduction

ASES SOLAR 2021 Proceedings Introduction

National Organizing Committee

50th Annual National Solar Conference

August 3-6, 2021 | Hybrid Conference | University of Colorado Boulder + Online

ASES SOLAR 2021 expanded knowledge, inspired action and strengthened community through a wide variety of formal and informal exchanges and networking among online and in person participants. Attendees celebrated 50 years of progress and joined together in deeper commitments to accelerate the energy transformation equitably in this decade of disruption. Here are a few of the many conference highlights.

50th Anniversary

To commemorate the 50th anniversary milestone, the opening reception recognized the local native lands with a special blessing by James Rattling Leaf. In a special commentary, ASES Executive Director Carly Rixham reviewed the organization's progress and pioneers. NREL Deputy Director Peter Green framed the future energy transformation that those advancements not only make possible but inevitable. ASES's 50 years of contributions were also celebrated in Larry Kazmerski's engaging video of our history and current events as part of the annual ASES Awards Banquet.

JEDI Commitment

ASES's commitment to justice, equity, diversity and inclusion (JEDI) principles is essential to achieving a 100% renewable energy and sustainable living. This was reflected throughout the keynotes and technical sessions. A key takeaway message of the opening keynote session with Dave Renné (Immediate Past President of ISES), Bill Ritter (Former Colorado Governor and founder of Center for New Energy Economy), and Alice Jackson (CEO Xcel Energy Colorado): we have the technology, and to a growing extent, the financing and policies to achieve 100% renewable energy world in the near future. However, stronger political will is needed to ensure an equitable transformation. The closing keynote by Amory Lovins, co-founder of Rocky Mountain Institute, provided a compelling reminder about the importance of design to achieve the transformation we envision. Both Lovins and Renné referenced a quote from Dwight Eisenhower; "If a problem can't be solved, enlarge it," an auspicious reminder about the importance of bringing more stakeholders into the discussion, even if they don't agree with you.

Building on the conference theme of "Empowering a Sustainable Future," the Social and Environmental keynote session focused on the topics of racism and social justice as they intersect with energy writ large and renewable energy in particular. Henry Red Cloud (Executive Director at Red Cloud Renewable), Michelle Romero (National Director at Dream Corps), Monique Dyers (President/CEO at Ensign Energy Consulting) and Pilar Thomas (Professor of Practice at the University of Arizona) shared their perspectives on working together to ensure that *all* communities benefit from the clean energy transition, and how empowering a sustainable future can benefit everyone without harming the most vulnerable among us.

Technical Sessions

SOLAR 2021 featured outstanding content in the technical sessions on social and environmental justice, modeling and scaling, solar advancements, sustainability, and policy, education, and finance deepened the discussions around equity, technology progress, challenges, and paths forward. Other sessions: the important role of local governments in accelerating solar adoption; programs to help low and middle income individuals access solar; incentives and rebates to accelerate EVs; recycling and life cycle of materials; carbon footprints; land use; how solar cookers can improve the lives of three billion people; modeling tools that advance grid scale solar energy adoption; nuances to battery system sizing; passive and active solar systems from design to maintenance; community solar; and workforce development needed in all of these areas.

Board Special Recognition 2021 – Tony Seba

For the first time, ASES's Board of Directors recognized an ASES member for exceptional contributions to our 100% renewable energy transformation goal. ASES Professional Member, Tony Seba, is a world-renowned thought leader, author, speaker, educator, angel investor and Silicon Valley entrepreneur. Recognized for simple, consistent and persistent explanations of the challenges and exponential opportunities related to solar and clean technology disruption, Seba envisions an electric grid run primarily on PV technologies with storage capacity that includes a fully electrified transport system. He has directly influenced cleantech leaders, corporations, investors, utilities, political decision makers and the general public. Seba's work focuses on technology disruption, the convergence of technologies, business model innovation, organizational capabilities and product innovation that leads to the creation of new industries and societies and the collapse of existing ones. Although his work has primarily focused on disrupting the U.S. electricity grid, his influence has spread worldwide as his vision is now being embraced by global cleantech industry organizations. In addition to his inspirational acceptance speech at the Awards Banquet, Seba also spoke at the Industry Roundtable as a Keynote speaker. Attendees were optimistic and energized about the exponential growth of solar's superpower status within this decade. His broad vision includes a new age of humanity, moving from the Age of Extraction to the Age of Creation.

ASES Fellows and Awardees

Six new ASES Fellows were inducted:

Everett M. Barber, Jr. has worked for more than 50 years as an inventor, designer, entrepreneur, manufacturer, educator, writer, and advocate inspiring thousands of this industry's leaders.

Lucas Dixon, a dedicated ASES leader, solar energy advocate, and energy-efficiency professional, served as Board Chair 2018-2019.

Robert Foster is known for his sustained contributions to the advancement of renewable energy in over 40 countries, as well as his lifetime dedication to education and community service.

David Hill, a long time ASES leader and Board Chair 2012-2013, is recognized nationally for his groundbreaking work to advance sustainable energy markets.

Orlo Stitt has dedicated his life to educating others about how to save energy and why doing so makes the world better for us and future generations.

Tom Stoffel is recognized as one of the international giants of solar resource characterization and a person who provided passionate service to the solar energy community for decades.

2021 Awards

Charles Greeley Abbot Award

Jan Kleissl, *University of California San Diego*

Citation: For groundbreaking and global leadership and contributions in the important field of solar energy meteorology and pioneering research leading to renewable-energy capacity building in the electricity grid system.

Women in Solar Energy (WISE) Award

Fayeann Lawrence, *Sologistics*

Citation: For leadership and outstanding contributions to technical achievement, policy advocacy, educational opportunities, and social change built upon her dedication to collaboration and inclusion—and specifically providing opportunities for women and minorities in solar.

Rebecca Vories Award

John Burke, *Maine Solar Energy Association & Downeast Alternative Design Solar (DADS)*

Citation: For a uniquely inspiring blend of ASES chapter and division leadership, generously topped with humor, caring, outreach, and dedication.

Leadership in Solar Architecture and Design Award

Alfredo Fernandez-Gonzalez, *University of Nevada Las Vegas*

Citation: For extraordinary leadership in advancing excellence in passive solar research, design, and education.

Leadership in Solar Policy and Market Transformation Award

Paul Fenn, *Local Power*

Citation: For exceptional efforts and successes in initiating policies that have led directly to the Community Choice Aggregation (CCA) model and having revolutionary impact on community solar development.

John and Barbara Yellott Award

Qihua Duan, *The Pennsylvania State University (Architectural Engineering)*

Citation: For her research in developing a model to decompose broadband solar radiation into narrowband visible (VIS) and near infrared (NIR) components and implementing this into current solar architecture design.

William Callahan, *Colorado School of Mines (Materials Science)*

Citation: For designing, modeling, and developing a functioning solar and thermophotovoltaic/ thermoradiative system and complementary fundamental research leading to new and transformative electronics for renewable-energy systems operating in harsh environments.

Networking Events:

WISE Forum where accomplished women share lessons learned and heartfelt stories to inspire women to become more technically involved in solar.

Emerging Professionals Forum provided opportunities to build networks and obtain guidance in navigating early career challenges.

Spirit and Sustainability Forum celebrated its 25th anniversary by acknowledging its founder Barbara Harwood (Pia Aitken) and inviting attendees to share their thoughts about bringing diversity into the energy transformation tent.

Industry Roundtable provided sponsors a platform for five-minute pitches for their businesses or offerings.

Special Events:

Attendees at the Awards Banquet were entertained by the Stand Up for Climate Change Comedy Show, an online show hosted by Max Boykoff and Beth Osnes, featuring select pieces developed by University of Colorado students and performed by stand-up comedians from across the nation. The show was emceed by recent graduates Ben Stasny and Megan McHugh. [See the whole show online.](#)

This year, as part of SOLAR 2021, ASES held a Climate Ride/Walk Solar Fundraiser. Online and in person attendees were challenged to raise funds for ASES through the event.

ASES also featured a special Colorado Spotlight Session highlighting a panel of local Colorado leaders and the work they are doing in the renewable energy sector.

Workshops & Tours

SOLAR 2021 featured two NABCEP registered workshops (Solar PV Intensive and Energy Storage, PV & NEC) and a workshop on DIY Energy Efficiency. Tours included Jack's Solar Garden, the nation's largest agrivoltaic research site which is located in Boulder, and a virtual tour of NREL.

SOLAR 2021 – 1st Hybrid Conference Success Statistics – Thank You

All sessions were hybrid with speakers and audience in person and online.

Opening reception – Carly Rixham, ASES Executive Director, Sarah Townes, ASES CFO and Zen Director, and Dale Miller, Conference Chair

Total number of registered participants hybrid and virtual: 435

Total number of JEDI scholarships awarded: 13

Total number of sponsors: 9

Total number of volunteers: 37

Total number of people who participated in the Caucuses: 40

A special thank you to the SOLAR 2021 National Organizing Committee (Dale Miller, Dave Ginley, Carly Cipolla, Carly Rixham, Robert Foster, Paulette Middleton, Dara Bortman, Paul Ndione), ASES staff, volunteers and interns, and everyone who contributed and participated in the conference.

Moving Forward

During the ASES Annual Membership meeting at the end of the conference, ASES board and staff reported on outstanding progress over the past year and underscored goals, focus areas and commitments outlined in our transformative five-year strategic plan.

Goals: Interact with and inform a broader and more diverse cross-section of solar stakeholders including individuals, communities, businesses, local governments and other organizations with similar missions and values; and strive to strengthen these partnerships and develop a more committed and active base of dedicated staff, interns and volunteers.

Focus Areas:

- Monitoring, integrating and disseminating information and resources particularly in policy best practices and technology innovation.
- Education and workforce development with special attention to providing resources to the knowledge base of professions influencing solar adoption and focused educational resources for emerging professionals.
- Facilitation of solar adoption by individuals and communities by supporting the global expansion of sustainable solar power (PV and solar thermal).

JEDI Commitment: Ensure that ASES's energy transformation work follows JEDI principles and advances these values more broadly in the organization.

Efforts in all ASES programs reflect these goals, focus areas and commitments.

All SOLAR 2021 is available online for people who registered for the conference.

See you next year in Albuquerque, NM, June 21-24 at ASES SOLAR 2022!

Solar2021

True Sustainability with Low Embodied Energy

Jonathan A. Clemens

Olympic Energy Systems, Inc.
Port Angeles, Washington, U.S.A.

Abstract

As more companies, institutions, governments, and individuals set and commit to carbon dioxide (CO₂) reduction goals, and as policies, technologies, and infrastructure grow to meet intermediate goals, we find ourselves facing an emerging challenge of embodied energy. Energy is invested or used in the manufacture of (energy-saving) products and (energy) infrastructure. In the near term, a bow wave of CO₂ emissions from infrastructure tends to counter the progress toward reductions from lower consumption. Will that bow wave undermine the important pace of reductions necessary to stave off runaway Climate Change?

Indeed, we must replace our consuming of our stored solar energy assets (fossil fuels) with our daily solar income (vast and renewable). But, a whole other challenge, of reducing the use of stored solar for building the new energy infrastructure, emerges. This challenge mandates a Doing More With Less program, as we are now still just doing more with not enough less. Our current state of the art for renewable energy infrastructure – mounting, PV panels, concrete ballast, Electric Vehicles, and storage – is metal and material intensive, high in embodied energy, and ultimately more costly than it could be. The science of tensioned cables for the mounting of solar photovoltaic panels can significantly reduce embodied energy to a fraction of conventional mounting. True sustainability will require lowering embodied energy, as energy infrastructure must be replaced as service lifetimes are met.

Keywords: Embodied, Invested, Production, Energy, Emissions, GHG, Sustainability, Carbon

1. INTRODUCTION

Embodied energy is the energy required to produce or make the things humans use or rely on. Sustainability is essentially what human civilization is actively pursuing at this time on a global scale, with Climate Change prevention and mitigation the primary goal. Accumulating Green House Gas (GHG) emissions, particularly CO₂ from human activity, is the leading cause of Climate Change. Efforts to build up the infrastructure for a sustainable future aimed to reduce the emissions will involve a grand accounting of emissions, from manufacturing and power generation to usage and consumption energy and to other GHG emitting activities. This paper, intended to generally inform on the subject of embodied energy in the transition to renewables, will address such accounting.

Sustainability is the ability to sustain life and future generations of life without diminishing the natural capital upon which all life depends. In essence, it means living on income rather than savings and respecting the natural cycles on earth – thermal, hydrological, carbon, and so on. True sustainability assures that the approach to obtaining sustainability does not itself lead to non-sustainability.

True sustainability with low embodied energy is a challenge, as the recurring remnant embodied energy works up against the GHG/CO₂ budget in the longer term, as well as cumulatively forming a bow wave of GHG/CO₂ emissions in the buildup of the low carbon infrastructure in the shorter term. We will see that staying within the carbon budget is more difficult than dealing with a surge in carbon emissions early in the transition to renewable energy.

2. EMBODIED ENERGY

The path toward 100% renewable energy will inevitably face the challenge of providing an alternative to the fossil fuels sourcing of the production, process, and high heat energy needed to make things. Ultimately relying on Carbon Capture technology leaves us reliant on non-renewable fossil fuels, which is not true sustainability. To deal with the availability and intermittency issues of renewable energy we will have lots of energy storage (at Utility Scale and/or widespread Distributed Generation), which means higher embodied energy and more CO₂ emissions.

A practical solution for achieving a sustainable future involves scaling up of the existing state of the art (SOTA), while embarking on Research & Development to reduce embodied energy and to advance the state of the art, especially in the areas of energy storage and reliability, but also in Carbon Capture and Nuclear power – our backup plan in light of our persistent embodied energy, high heat challenges.

Embodied energy (aka Invested Energy) is inescapable, as it accompanies the buildup and maintenance of renewable energy infrastructure and large scale electrification of the economy, done so to prevent further Climate Change and to transition away from nonrenewable fossil fuels. It is all about GHG emissions, especially CO₂. We can discuss emissions baselines, targets, and annual reductions, but the CO₂ Budget metric (of about 900 Gigatons, or billion tons) is perhaps the most important. As of 2016, globally we had about 900 Gigatons of CO₂ emissions left before worsening Climate Change and passing Tipping Points (of irreversible, accelerating Climate Change).

Embodied energy is a three part problem:

- A CO₂ Bow Wave from initial infrastructure buildup (constituting embodied energy)
- Breakthroughs and technology advances over the next decades that reduce operational energy CO₂ emissions at the cost of higher embodied energy, a second Bow Wave of sorts when those breakthroughs are built up (commercialized)
- Remnant embodied energy to maintain the lower operational energy infrastructure in the face of an exhausted CO₂ Budget, amounting to billions of tons CO₂ emissions per year (a fraction of the projected 51Bt/y) when the remaining CO₂ Budget has dropped to zero.

The somewhat politically charged goal of global Zero Net Carbon by 2050 is not practical, as it largely depends on technology, know-how, and breakthroughs not even developed, yet. Global zero net carbon by 2100 is a more practical scenario. The 2050 goal essentially ignores the embodied energy issue. The 2100 goal provides time to resolve the embodied energy issue. We do not want the Perfect (Zero Net Carbon) be the enemy of the Good (highly reduced CO2 emissions).

Approach to CO2 Emission Reduction Calculations

The two prongs of the approach to calculating CO2 emission reductions reflect the fundamental nature of the categories of emissions. The approach to calculating CO2 emission reductions is illustrated in Figure 1.

The Top / Down Prong identifies reductions by added infrastructure and products and has 6 main development areas: Solar PV, Wind, EVs, Efficiency, Energy Storage, and Buildings. The focus is on consumers and products, with calculations based on direct assessments and analysis.

The Bottom / Up Prong identifies reductions by modifications of existing infrastructure, especially in manufacturing and production of material, which are energy intensive (not amenable to the diffuse less intensive renewable energy). The focus is on suppliers and providers, with calculations based on historical data.

Forestry, agriculture, and aviation will follow another path to Zero Net Carbon, and will somewhat depend on the progress in the other categories (two prongs). This third prong (or path) is beyond the scope of this paper, as the solutions and implementations go beyond technology and scaling up, facing revolutionary change politically and socially. Aviation, though extensive in our modern world, is basically a non-essential activity and, thus, could be scaled down. Renewable fuels and electric propulsion are already in development and show promise, as progress has already been demonstrated. Agriculture can also look at renewable fuels to power its operation and to organics to help replace the use of fertilizers. Forests provide a sink for carbon, but tropical deforestation contributes about 1/5 of global GHGH emissions. Forests are not so much a technology issue, as they are socio-political – we choose to allow their overuse and destruction. We could choose less consumption of forest resources, and we can choose to manage sustainable forests.

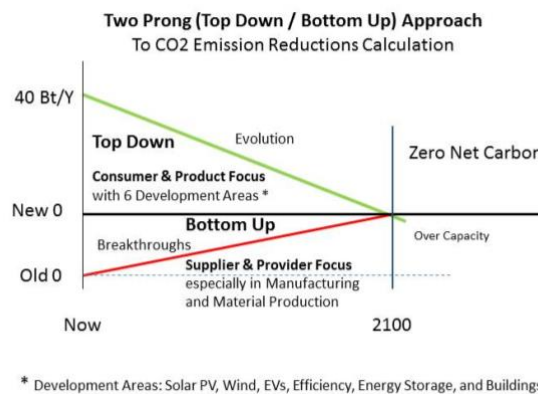


**Figure 1: Emissions Reductions Approach
Considerations for Calculating Infrastructure Build Up CO2 Numbers**

Actual calculations, raw data, and derivations are documented in a white paper titled “True Sustainability With Low Embodied Energy” [Clemens, 2021]

Service Lifetimes (assumed 30 years for Solar PV and Wind, 15 years for EVs, Energy Storage 10 to 20 years)

Invested Energy (per Watt, capacity)

Production (Emission Free)

Timeframes 2021 – 2050 (30 years) and 2050 – 2100 (50 years)

Build Up linearly over Timeframe

Costs in 2020 year dollars

Physical constants

Conversion data from public available sources (Ex., 1 KWh = 3412 BTU = 3,600,000 Joules)

Capacity (of Build Up) to meet established goals with practical assumptions (Ex., 30% solar electricity)

Gasoline when burned releases 157.20 lbs CO2/MBTU (without ethanol) [1 pound (lbs) = 0.454 kilogram]

CO2 Avoided depends on power plant fuel (electricity):

Coal (Anthracite) 228.6 lbs emitted per MBTU

Natural Gas 117.0 lbs emitted per MBTU

(A composite of sorts averages the two values for 170 lbs CO2 emitted per MBTU)

Build Up Goals / Targets:

Solar PV in U.S. to have 30% Solar Electricity by 2050: 1500 GW [100% by 2100: 3000 GW]

Wind power in U.S. from 107.4 GW to 425 GW by 2050, additional growth thereafter

EVs replace the world's 1.6 B vehicles about 15 years (depends on manufacturer plans)

Efficiency measure reduce energy consumption 20% across all sectors (affecting 2/3 of emissions)

Buildings (1 M in U.S.) replaced/built per year and saves 20% in energy

Top down CO2 emissions reductions from added infrastructure in 6 main development areas are calculated based on build up rates. Build up rates are estimated based on CO2 reduction targets and EIA projections and the associated expected performance of the added infrastructure. Invested Energy (IE) and associated CO2 emissions, based mainly on material content and quantity, for the U.S. through 2050 and 2100 are calculated first, then global IE and CO2 emissions are calculated based on their current relative size. Global energy consumption and CO2 emissions are roughly 4 to 1, global to U.S., as China grows. Calculation of embodied energy starts with calculating material content and quantity, then determining the energy to produce the material (Table 1), followed by calculating CO2 emissions from sourcing of energy used to produce the material.

Table 1: Energy Required To Produce Material

Energy Required To Produce Material [source: www.lowtechmagazine.com]

Wood from standing timber	0.830-1.950 KWh/kg (3-7 MJ)
Steel from recycled steel	1.665-4.170 KWh/kg
Aluminum from recycled Al	3.15-4.75 KWh/kg
Iron from Iron Ore	5.55-6.95 KWh/kg
Glass from sand, et cetera	5.0-9.7 KWh/kg
Steel from Iron	5.55-13.9 KWh/kg
Silicon from silica	63.9-65.3 KWh/kg
Aluminum from bauxite	63-95 KWh/kg
Electronic grade Silicon Si	2,108-2,154 KWh/kg

The Practical Scenario

The practical scenario for achieving ongoing CO2 emissions reductions recognizes the technological realities and limits of today to achieve significant reductions by 2050, with Solar at 30% of electricity generation and Wind at fully developed optimal sites. Solar grows to 15 times and Wind to 4 times current capacity in the United States and similarly elsewhere, summarized in Table 2.

Table 2: CO2 Numbers Through 2050

Categories (Energy – related)	Invested Energy (U.S.) CO2 Level	Invested Energy (U.S.) thru 2050 CO2 released	U.S. CO2 Reductions through 2050	Global CO2 Reductions thru 2050
Solar PV	195 Mt/y	5.85 B tons	(522Mt/y) 15.7 B	62.8 B
Wind	30 Mt/y	900 M	(490Mt/y) 14.7 B	58.8 B
Electric Vehicles	169 Mt/y	5.07 B	(501Mt/y) 15 B	60 B
Efficiency	236 Mt/y	7.08 B	(507Mt/y) 15.2 B	60.8 B
Energy Storage	16 Mt/y	480 M	0	0
Buildings (1M/Y)	8 Mt/y	240 M	(35Mt/y) 1.0 B	4 B
TOTALS	654 Mt/y	19.6 Bt total (78 Bt Global)	61.6 Bt (U.S.)	246 Bt (Global)

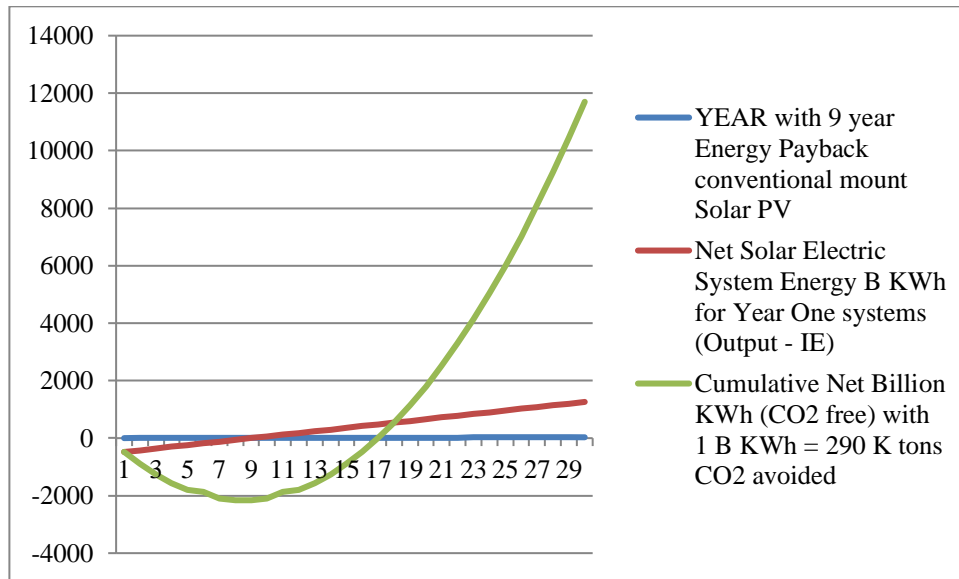
The efficiency category is most interesting. With a reasonable assumption that across all sectors there is a feasible reduction of energy consumption (thus CO2 reductions) of 20%, the returns continue on past the 2021 to 2050 timeframe. Be efficient now and save indefinitely. The investment (invested energy) is not insignificant, as energy-saving equipment, machinery, resources, and appliances across all sectors are replaced. The practical scenario for achieving ongoing CO2 emissions reductions (to Net Zero Carbon from 40 Bt/y in 2019) by 2100 involves adding more solar PV, wind capacity, and energy storage and is summarized in Table 3.

Table 3: CO2 Numbers Through 2100

Categories (Energy – related)	Invested Energy (U.S.) CO2 Level (2050+)	Invested Energy (U.S.) thru 2100	U.S. CO2 Reductions through 2100	Global CO2 Reductions through 2100
Solar PV	195 Mt/y (390)	25.5 B tons	(1562 Mt/y) 93.8 B	375 B
Wind	30 Mt/y (60)	3.9 B	(1273 Mt/y) 78.1 B	312 B
Electric Vehicles	169 Mt/y (169)	13.6 B	(1.03) Bt/y 51.5 B	206 B
Efficiency	236 Mt/y (0)	7.1 B	(1.13 Bt/y) 56.5 B	226 B
Energy Storage	16 Mt/y (51)	3.1 B	0	0
Buildings (1M/Y)	8 Mt/Y (8)	0.6 B	(70Mt/y) 3.5 B	14 B
TOTALS	654 Mt/y (678)	54 Bt total U.S. (216 Bt Global)	283 Bt (U.S.)	1133 Bt (Global)

The transition to Electric Vehicles will produce good net reductions in CO2. An average passenger EV has an IE (assumed similar to that of ICEVs) of 11 tons of CO2 emissions, while annually reducing almost 3 tons of CO2 over an ICEV. If the entire 1.6 B ICE Vehicles in the world were EVs, we would be expending about 1 B tons of CO2 per year to save/reduce/avoid about 4 B tons of CO2 annually.

The practical scenario will have achieved a 100% renewable clean electric grid by 2100, along with expanded electrifications of transportation and other sectors, but, will have used up the 900 Bt CO2 Budget. There remains the reference 1990 level of energy consumption...mainly the heavy industries producing machinery, ships, structural steel, cement, and automobiles. To contend with this (Bottom/Up) part of the challenge, the approach to manufacturing and such will have changed. Annualized Invested Energy from the new infrastructure buildup (of renewable energy generation, energy-saving non-generation, and Electric Vehicles) totals about 4 Bt CO2 per year. Solar KWh production from the buildup is illustrated in Figure 2.



CO2-free KWh from Solar PV in U.S.

Note: In 2020, U.S. annual electricity production was 4,009 B KWh [expected to rise to 5,700 B by 2050]
 Annualized Solar PV KWh production from added PV in 2021-2050 is $11,700/30 = 390$ B KWh/Y (10%)
 Solar PV KWh production from added PV by 2050 is 1500 B watts x 1.2 KWh/W/Y = 1800 B KWh/Y (30%)

Figure 2: Solar PV Build Up KWh Production

In summary, from 2021 to 2100 (80 years), globally we have released about 216 B tons of CO2 to build the infrastructure that reduces, saves, or avoids 1133 B tons of CO2. Projected infrastructure includes:

- 12,000 GW Solar PV 55% of grid capacity (enough solar panels to cover half of Texas)
- 1,800 GW Wind 45% of grid capacity
- 1.6 B Electric Vehicles
- 20% Demand Reduction via Efficiency across all sectors
- 10 B KWh (7 B KWh Utility Scale plus 3 B KWh Distributed Generation) Energy Storage
- 100% Residential & Commercial Energy Storage (10 KWh each, then to 20 KWh by 2100)
- 20% Lower Operating Energy in most or all Buildings

Hydropower, Nuclear power, and Coal/NG powered electricity generation 10% of grid capacity as a Backup

Carbon Capture, Renewable Hydrogen, and Concentrated Solar Thermal TBD

The practical scenario acknowledges the achievement of a 100% renewable energy electric grid in 2100, requiring recurring IE (after 2100) causing the release of 1 to 10 B tons of CO2 per year, and the exhaustion of the (900 Bt) CO2 Budget by 2050, necessitating measures to either Capture Carbon, use Hydrogen (sourced from RE), or develop concentrated solar thermal - all with cost and technology risk implications.

Groundrules & Assumptions

Some key groundrules and assumptions to note in the practical scenario:

- 1) Energy demand is assumed flat between 2050 and 2100 (mainly due to efficiency measures, economic reality, and policies), with increased demand met with CO2-free supply.
- 2) The quantity of automobiles ceases to increase. The transition to EVs is complete before 2100. The Invested Energy of EVs is assumed the same as that of Internal Combustion Engine vehicles.
- 3) An aggressive Electrification “of everything” is pursued to the greatest extent possible.
- 4) Hydropower capacity is assumed to remain flat (w.r.t. production capacity).

- 5) Nuclear power is assumed to fall off by natural attrition, as plants reach the end of their Service Life times. Nuclear will need breakthroughs before again growing in capacity.
 - 6) There will be a significant contingency of coal and natural gas powered electricity plants in 2050.
 - 7) In the 2020 – 2050 interval efficiency measures are assumed across all sectors, resulting in a 20% energy demand reduction. These are economically beneficial investments that have been happening for decades.
 - 8) Energy storage can be embodied energy intensive and significant R&D effort is assumed in 2050 – 2100, service life times of 10 years through 2050 expanding to 20 years through 2100.
 - 9) Reliability (service life) improvements will play a positive role in reducing GHG emissions.
- GHG emissions globally in 2021 (starting in 2019) are at 40 B tons CO₂ (equivalent) per year.

The Paris Agreement, established at (Conference Of Parties) COP 21 in 2015-2016 and organizing commitments by member countries to document releases and reduce emissions, allows for a GHG Peak to occur in the near future, estimated to be around 2030 and achieve Zero Net Carbon by 2100, or 0 Bt CO₂ per year.

Swedish scientist Svante Arrhenius considered in the 1890's what would happen if we doubled the amount of carbon dioxide in the atmosphere, stating that the average temperature of the earth would rise 5 degrees Celsius. One hundred years later we are seeing that scenario play out, with the near future temperature rise scenarios shown in Figure 3 below. With no climate policies in place, we are heading to a 4.8 degree Celsius rise. The best we can hope for is a 1.5 degree Celsius rise, which would involve humanity going to Net Zero Carbon.

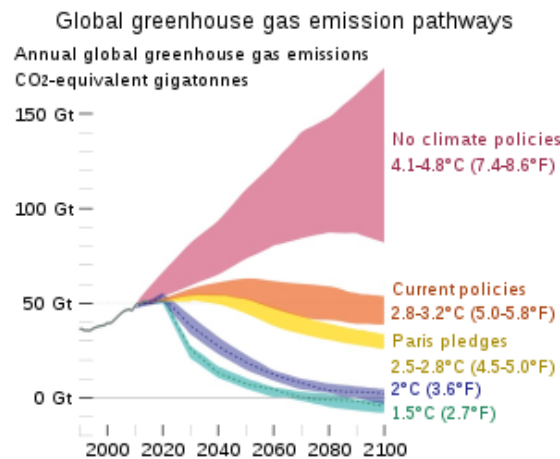


Figure 3: Global greenhouse gas emissions pathways

The Intergovernmental Panel on Climate Change (IPCC), formed in 1988, is the United Nations body for assessing the science related to Climate Change. The IPCC periodically releases assessments that determine the state of knowledge on Climate Change, including where there is agreement in the scientific community. The IPCC looks at various scenarios reflecting the different possible temperature rises in the future, from the desired limit of 1.5 degrees C (since pre-Industrial Age), up to 4.8 degrees C (amounting to a doubling of pre-Industrial Age CO₂).

In his book “How to Avoid a Climate Disaster”, Bill Gates breaks down 2020 GHG emissions into 5 categories by % and establishes the goal to be Net Zero Carbon by 2050:

Making Things	31%	12.4 Bt/Y re 2019
Plugging In	27%	10.8
Growing Things	19%	7.6
Moving Around	16%	6.4
Keeping Cool/Warm	7%	2.8

Innovation and breakthroughs will be required to meet the 2050 target, what might be called the best case scenario (called the Breakthrough Scenario herein). Gates pushes for electrification of just about everything (transportation, home heating and cooling, manufacturing processes, etc.). Without breakthroughs, growth in Nuclear power would be needed to get to Zero Net Carbon by 2050. Gates recognizes the ultimate challenge in zeroing out carbon in Making Things and relies on yet to be fully developed and scaled up Carbon Capture, alluding to Invested Energy (IE), the energy to Make Things, now mainly dependent on burning fossil fuels. As of 2021, there are no operating Carbon Capture systems due to the exorbitant cost.

The Paris Agreement stresses the importance of (Developed Countries like the U.S. and China) helping Developing and Poor Countries toward low carbon economies, through financing and technology transfer. But, how do High Carbon countries do this helping? Chemistry Professor Neocles Leontis of Bowling Green State University (BGSU) in Ohio has noted a CO₂ Budget of 900 B tons of CO₂ to limit temperature rise and avoid worsening Climate Change. Using only current state of the art (and not relying on new breakthroughs) and acknowledging the current 40 Bt/Y, one can see a CO₂ Budget Gap emerging before 2050. Invested energy emissions are a significant and persistent portion of the CO₂ Budget.

The practical scenario leaves us with about 1 Bt/Y for IE(RE) and 1 Bt/Y for IE(EVs) through 2050. The IE(Non-RE/EVs) is the toughest to predict or levelize – if ½ of the Making Things CO₂ Budget (of 12.4 Bt/Y) were eliminated by evolutionary technology, planning, and policy, then there would remain an IE(Non-RE/EVs) of 6 Bt/Y. We are looking at a total of 8 Bt/Y of Residual IE by 2100, down from a projected peak of 51 Bt/Y from all sources. Accounting for residual emissions for Growing Things and Moving Around (as for heavy equipment, airplane operation, trains, and trucks), and unless Energy Storage, Carbon Capture, Hydrogen, and Nuclear power are advanced, we will likely see a 21st Century CO₂ Budget Gap of over 500 B tons of CO₂.

Meeting the CO₂ Budget in time to achieve Zero Net Carbon (and maintaining thereafter), and staving off worse Climate Change, must involve minimizing the Invested Energy used to build the energy infrastructure.

In the decades ahead, Making Things will increasingly be the major GHG contributor [in 2100]:

Making Things	90%	8 Bt/Y
Plugging In	0%	
Growing Things	5%	1 Bt/Y
Moving Around	5%	1 Bt/Y
Keeping Cool/Warm	0%	

3. LOW EMBODIED ENERGY SYSTEMS

Innovation to reduce the embodied energy (invested energy, IE) of renewable energy systems should be addressing the 1 Bt/Y of CO₂ emissions. The Tensioned Cable System (TCS) for mounting solar panels (first produced and installed for the University of Findlay in Ohio in June 2012 – See Figure 4) is low embodied energy and reduces energy payback of conventionally ground mounted solar electric systems from 9 years to 6 years. If the 3000 GW of Solar PV (in the U.S. by 2080) capacity modeled in the practical scenario were TCS mounted, then about 70 Mt/Y of CO₂ emissions could be eliminated in the U.S., or about 280 Mt/Y globally – that is ¼ of the residual IE(RE). With less impact to land, the TCS also has lower Disposal Energy, as there is less mined material and less concrete to repurpose, resulting in lower Disposal Cost. Such technology exists now and can reduce system installed cost.

The economics of low embodied energy systems are favorable, even without anti-carbon policies or carbon disincentives such as Carbon Taxes. Material-intensive, high embodied energy systems, are costlier (to account for extraction and processing), and will become more costly as demand increases during the infrastructure build up and as fossil fuel production decreases past Peak.



Absent are metal post, beams, stringers, and concrete

Figure 4: TCS G1 in September 2020

The practical place to implement low IE RE is in Developing Countries, where the Paris Agreement intends to develop low carbon economies. The high carbon U.S. is rapidly developing large utility-scale solar farms, which can operate well in its highly developed electrical transmission and distribution system. What about Developing and Poor Countries lacking such infrastructure? Smaller scale, low impact, versatile solar electric systems would be appropriate and affordable.

The cost of material-intensive products correlates to their embodied energy. Implicitly and generally, lower embodied energy products mean lower cost. In summary, the case for low embodied energy renewable energy systems rests on these main points:

- Helps preserve the limited CO₂ Budget for preventing worse Climate Change in the longer term.
- Helps relieve the CO₂ Bow Wave concurrent with large, fast buildup of renewable energy and energy efficient systems, thus, helping to prevent arrival of Climate Tipping Points, where accelerating Climate Change could happen irreversibly.
- Tends to lower costs of renewable energy and energy efficient systems.
- Reduces the development risk otherwise associated with the pursuit of breakthroughs, while the natural pursuit of doing more with less leads to time-proven positive results.

Economics

The industrial age has prospered with the availability and low cost of energy – coal, oil, and natural gas. Not without some investment (in exploration technology, extraction equipment, transportation and distribution systems, etc.). There are enough fossil fuels left to serve us a few more generations. But, we are spending our (solar) energy savings, and quite rapidly, despite billions of earth's inhabitants in poverty. Sustainability will require a transition to our (solar) energy income and will require technology and global cooperation (and tens of trillions of dollars in investment). True sustainability will require scientific truth, transparency, global perspective, and an appreciation for the long term.

The Paris Agreement prescribes financial help and technology transfer to Developing and poor countries, hopefully not to take the Western (Developed) world's path to prosperity, but to create a low carbon economy that provides the basics to survive and thrive. Of course, Climate Change is set to hit the Developing and poor countries worse, with sea-level rise (flooding), drought, etc. affecting them to the point of inducing mass migrations. Developed countries, such as the U.S., face a lot of challenges handling immigration.

The U.S. and other Developed countries have high carbon economies. To date, the Industrial Age has caused the emission of about 2000 Gigatons of CO₂. Scientists claim that a budget of about 1000 Gigatons

remains before worsening Climate Change, which will bring about catastrophic damages and big hits to the economy. Interestingly, Europe achieves each unit of GDP with a quarter less energy than the U.S. Architect, inventor, and design science advocate R. Buckminster Fuller recognized the geologic value of gasoline at about \$1M per gallon. Forty years ago Bucky Fuller suggested that it was cheaper to pay people to stay home, to avoid the gas guzzling trips to work, which did not necessarily contribute to the productive economy, though part of the consumptive economy. Bucky also had the foretelling suggestion that we build a global transmission system, so that the sunlit day side could power the dark night side, without large scale energy storage.

As we learn to more efficiently utilize fossil fuel energy, an ironic paradox emerges – Jevon’s Paradox, identified at the start of the Coal Age – the more efficiently we use a limited resource, the more of that limited resource we will use. Efficiency steps up demand, and demand induces greater supply, and supplied demand consumes the limited resource, be it coal, oil, or natural gas.

Given any progressive technology, reliability and efficiency improvements historically have followed, such as in Solar PV panels (from years to decades in Service Life) or in cars (from 100 to 300 thousand miles and from 15 to 35 mpg). We will rely on such improvements in the decades and century ahead. Jevon’s Paradox and Capitalism’s emphasis on consumption will be huge challenges to overcome, as profits get conflated with progress on the path to sustainability, low carbon, and avoidance of a climate disaster. Before geologic discoveries of large deposits of coal (and oil), and efficient ways to extract or use it, costs were high and production low. Efficiency became the key. Efficient boilers and machines to get more work with less coal stepped up the demand and consumption of coal. A similar phenomenon occurs with embodied energy and renewables (solar and wind) – as we use less energy in making the infrastructure, we see demand (for low embodied energy products and systems) going up, as acquisition costs (leveraged by the lower embodied energy) go down. This paradox of sorts can induce transition to solar in the midst of economic stress and high material costs, of which we clearly face in the future.

There is a tendency to focus on operational or end use consumption of energy and accompanying emissions. The ongoing electrification of our economy and lives will leave Making Things the clear leader in GHG emissions. Embodied energy (from Making Things) will be an increasing hurdle to achieving Zero Net Carbon (and, thus, True Sustainability) without busting the CO₂ Budget (for avoiding worse Climate Change). The process energy for Making Things is not naturally occurring. Solar and wind energy is diffuse and low intensity, while process energy is concentrated and high intensity. Carbon Capture and continued fossil fuel use is not a long term sustainable solution.

It is important that we know our CO₂ (emission) Budget to stave off worsening Climate Change, particularly warming. There are currently at least 15 phenomena in nature that are at risk of runaway behavior, worsening Climate Change, such as polar ice melting, carbon sink forests diminishing, and ocean circulation changes. As of 2016, 900 Billion tons of CO₂ was the Budget before we pass Tripping Points. No scenario realistically gets us to Zero Net Carbon by 2050, which would have reliably assured a Stable Climate. Indeed, assuming that breakthroughs do happen as hoped, there is a chance to reach Zero Net Carbon by 2050, albeit not practical or probable. As annual reductions increase over time, the Invested Energy (IE) needed to build up and maintain the clean energy and clean living infrastructure, and the associated emissions, will be increasingly significant, as it chips away at the CO₂ Budget and contributes to the CO₂ Budget Gap.

The dilemma of embodied energy (invested energy for the infrastructure to fight Climate Change) is in the near term somewhat mitigated by following the old adage of the early environmental movement: REDUCE, REUSE, and RECYCLE, and mostly in that order. In the long term, recycling will be essential, and low embodied energy infrastructure is inherently easier and less costly to recycle. Implement low embodied energy now to reduce the CO₂ Bow Wave, to prepare for recycling in the future, and to reduce hurdles to achieving Zero Net Carbon.

The combined Bow Wave from all CO₂ reduction measures represents a temporary uptick of several billion tons of CO₂ in a 10 year or longer period, coinciding with the near term increases in CO₂ emissions from infrastructure buildup. Net reductions occur only after the Energy Payback period.

Pursuing low Invested Energy infrastructure means lower rates of fossil fuel consumption, less costly recycling, lower risk of Climate Change worsening, and lower cost risk in the future, when energy and material costs are likely higher. Identifying the advantages of lower IE will justify incentivizing the development of IE-reducing technology, such as structural alternatives (to steel, aluminum, concrete, and glass), design with less material, hydrogen, concentrated solar thermal, and even Carbon Capture.

4. CONCLUSIONS

There may be a conclusion to a study, an article, or a white paper, but there is no conclusion to the sustainability story. True sustainability is technically impossible if we are consuming the resources that now sustain us. Climate Change is the blaring red flag that tells us we are using up our limited resources. We would have reached the Embodied Energy challenge whether we experienced (human induced) Climate Change or not. At least we are acknowledging Climate Change and are making plans to fix, or rather, to mitigate it.

The translation to a clean energy economy seems destined to be led by the free market system, with low cost and high profit the operative principles. Climate Change represents an added (emerging) cost to the market equation. The lure of free solar energy and the promise of technology is the market's answer to the greatest Incurred Cost imaginable, Climate Change. But, is this a setup to the greatest Paradox of our time? That we may be designing more efficient means of consuming even more of the limited resources we call fossil fuels?

Low embodied energy (i.e., low invested energy in Making Things) is a logical pursuit in our transition from quantity limited fossil fuels to renewable fuels, electricity, and materials. It is logical to incentivize the pursuit of low embodied energy in our free market economy. Certified Low Embodied Energy may one day coexist with Certified Organic, Low Sugar, Fat Free, and Gluten Free in the lexicon of the market. The first order, material-based Invested Energy estimating approach herein would need to be more rigorous and inclusive of all invested energy sources, such as machining, transportation, and installation energy. Encouraging is the fact that these secondary embodied energy demands can be supplied by the new clean energy infrastructure. Material production stands as the main challenge in achieving low embodied energy and true sustainability.

Despite identification and planning for Climate Change (Global Warming) going back decades, the past decade has seen at least a 15% increase in global GHG emissions, attributable to population induced demand growth and perhaps to the renewable energy build up already in progress. The buildup (of Solar PV, Wind, and Electric Vehicles) has only just begun, with the bow wave of associated CO₂ emissions coming in the next decade. We can only hope to begin the sustained decline in CO₂ emissions by 2030. The CO₂ Bow Wave, though seemingly lost in the current rise of global emissions, is foretelling of the challenge ahead, that is, the needed revolution in the approach to Making Things. We are prioritizing the reductions in end use emissions, and expanding emission-free electric generation, while not emphasizing lower embodied energy. It is not profitable, yet, to find alternatives to coal and natural gas for Making Things.

Incentivizing low embodied energy now can be relatively less expensive than dealing with worse Climate Change mid-century, as we are already facing trillions of dollars in losses to the economy in the decades ahead due to Climate Change. The new (Buildup) Invested Energy portion of the CO₂ Budget going forward, at about 200 Bt of CO₂, is too large to ignore. The old legacy Invested Energy of the current

manufacturing-focused Industrial Complex (with emissions on the order of 10 Bt/y of CO₂) is also too large to ignore.

The goal of doing more with less can cost less. The Tensioned Cable System for mounting Solar PV panels (G1 or all metal G1M) costs less than conventional mounting, reduces Invested Energy CO₂ emissions, creates semi-skilled jobs, and is amenable for broad use in Developing Countries. The Practical Scenario addressed herein for the U.S. will cost about \$4.5 - 6T through 2050, still less than the cost of the Cold War (\$6T in 1980 dollars), which went a long way to preserving the fossil fuel-dependent economy of the post WWII years.

The significance of Invested Energy and associated CO₂ emissions grows over time. Ultimately, we face releasing 4 Bt of CO₂ per year to maintain the 100% renewable energy/clean Electric Grid and perhaps 6 Bt of CO₂ per year to Make Things. The last 20% of annual reductions are faced at a time (mid-century and beyond) of Climate Tipping Points – including sea level rise, carbon sink forest loss, and ocean circulation changes. The real deal will be finding new ways to produce material without burning fossil fuels, sooner rather than later.

Let us develop a Design Science of Doing More with Less and direct investment and effort into reducing Invested Energy (embodied energy), optimizing and economizing the global plan for reducing GHG emissions.

5. ACKNOWLEDGMENTS

The author is not a scientist or professional researcher and relies on the contributions of numerous individuals, organizations, and agencies. The idea for addressing embodied energy (in a white paper) comes from a conference in Ohio in 2016, where BGSU Chemistry Professor Neocles Leontis spoke to Climate Change and tipping points. A list of referenced individuals, institutions, agencies, and websites is included in the related white paper cited in the References section herein.

6. REFERENCES

- Clemens, J. A., 2021. True Sustainability With Low Embodied Energy.
www.olympicenergysystems.com/uploads/TrueSustainability.pdf.
- Gates, Bill, 2021. How To Avoid A Climate Disaster. Alfred A. Knopf, New York.
- Fuller, R. Buckminster, 1981. Critical Path. St. Martins Press.
- Fuller, R. Buckminster, 1969. Operating Manual For Spaceship Earth. Southern Illinois University Press.

SOLAR FOOD DRYING FOR AFGHAN COMMUNITIES

Prof. Robert Foster
College of Engineering
New Mexico State University (NMSU)
Las Cruces, New Mexico USA
rfoster@nmsu.edu

Eng. Fazlullah Fazli
Da Afghanistan Breshna Sherkat (DABS)
Kabul, Afghanistan
fazli28@gmail.com

Abstract

Solar food drying is a thousands years old technique used for food preservation. Bacteria, yeast, and mold are prevented from spoiling the food due to a low moisture content. Dried food takes up less room and is light and easier to transport. Afghanistan is a leading exporter of dried foods, but often still using inefficient traditional outdoor direct drying methods with longer drying times. Traditional outdoor drying is also less hygienic and subject to contamination from dust, insects, birds, and animals.

New Mexico State University (NMSU) introduced more efficient active and enclosed passive solar food drying techniques to Afghanistan in 2009 with faster drying times, better hygiene, and improved quality of dried foods. Food is normally dried between 50 to 80°C, which is a desirable range for drying and pasteurization. Solar drying reduces moisture content typically from about 10 to 20 percent. There are now over a dozen Afghan vendors supplying solar dryers. Many farmers also rent out their food dryers to after they have dried their own crops. This paper discusses solar dryer theory, operation, drying results, vitamin and color retention, business development, and applications in Afghanistan.

Keywords: solar energy, food drying, Afghanistan

1. SOLAR FOOD DRYING

Solar food drying was the only method for long term food preservation for thousands of years until canning was developed at the end of the 18th Century. Bacteria, yeast, and mold are prevented from spoiling the food due to a low moisture content. Dried food takes up less room and is light and easy to transport. Food is normally dried between 50 to 80°C, which is a desirable range for drying and pasteurization. Solar drying reduces moisture content to 10-20%.



Figure 1. Traditional outdoor direct solar food drying in Afghanistan has been used for thousands of years like drying apricots on a rock, but this slower drying method often leads to mold and allows access for insects, birds, and vermin.

Traditional outdoor food drying techniques commonly use rocks, rooftops, and tarps which generate relatively low drying temperatures highly dependent on the ambient temperature and available sunlight. Traditional methods rely on longer drying times that often take five or more days. These slower drying times make food more susceptible to spoilage from mold, bacteria, and yeast if the weather does not cooperate and the sky clouds up for a day or more in

the middle of the drying process. Traditional outdoor food drying is also less hygienic and subject to contamination from dust, insects, and animals.

Afghanistan has a centuries old tradition of using indirect solar food dryers in the form of adobe type barns (keshmesh khanas – literally raisin houses), but only for drying grapes into raisins. Fifty years ago before the wars, Afghanistan provided over ten percent of the global raisin supply (AFP, 2017).

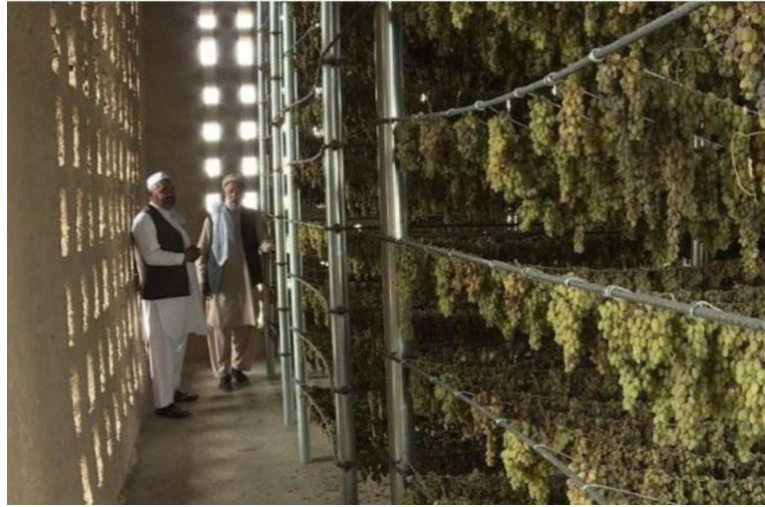


Figure 15. Traditional raisin drying adobe barns (keshmesh khana) have been used for centuries in Afghanistan. (AFP, 2017)

The input energy to a solar dryer and the energy output of solar dryer is given below. For I is the amount of solar energy falling on a solar dryer, A is the aperture area of the solar cooker and Δt is the period of time; the amount of energy received by the solar dryer (E_{in}) is calculated by the following expression:

$$E_{in} = IA\Delta t.$$

The energy output of a solar dryer is the increase in energy that the food has due to the temperature increase and moisture driven out. From this point of view, energy output of the solar dryer (E_{out}) is given as follows:

$$E_{out} = m_f c_{pw} (T_{ff} - T_{fi})$$

where m_f is the mass of food, c_{pw} is the specific heat capacity of water (which is driven out of the food), T_{ff} is the final food temperature and T_{fi} is the initial food temperature (for any solar day). The basic concept is shown below where solar energy is used to dry food either passively or actively in a vented solar dryer that removes the moisture to a desirable moisture content level.

2. Solar Dryer Types

2.1 Rack Dryers

This is the simplest dryer to build and is a completely passive natural air dryer, a simple rack or even cardboard box can be used with cheese cloth or netting on top to keep the flies out. It's preferable to use some kind of screen underneath the food to allow for greater airflow and faster moisture removal.



Figure 2. Outdoor rack type dryer drying apricots in Afghanistan which allows for better air circulation underneath the product.

2.2 Direct Dryer (Greenhouse or Tunnel)

Direct dryers come in several configurations such as greenhouse or tunnel dryers and moisture is removed either passively or actively. Glazing is used and important as it allows the visible short wavelength sunlight to pass through, but and helps trap heat inside the box from the reflected long wavelength radiation through the greenhouse effect. The glazing should seal the top of the dryer in order to minimize heat from leaking out. Glazing facing the sun (perpendicular) achieves a higher solar heat gain.



Figure 3. Direct greenhouse dryer used by the French NGO GERES in Afghanistan for apricots.

2.3 Indirect Solar Dryer

Indirect solar dryers are the best type since the food is not dried in direct sunlight, which has strong UV rays that break down vitamins and color in food. Thus, indirect solar dried food has better vitamin quality and improved food color retention. There is no need for sulfur or blanching techniques sometimes used with some commercial food dryers designed to prevent spoilage and rot. Indirect dryers provide better control of the food drying process, which can more easily regulate the interior dryer temperature through passive or active (e.g. electric fans) venting.

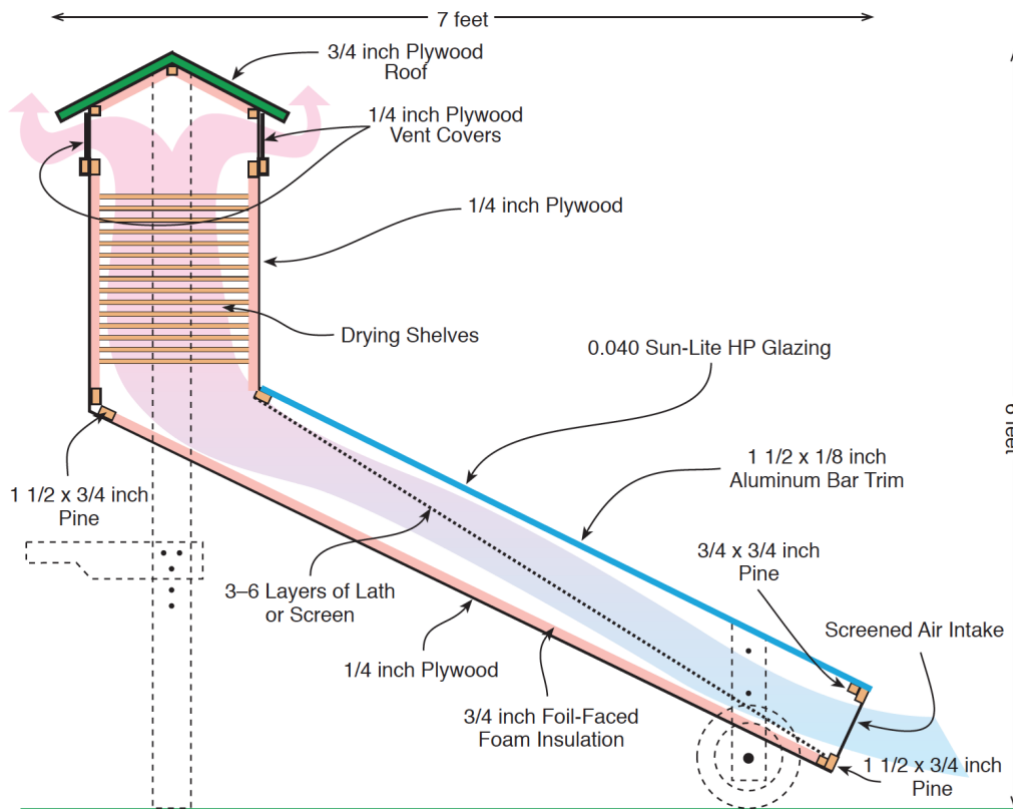


Figure 4. Indirect solar food dryer design originally developed by Appalachian State University, which dries food about 3 times faster than outdoor drying, reducing spoilage. NMSU introduced this design to Afghanistan in 2009. Black metallic window screen was folded over about 5 times over to serve as an excellent absorber plate with great air mixing abilities (Scanlin, 1997)

3.0 Solar Dryer Operation

Successfully drying foods depends on two primary parameters: temperature and airflow. The goal is to keep air temperatures low enough to avoid cooking the food or causing it to crust, while maintaining enough warm air to discourage the activation of enzymes that would begin the spoiling process. The high sugar and acid content of fruits make them safe to dry in the sun. Vegetables are low in sugar and acid and at greater risk of spoilage. Meats are high in protein making them ideal for microbial growth when heat and humidity cannot be controlled. The target temperature is typically between about 40 and 75°C depending on the type of food. Airflow is also important, as it helps to create balance in the drying process and removes moisture.

Proper food preparation requires cutting it into thin slices, no more than about one centimeter thick, and spread them out over the drying trays, allowing plenty of room for air to move around the individual pieces of fruit or vegetable. Add the food to the drying trays and place inside the solar food dryer. You can rotate the dryer to track the sun each day for faster drying until the food is completely dried. This helps to create a uniform drying process.

A solar dryer is turned towards the sun and left until the food is properly dried. The solar dryer may be checked every few hours, to rotate the dryer to track the sun more precisely and to ensure that shadows from nearby obstacles like buildings or trees are not blocking the direct sunlight. The long absorber is made of black wire screen, which collects heat under a glass cover. Small wooden vents in the front and at the top assure that air is drawn through. Moisture is eliminated through the vent at the top as air flows naturally.

The drying time depends primarily on the solar dryer type of equipment used, the amount of sunlight at the time, and the quantity of food that needs to be dried and its moisture content. Air temperature and airflow affect performance and drying time. Some foods with lower moisture content (e.g., onions) dry faster in maybe 1.5 days, while other foods with a higher moisture content (e.g. tomatoes) take longer as long as 3 days to dry. Larger quantities of food, and food cut in larger pieces, take longer to dry.

3.1 Ideal Food Drying Temperatures

- Fruits and Vegetables: 40-55°C
 - Temperatures over 65°C can result in sugar caramelization of many fruit products
- Meats: 60-65°C
- Fish: 55-65°C
- Herbs: 35-40°C
- Rice, Grains, Seeds: 45°C
- Livestock Feed: 75°C

3.2 Solar Dryer Usage

1. Place the solar dryer outside in a location that will have FULL sun exposure all day.
2. Cut the food into thin strips placed on the drying trays/racks to be placed in the solar dryer.
3. If using a vented dryer, adjust the vents leaving them wide open for the start of the drying process to remove more moisture and gradually closing them down to bring up the interior temperatures as the food dries over the next 2 to 3 days.
4. For faster drying, have the dryer aimed directly towards the sun, moving it every couple of hours to track the sun which moves about 15° per hour across the sky. By pointing the solar dryer ~20° ahead of the sun's path through the sky, you will have less need to move the dryer throughout the day.
5. Occasionally want to reorder racks or move food around on trays for more even drying; the food will not burn.
7. Avoid opening the dryer too often as this lets the heat out. Be careful when opening the solar dryer as the temperatures are hot enough to burn you. Drying racks are hot and should be handled with oven mitts. Always exercise caution with solar dryers. Sunglasses, long sleeves, and hats are useful when working outside with a solar dryer.

4.0 Afghanistan Solar Food Drying

NMSU introduced indirect solar food dryers into the country initially through the USAID Afghanistan Water, Agriculture, and Technology Transfer (AWATT) in 2009 working with NGOs like MEDA and Global Partnership for Afghanistan. as a faster and more hygienic method for drying food. Later this effort was further expanded by NMSU in collaboration with Winrock International under the USAID Afghanistan Clean Energy Program (ACEP) working with MAIL and FAO to disseminate to all provinces in the country.

Food can be dried about three times faster than traditional outdoor drying. With indirect solar dryers, the food is also no longer exposed to direct UV rays as in traditional outdoor drying; the UV causes vitamins and natural food colors to break down. Indirect solar dried food improves vitamin quality and improves food color retention which is

aesthetically more appealing. There is no need for sulphur, blanching, etc. Indirect drying also provides better control of the drying process - can more easily regulate the temperature through passive (or active) venting.

NMSU chose a solar food dryer designed in the early 1990's by Appalachian State University as an economical and efficient food preserver, which was created by Professor Dennis Scanlin. Solar dryers are easy to build with locally available tools and materials and operate simply by natural convection. The solar food dryers designed at ASU are basically wooden boxes with vents at the top and bottom. Food is placed on screened frames that slide into the boxes. A properly sized solar air heater with south-facing plastic glazing and a black metal absorber is connected to the bottom of the boxes. Air enters the bottom of the solar air heater and is heated by the black metal absorber. The warm air rises up past the food and out through the vents at the top.

The dryers produce temperatures of 130° to 180° F, which is a desirable range for most food drying and for pasteurization. With these dryers, it's possible to dry food quicker, even when it is partly cloudy, hazy and very humid. Inside, there are 13 shelves that will hold 35 to 40 medium-sized apples or peaches cut into thin slices (Hartley, 2009).



Figure 5. NMSU trained Afghan carpenters such as Mr. Hakim on how to build indirect solar food dryers using all local materials.

Afghans have long been known for their excellent quality raisins and other dried fruits which they have exported for centuries to Pakistan, India Iran and more recently to UAE. With these newer indirect food dryers, not only can farmers triple production, the quality of the dried fruit and vegetables is much higher than the traditional outdoor drying. The enclosed indirect dryers eliminate dust, flies, and mold, as well as ultraviolet rays from direct sunlight which discolor fruit and damage the vitamins they contain. Birds and other animals also are blocked from attacking the drying food in the newer solar dryers.

In two or three days, five kg of fruit or vegetables can be dried and ready for use or sale. During the four month summer season, this would mean 600 kg can be dried, producing 120 kg of dried fruit which sells for up to \$5 per kg – a profit of \$600 per summer. The indirect solar food dryer, which can last for many years, can be built for \$120 and Afghan carpenters sell them for about \$200 – a sum that can be made back in less than half a summer of dried food production. Larger dryers can go for \$350 or more. Units are distributed across the country.



Figure 6. Indirect solar food dryer developed by NMSU disseminated with local NGO partner MEDA. Afghan women are very entrepreneurial, and when they were finished drying products, they rent out the solar food dryers to their neighbors.

4.1 Solar Dryer Value Added

AWATT designed and conducted trainings on the construction and use of solar fruit and vegetable dryers initially in Parwan and later Nangarhar. Drying helps preserve and extend the market window for many fruit and vegetable products. This work produced direct benefits for women in the region. Initially five Afghan carpenters were taught to build indirect dryers. Commercialization of the solar dryers was rapid with the receipt of nearly three dozen orders during the first growing season. Through the NGOs the dryer technology diffused throughout the country. Within two years of introduction over 1,000 solar food dryers were sold throughout Afghanistan, generating over US\$250,000 in local manufacturing sales in a couple of years.

The drying units create value added for Afghan farmers by offering an improved alternative to the way fruits and vegetables are traditionally dried outdoors. Initially when first introduced, women's groups cost shared half for each dryer (US\$250 each) with NGO support. The owner's learned to also rent out the dryers to their neighbors typically for about 20% of dried food production (NMSU, 2011). NGOs like MEDA and Global Partnership also worked with the women's groups on how to package and market solar dried food.



Figure 7. Business development and market development for dried products for export are essential components for successful selling solar dried foods. Organically grown solar dried products from Afghan women's groups have strong market appeal.

4.2 Capacity Building

Capacity building and business development are important to solar drying promotion. AWATT and later ACEP conducted a series of solar food drying workshops for female participants from Afghan women's groups, universities, government development promoters in Jalalabad, Parwan, and Kabul provinces. The goal with MAIL was to Train the Trainers for women agricultural extensionists across the country. The participants learned solar drying fundamentals including food preparation, sanitation, solar energy fundamentals, drying processes, dryer components, performance, and dynamic evaluation of the food drying process and product quality. The training deployed solar food dryers designed by NMSU who taught local carpenters to build units. Indirect solar food dryers have proven popular, with over 250 units sold in the past year. The units are passively vented and no electricity is used. Solar dryers are used to prepare dried apples, raisins, apricots, eggplants, onions, tomatoes and other high value fruit and vegetables. Farmers have tripled drying production, while the color, quality, and vitamin content of the dried fruit and vegetables is better since the food is not exposed to the sun's UV rays. Likewise, dust, flies, and birds cannot get into the enclosed drying chamber. In two or three days, 12 kg of food can be dried. The faster drying times reduces spoilage from mold and fungus as compared to outdoor drying.

Besides training NGOs, NMSU also assisted PRTs (Provincial Reconstruction Teams) with solar food dryer education and dissemination. The Kentucky Agribusiness Development Team in Kapisa taught men how to build solar food dryers, and the women on how to hygienically prepare food, as well as operate the dryers. The women were typically proud their male relatives had built the indirect food dryers. Both men and women learned how to price their products for sale. One woman relayed the story of how her mother-in-law had praised her dried eggplant. Now that is a success story in any culture (Getchell, 2011).



Figure 8. NMSU AWATT indirect solar food drying workshop held in Dari language with Afghan women's groups in Jalalabad in 2009 with the Afghanistan Ministry of Women's Affairs.



Figure 9. Engineering students undergoing solar food drying class at the Kabul University Renewable Energy (KURE) Lab.

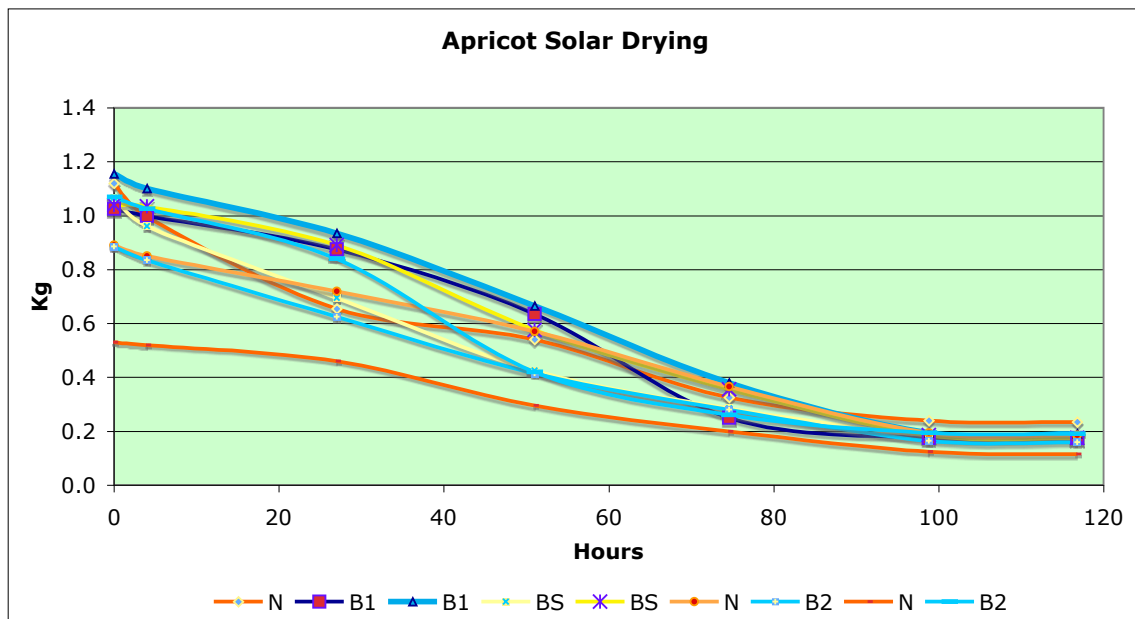


Figure 10. Apricot drying results from KURE Lab by weight (kg). Roughly takes 3 days to dry the product.

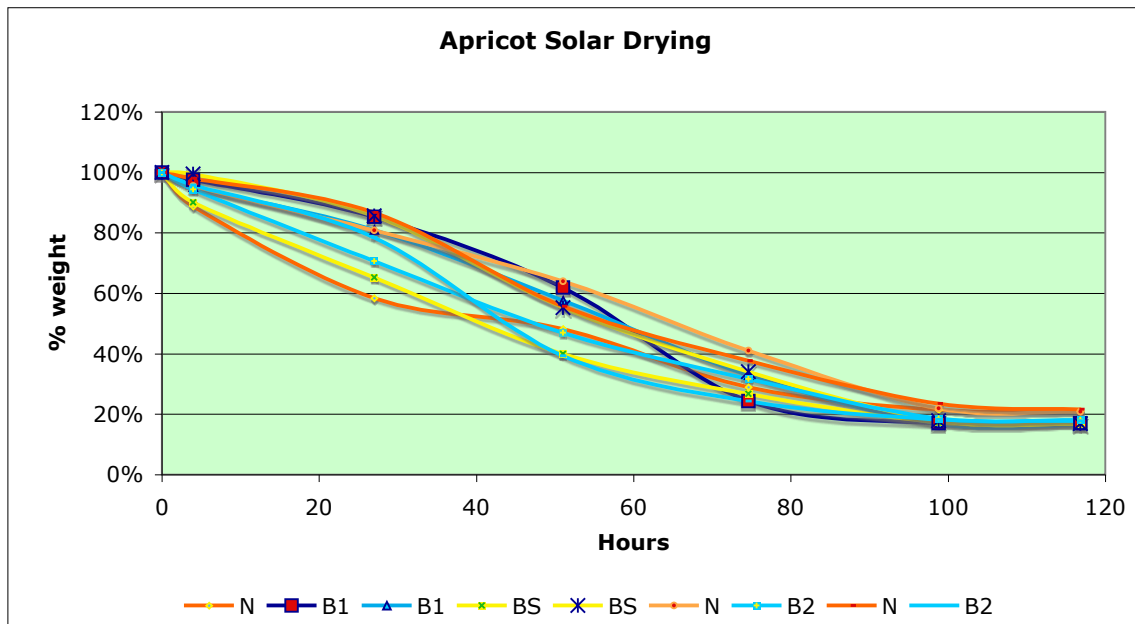


Figure 11. Apricot drying results by moisture content from the KURE Lab.



Figure 12. ACEP Train the trainers solar food drying workshop in Kabul with MAIL/FAO women extensionists who work nationally to teach farmers on how to utilize driers. They helped spread the concept across the country to even the most remote provinces.

4.3 Antioxidant Comparison: Direct vs. Indirect Solar Food Dryers

AWATT partner Southern Illinois University (SIU) conducted an antioxidant analysis comparing direct and indirect solar dried food. Antioxidants are compounds that prolong the shelf life of foods by protecting them against deterioration caused by oxidation, such as color changes. Direct photooxidation is caused by free radicals generated by radiation from UV light and then proceeds by normal free radical chain reactions. Phenolics are a group of phytochemicals that are biosynthesized from all kinds of plants. Common phenolics such as quercetin, chlorogenic acid, gallic acid, or syringic acid are widely found in a variety of fruits and vegetables like apricots and peppers. Antioxidants play an important role in promoting human health and combating chronic diseases. Total phenolic content and DPPH assays are useful assays for evaluating the antioxidant activity of food products.

The conventional phenolic content, scavenging DPPH free radical assays are used for antioxidant evaluation. SIU studied the correlation between DPPH free radical activity, total phenolic content, and ABTS (Vitamin C) compared between the direct dried and indirect dried food products. Determination of total phenolics was made using the Folin-Ciocalteu Method. A determination of antioxidant activity was made using an ABTS radical assay. Finally a determination of antioxidant activity was also made using a DPPH assay (Huang, 2005). From Table 1, you can see that the DPPH average was higher with the indirect dried food product than direct dried products, generally indicating a higher percentage antioxidant content as would be expected for the indirect dried product not exposed to UV light, especially for red peppers and prunes.

Table 1. Antioxidant Comparison between Direct and Indirect Solar Dried Fruits

Sample Name	Total Phenolics (umole/g)	Total Phenolics Average	ABTS Assay (umole/g)	ABTS Average	DPPH Assay (umole/g)	DPPH Average
Prune - Direct Drying - 1	88.331		138.253		82.277	
Prune - Direct Drying - 2	76.395	82.363	129.771	134.012	82.475	82.376
Prune - Indirect Drying - 1	87.76		123.715		86.003	
Prune - Indirect Drying - 2	98.794	93.277	128.731	126.223	95.587	90.795
Berry - Direct Drying - 1	51.395		114.724		58.721	
Berry - Direct Drying - 2	48.417	49.906	117.544	116.134	50.924	54.8225
Berry - Indirect Drying - 1	45.84		106.886		53.947	
Berry - Indirect Drying - 2	44.684	45.262	103.782	105.334	59.05	56.4985
Tomato - Direct Drying - 1	51.781		107.848		43.938	
Tomato - Direct Drying - 2	42.966	47.3735	100.66	104.254	43.52	43.729
Tomato - Indirect Drying - 1	49.672		107.668		44.78	
Tomato - Indirect Drying - 2	47.97	48.821	112.27	109.969	38.03	41.405
Red Pepper Direct Drying - 1	62.066		132.63		51.332	
Red Pepper Direct Drying - 2	53.717	57.8915	133.345	132.9875	47.733	49.5325
Red Pepper Indirect Drying - 1	63.787		122.101		65.548	
Red Pepper Indirect Drying - 2	59.628	61.7075	134.42	128.2605	58.249	61.8985
Peaches/Apricot Indirect Drying -1	53.654		105.71		83.799	
Peaches/Apricot Indirect Drying -2	47.565	50.6095	98.404	102.057	77.39	80.5945

Source: Southern Illinois University 2009

4.4 Afghan Industry Solar Food Dryers

Historically, Afghanistan has produced high-quality and organic dried fruits and vegetables for centuries, renown for their superior taste and quality. These traditional Afghan dried fruits includes raisins, apricots, figs, cherries, prunes, dates, and mulberries. In the country, the process of drying fruits is a family business that has been passed down from one generation to another for many years. People typically dry their fruit in an entirely natural way either in direct sunshine or in the case of raisins in well aerated drying barns. From 2005 to 2015, when the security situation was better, there was solar food dryers development and using solar fruit dryer in the country by the international committees, with some local private companies trained and encouraged to start manufacturing of solar fruit dryers for both small and large scale drying.

One of the key challenges is educating farmers about the benefits of solar technologies to increase production of solar-dried fruits. If farmers use improved solar dryer technologies, they can increase production, reduce spoilage, improve hygiene, and sell an overall higher products will quality product. Most companies shown in Table 2 typically sell from two to five units per week during the summer and fall season. The great thing about the indirect solar food dryers is that they are made in country with local materials by local shopworkers, regardless of who is in power nationally.

Table 2. Afghanistan Renewable Energy Union Members solar dryer vendors (2021)

Company Name	Location
Qaderdan Rural Technology and Development Workshop	Kabul
Zaib Pamir Elect Engineering Company	Jalalabad
Silicon Solar Company	Kart-e-Parwan
Behroz Rayan Technical Engineering Company	Herat
Royal Group Co Ltd	Kabul
Afghan Lucky Door Logistics Services Company	Kabul
Takwin Electrical and Electronics Engineering	Kabul-Logar Road
Yosouf Mosawer Solar Manufacturing Company	Kabul



Figure 13. Indirect solar dryer innovation in 2021 by Zaib Pamir Co. with the addition of an active fan powered by a PV module to increase drying rates and productivity.



Fig. 14. Modern commercial scale indirect solar food dryer in central Afghanistan with active fans for large scale food drying increases production and reduces spoilage.

5.0 References

(AFP, 2017) Afghan raisin houses get a facelift to boost productivity,” *Arab News*, <https://www.arabnews.com/node/1211891/food-health>

(Getchell, 2011) KY ADT’s Solar Food Drying Project is a Family Affair, *Afghanistan Gazette*, USDA, Kentucky Agribusiness Development Team, Vol. 2, Issue 25, November 10

(Hartley, 2009) J., “Solar Food Dryers Designed at ASU Preserve Food Worldwide,” High Country Press, Boone, North Carolina. http://www.highcountrypress.com/weekly/2009/07-16-09/solar_food_dryers.htm

(Huang, 2005) D., Ou, B., & Prior, R. L. The chemistry behind antioxidant capacity assays. *Journal of Agricultural and Food Chemistry*, 53(6), 1841-1856.

(NMSU, 2011) Final Project Report: USAID Afghanistan Water, Agriculture, and Technology Program (AWATT), submitted to USAID Afghanistan, Kabul Afghanistan, 2011

(Scanlin, 1997) D., M. Renner, D. Domermuth, H. Moody, “Improving Solar Food Dryers,” *Homepower #57*, February/March.

A review on Solar Thermal System Design, Integration, and Techno-economic Modeling for Industrial Heating and Cooling Processes

Yacob G. Hiben^{1, 2*}, Mulu B. Kahsay¹, Johan Lauwaert²

¹Thermal and Energy Systems Chair, School of Mechanical and Industrial Engineering, Mekelle University, Endayesus Campus, Mekelle, Ethiopia

²Department of Electronics and Information Systems, Faculty of Engineering and Architecture, Ghent University, iGent-tower, Technologiepark-Zwijnaarde 15, 9052 Ghent-Zwijnaarde

*yacob.gebreyohannes@mu.edu.et

Abstract

The utilization of solar thermal energy has been ranging from simple fire starting using a pocket mirror to the solar architecture used in various ways. Solar thermal applications are indispensable and crucial technologies with increasing attention in renewable energy research for their high energy conversion efficiency and energy storage density. Solar collectors can absorb nearly the entire solar spectrum; around 50% of the sun's energy is invisible to the human eye in the infrared spectrum, as heat. Thermal energy storage (TES) can store on average around 10,000 kW for about 6 hours. Financially, solar thermal energy conversion systems in many locations have reached grid-parity (EUR 0.02 - 0.05/kWh for low-temperature and EUR 0.05 - 0.15/kWh for medium-temperature applications). Thus, solar heating and cooling (SHC) systems are identified as typical application areas for the huge technical potential of solar thermal integration (up to 5.6EJ in 2050) available within industries that are predominantly being met with environmentally unfriendly and less available fossil fuels. The scope of this review is, therefore, to demonstrate the state-of-the-art for basic energy generation and supply concepts of solar thermal systems for industrial application. The paper presents the basic solar thermal system design, configuration, operation, and possible integration concepts with an existing conventional system. It also describes the techno-economic mathematical models and analysis techniques for solar thermal system key performance indicators. Accordingly, this paper can be used as a brief extract and guide to systematically approach industrial solar system development projects using best practices adopted to explore the contributions of the researchers in the literature.

Keywords: Solar thermal, System design, Techno-economic modeling, SHC, Industry

1. Introduction

Solar radiation incident on the solar collector's aperture is focused on the absorber/receiver tube to heat the fluid passing through it. The heated fluid (usually air, water, or oil) is then used for applications and processes based on the specific end-use in water-heating (domestic, commercial, and industrial), space-heating, and pool heating systems (Lund et al., 2008) or to charge a thermal energy storage tank from which the heat can be drawn for use later (at night or cloudy days) (Prakash, 1994). Solar cooling is also identified as a potential application area, especially in the range of middle and small cooling capacities (Gebreyohannes et al., 2021). Solar collectors are the key components of solar thermal systems and can absorb nearly the entire solar spectrum; around 50% of the sun's energy is invisible to the human eye in the infrared spectrum, as heat (Penn State University, n.d.). Another key component of the system, Thermal energy storage (TES), is also one of the highest density energy storage systems with an average value of around 10,000 kW for about 6 hours (Global Energy Systems Program, 2020).

As one of the identified application areas, in 1976, the U.S. Department of Energy had funded about ten Solar Heat Industrial Process (SHIP) projects as a contribution towards the commercialization of solar thermal utilization. A few years after their operation, a report summarizing the data regarding application studies, output, performances, and economic analysis of these projects was published (Brown, 1978). It was observed that there was a need to reduce cost and minimize design and installation errors. Another handbook was then released that provided a step-by-step procedure for designing SHIP systems. It also presents specific design information regarding the selection and sizing of components such as collectors, storage, piping, insulation, pumps, valves, heat exchangers, and heat transfer fluids (Uppal et al., 2015). A different report that comprises the design and integration aspects of SHIP systems and additional performance prediction procedures using computer-based simulations was also published in 1982 (Kutscher, 1983). Since then, many promising projects on SHIP have been implemented ranging from small-scale

demonstration plants to very large systems capacities. In 2017, operating 124 new SHIP installations, totaling 192,580m² collector area was started. This increased the documented world total SHIP system by 25% in the number of installed plants and by 46% in the installed collector area. At least 624 SHIP systems, totaling 608,994m² collector areas were in operation at the end of 2017. Investigations projected the global SHIP potential to 5.6 EJ for 2050 (Gebreyohannes et al., 2021).

In a preceding couple of decades, though the dominant means for supplying cooling capacities have been compression refrigeration systems driven by electrical energy, the use of sorption refrigeration machines, which can be driven with thermal energy in the temperature range of 55-180°C have been used to supply cooling. Having been commercially available, absorption chillers are also mature and reliable technologies (Gebreyohannes et al., 2021). Currently, there is increasing use of solar cooling solutions for large public and private buildings as well as industries. According to (Justus et al., 2005), more than 100 commercial solar cooling systems with a cooling power of 9 MWth are reported in Europe. These systems show high potential in energy saving compared with conventional electric systems. By the end of 2015, an estimated 1,350 solar cooling systems were installed worldwide (Gebreyohannes et al., 2021).

Financially, the total investment costs for solar thermal systems, with few exceptions and differences at the national levels range from EUR 180 - 500/m². This equates to solar thermal systems in the range of EUR 450 - 1100/kWth and leads to an average energy cost of EUR 0.02 - 0.05/kWh for low-temperature and EUR 0.05 - 0.15/kWh for medium-temperature applications and is comparable to grid-parity in many locations (Gebreyohannes et al., 2021).

The aim of this paper is, therefore, to present a comprehensive review of several possible designs and integration prospects of solar thermal systems for industrial application. The methods and techniques for the techno-economic modeling of the systems are also briefly explained in the following sections. A systematic review method was established with two major steps included in the review process: (i) collection of system installation concepts and (ii) collection of system techno-economic modeling techniques. Hence, the study helps as a quick installation and modeling guide for Solar Heating and Cooling (SHC) installations of industries depending on the thermal energy requirements.

2. System installation concepts

2.1. Solar thermal applications and energy flow

Most of the energy consumed by the industrial sector is either in the form of thermal or electrical energy. Thermal energy is mainly used in process heating applications (cooking, washing, dyeing, bleaching, drying, etc). There is also increasing energy consumption for refrigeration and air conditioning, especially in the range of middle and small cooling capacities.

Solar thermal energy is often assumed as some unique source that must have complex technology to convert it to useful work. However, solar thermal energy is no different from any other type of thermal energy. Different temperatures and operating temperature ranges can be obtained depending on the collector setup and working fluid. This heat can then be applied for several thermal processes that would normally be driven by some other heat source such as natural gas, propane, or electric resistance heat. Cooling needs are also an excellent fit for solar thermal energy because of the often synchronous nature of the energy source and load schedule (Gebreyohannes et al., 2021). The energy collected by the solar field and stored in the warm reservoir can be used for process heating and driving thermal chillers. When not enough solar energy is available a traditional heating and cooling system can be started to produce the required heating and cooling effect (Burckhart et al., 2014). A typical schematic diagram of the thermal energy flow and distribution for heating and cooling applications is shown in Figure 1.

2.2. Basic system designs and configurations

i. Low-temperature systems

The system consists of an array of non-concentrating solar collectors, a circulating pump, and a storage tank. It also includes the necessary controls and thermal relief valve, which relieves energy when the storage tank temperature is exceeding a preset value. When the stored water temperature is above the required process temperature, it is mixed with mains water to attain the required temperature. If no water of sufficient temperature is available in the storage tank, its temperature is topped up with an auxiliary heater before use (Schmitt, 2016). A schematic of a typical diagram of a low-temperature solar system is shown in Figure 2. This once-through system (i.e. no hot water returns to the storage tank) is what usually happens in many industrial applications. The used hot water is replaced by mains

water.

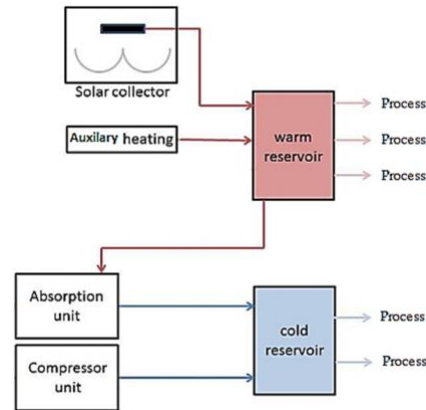


Fig. 1: Flow of thermal energy for heating and cooling processes

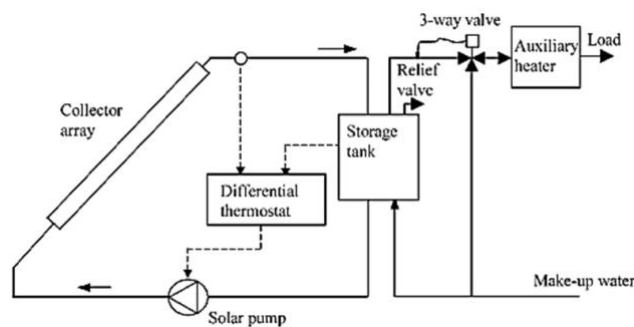


Fig. 2: Low-temperature solar system using a non-concentrating solar collector

In the case of low-temperature applications, higher efficiencies are achieved due to the low input temperature to the solar system. Thus, low technology collectors can work effectively and the necessary load supply temperature has little or no effect on the solar system performance. The system would need to be pressurized to allow storage at temperatures higher than 100 °C (Schmitt, 2016).

ii. High-temperature systems

Schematics of typical solar concentrator-based systems integrated with the backup boiler, with and without thermal energy storage are illustrated in Figure 3.

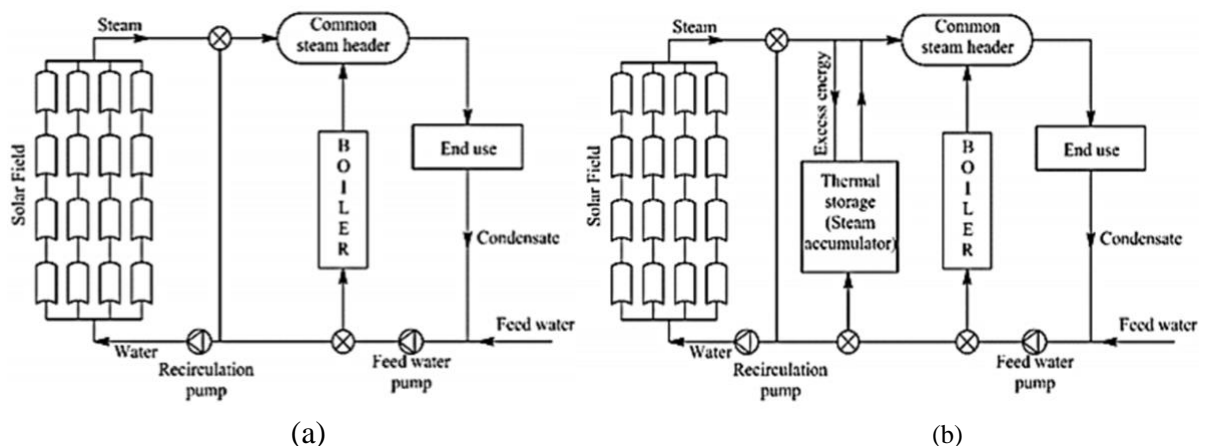


Fig. 3: High-temperature solar systems (a) with and (b) without provision of thermal storage

In concentrator-based systems, steam is generated in indirect and direct methods. In the indirect method, the heat transfer medium is heated in the solar collector loop and is then supplied to generate steam indirectly in the end-use loop. The indirect steam generation method can be in two different types of designs: unfired boiler (heat exchanger) based and flash boiler-based systems. In the unfired boiler-based system heat transfer fluid (e.g. water and air) is heated in the solar collector loop to provide the required heat that could be used to convert a secondary fluid to generate steam, pressurized hot water, or hot air as per the requirements of the end-use (Figure 4a). In the flash boiler-

based system, pressurized water is heated in the solar collector loop and is passed through a throttling valve. Due to the pressure change in the valve, a part of it is converted into steam (Figure 4b). This steam is transported to the end-user as per the requirements. The rest of the water is re-circulated through the collector field. Make-up water is fed from the feed water tank. In this case, a circulating pump is used in the loop that always maintains the pressure of water to prevent boiling in the collector loop and piping (Sharma et al., 2017).

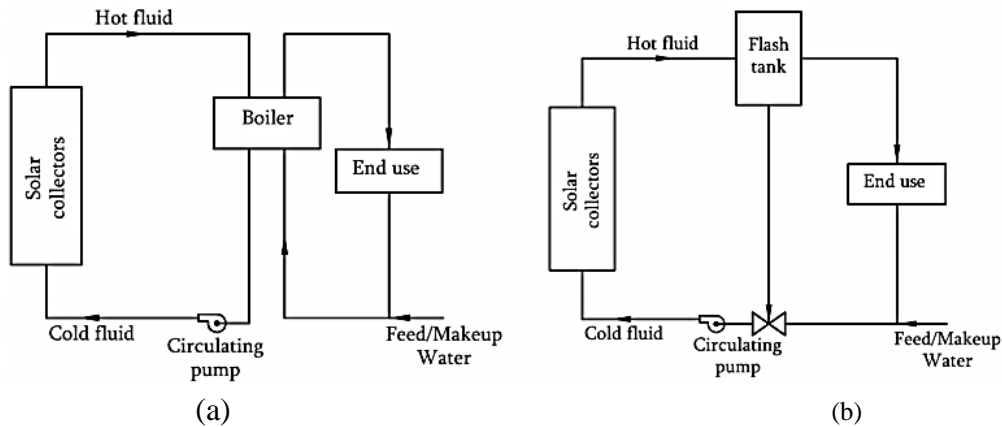


Fig. 4: Indirect steam production systems (a) Unfired boiler-based, (b) Flash boiler-based

In the direct (in situ) method, the water is boiled in the solar collector loop. In the case of partial heating, water is circulated through a steam drum where steam is separated from the water. Feed/Make up water is supplied to the steam drum or mixed with the re-circulated water at a rate regulated by a water level controller as shown in Figure 5 (Sharma et al., 2017).

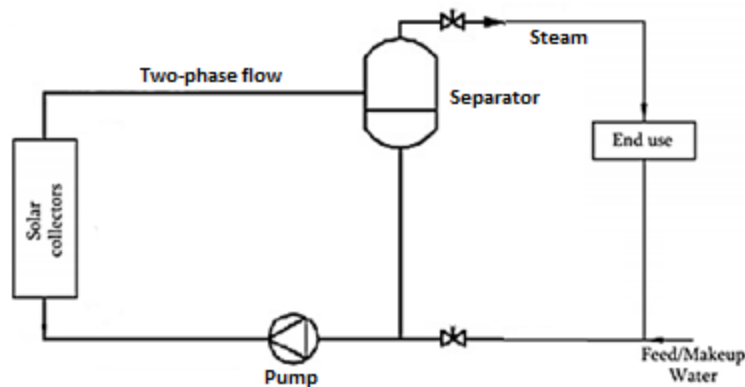


Fig. 5: Direct steam production system in a solar collector

A solar thermal system should enable continuous operation for meeting the process heating and cooling demand. This is possible with hybrid solar thermal systems where auxiliary boilers backup the system and ensure delivery of steam at a required temperature and pressure even in off-sunshine hours. Depending on the process heating and cooling demand and other requirements, the aforementioned solar thermal systems can be configured in parallel or series modes as per the requirements of the application shown in Figure 6 and Figure 7 (Sharma et al., 2017).

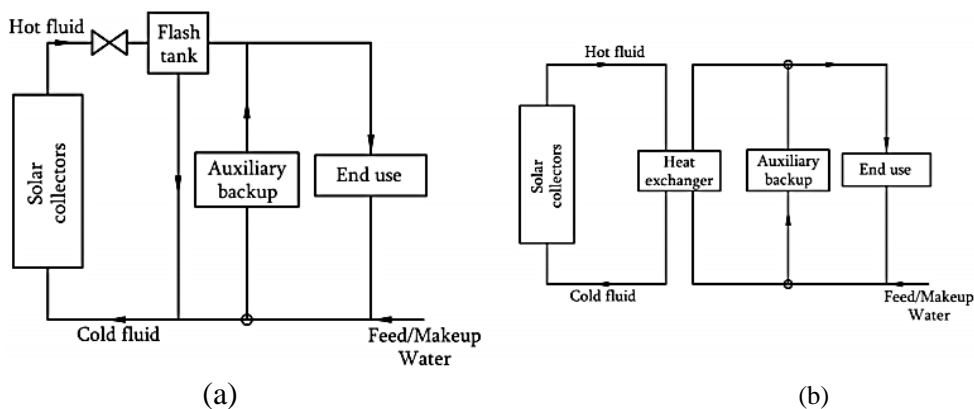


Fig. 6: Indirect steam production configurations with auxiliary backup in parallel for (a) Flash boiler, (b) Unfired boiler

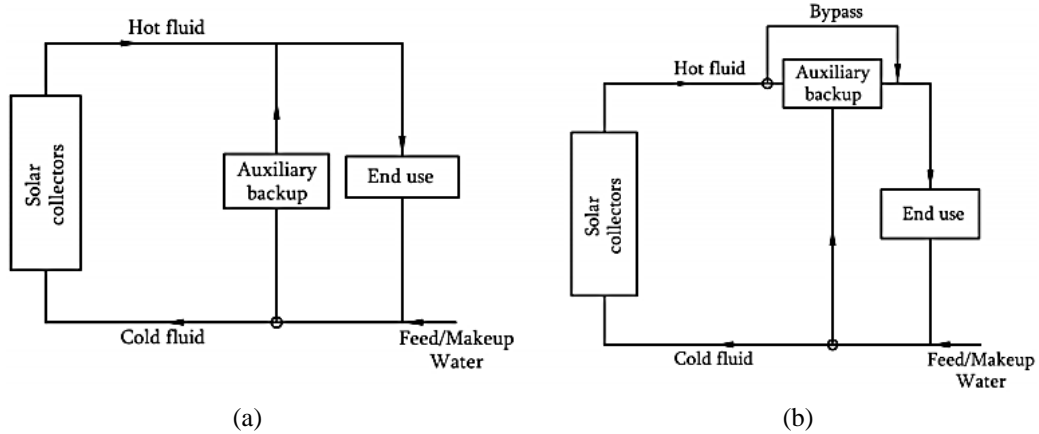


Fig. 7: Direct (in situ) steam production configurations with auxiliary backup in (a) Parallel, (b) Series

2.3. Basic system integration concepts

Perhaps the most common difficulty in the use of solar energy in a continuous operation is how and where to integrate it. A manual has been developed by the International Energy Agency (IEA) summarizing the guidelines for integrating solar systems with conventional systems (Aidonis et al., 2005). Different suitable integration concepts and configurations are identified by the guidelines for the integration of solar heat on supply and process levels. On the supply level, the respective heat transfer medium and integration point directly leads to a possible integration concept. On the process level, the category of a heat sink in combination with its conventional energy supply is decisive for the integration concept (Muster et al., 2015). Both direct and indirect integration configurations are applicable for integrating solar energy in the processes of existing industries.

Hot water or low-pressure steam at medium temperatures (less than 150 °C) can be used either for preheating of water (or other fluids) or for steam generation or by direct coupling of the solar system to an individual process processes such as washing, dyeing, etc. working at temperatures lower than that of the central steam-supply. The central system heat supply in most industries uses hot water or steam at a pressure matching to the highest temperature needed in the different processes. Typical maximum temperatures are about 180 – 260 °C (Schmitt, 2016).

In Figure 8 and Figure 9 two means (i.e. supply and process) for the direct integration of solar heating are shown. Figure 8a illustrates the solar array acting effectively as an inline heat exchanger preheating the water, or heating fluid, returning from a process before entering the heat source or boiler. In Figure 8b the flow can be diverted such that instead of using the heat source or boiler, the heat can be provided by the solar array (Epp et al., 2017; Schweiger et al., 2015).

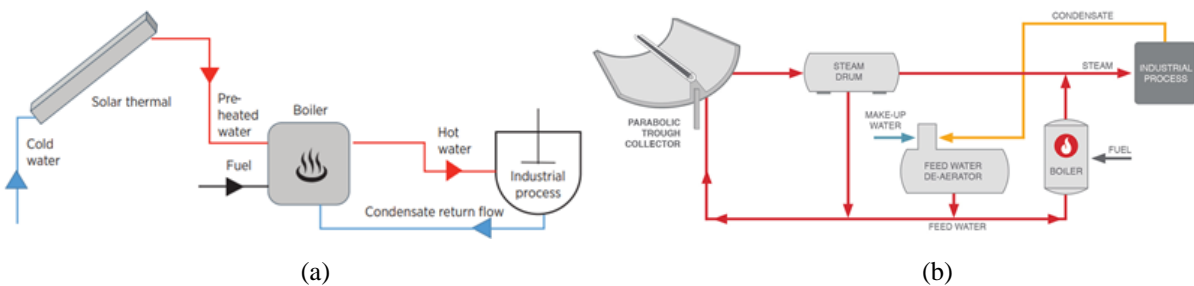


Fig. 8: Direct integration of heat from solar array (a) non-concentrating (b) concentrating

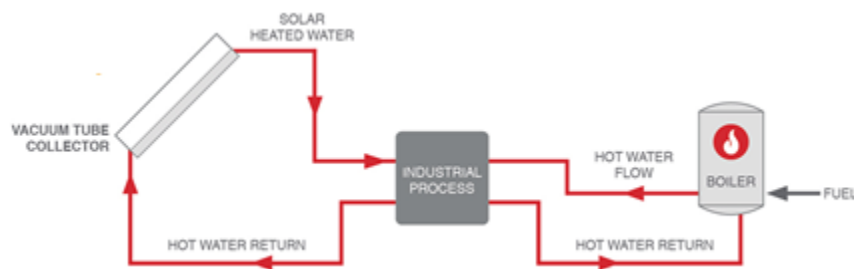


Fig. 9: Direct integration of solar heat into a process

There are some arguments for and against using direct integration as shown in Figure 8 and Figure 9. Typically the setup cost for these systems tends to be relatively low; however, they do require continuous control and by their

nature limit the size of the solar array to ensure that they do not provide energy at a higher temperature than is required by the process. Furthermore, these systems will only function during the day. These shortcomings can be overcome by the use of an indirect, storage-based system as shown in Figure 10. By installing an intermediate storage tank, heat can be added to the tank by the solar array and used as required. As such the system does not need to be continuously controlled as with a direct system and by adding a storage vessel heat can be stored and used during periods of low or no solar radiation. The main drawback of an indirect system is that they tend to have a higher initial cost and also a longer payback time (Anderson et al., 2008).

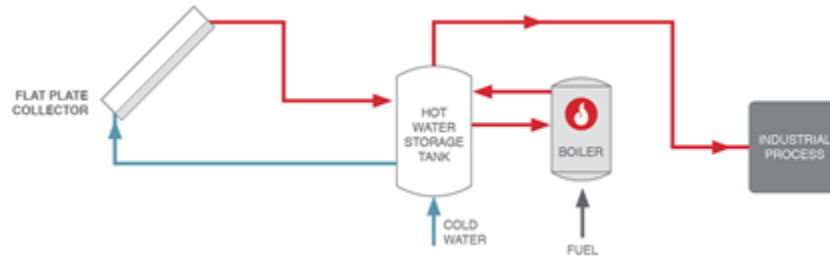


Fig. 10: Indirect heat integration from a solar array utilizing a storage system

One common method used in the determination of where heat sources should be integrated into a process is the pinch method. The pinch method uses combined heating and cooling curves as a graphic representation of heat and temperature demand in process industries. It shows the pinch point above which it is required for heat to be added and below which cooling is necessary. The minimum allowed temperature difference (ΔT_{\min}) between hot and cold streams limits the maximum heat that can be transferred in a heat exchanger (March, 1998; Brunner et al., 2008a).

Tab. 1: Typical ΔT_{\min} values for various processing industries

Industrial Sector	Experience ΔT_{\min} values (°C)
Oil Refining	20 - 40
Petrochemical	10 - 20
Chemical	10 - 20
Low-temperature processes	3 - 5

Table 1 confirms that the use of solar energy is ideally suited for low-temperature process application, as SHC systems would be able to deliver energy both above and below this point. The task is finding the optimal network of heat exchangers, external heaters, and external coolers for the capital and annual operating costs. In practical applications, $\Delta T_{\min} \neq 0$ is always valid. To cut the size of the heat exchanger into an acceptable level with a reasonable price, it is expected that there always exists a temperature difference.

3. System techno-economic modeling

As mentioned earlier, the choice of configuration or design of a solar system is typically based on the specific requirement of process heating and cooling. Another important consideration is the economic viability of the systems. Many studies involving new design and integration concepts of industrial solar systems have been reported in the literature. Analytical formulae to evaluate the annual useful energy supplied by these design and integration configurations have been developed. These formulae internalized the effect of system parameters or variables such as characteristics of solar collector, storage tank, heat exchanger, piping, flow rates, and user demand/load. This

approach can also be used for analysing system performance. These results are expected to be useful in performing sensitivity and optimization studies (Collares-Pereira et al., n.d.; Klein et al., 1976; Klein et al., 1979; Klein et al., 1975; Brunner et al., 2008b; Hess et al., 2010; Evans et al., 1997; Aidonis et al., 2005; Wallerand et al., 2016; Baniassadi et al., 2015; Walmsley et al., 2015; Baer et al., 1985; Gordon et al., 1982; Collares-Pereira, Gordon, Rabl, et al., 1984; Kulkarni et al., 2007; Kulkarni et al., 2008).

3.1. System yield assessment

The annual system yield is the most important value for assessing the economic feasibility of a solar thermal system besides system cost. This yield is influenced by many factors like temperature level, load profile, collector type, and location. There are many solar energy analyses in different papers and articles. A typical and simplified layout of solar thermal system with process steam production, primary and secondary circuits are made together combined, is shown in Figure 11 as a case study (Manfrida et al., 2009; Santbergen et al., 2010a; Gupta et al., 2010; Adnan M. Shariah et al., 1995; A.M. Shariah et al., 1999; Zondag, 2008; Santbergen et al., 2010b; Sarhaddi, Farahat, Ajam, & Behzadmehr, 2010; Zondag et al., 2003; Duffie, 2013; Sarhaddi, Farahat, Ajam, Behzadmehr, et al., 2010).

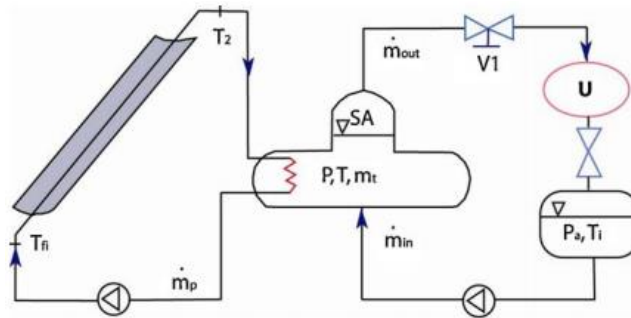


Fig. 11: Schematic diagram of a typical solar thermal system

In Figure 11, heat is transmitted from the primary circuit to the secondary circuit. The water vapor of the secondary circuit is stored in Steam Accumulator (SA). This model is assumed as a perfectly stirred adiabatic system, where heat is controlled by two limiting liquid levels with a liquid-vapor separation interface. Saturated steam is delivered to the thermal end-user or production plant (U) from the top of the SA at a mass flow rate of \dot{m}_{out} . Water comes into the SA at its bottom after leaving the condensate recovery tank of U with a mass flow rate of \dot{m}_{in} at sub-cooled conditions. When heat demand is increased by the user, the system valve V1 is opened to increase the system flow rate. During this transient period, the level in the SA falls and SA is depressurized to produce flash steam. To restrain this level from dropping below the minimum limit, more heat has to be provided by the solar collector or the condensate mass flow rate has to be raised. The former is dependent on weather conditions. On the other hand, if no heat is extracted from the SA ($\dot{m}_{out} = 0$), the continuous heat input from the primary circuit and the condensate inlet mass flow rate ($\dot{m}_{in} \neq 0$) leads to a rise in the SA filling level. Considering common conditions for steam production, a limitation for the SA filling level and operating pressures should be included.

The mass balance equation of the SA and the energy balance for the dynamic model of the SA, under the assumption of no thermal stratification, can be written as summarized in Table 2.

Tab. 2: The mass balance, energy balance, and system yield for the dynamic model of the SA

Mathematical Equation	Remark
$\dot{m}_{PT} = \frac{dM}{dt} = \dot{m}_{out} - \dot{m}_{in}$	\dot{m}_{PT} is mass flow rate exiting from the system accumulator (kg/s)
$\frac{du}{dt} = \dot{m}_{in}h_{in} - \dot{m}_{out}h_{out} + \dot{Q}_c$	\dot{m}_{out} is mass flow rate exiting from the SA (kg/s)
$\frac{du}{dt} = \dot{Q}_{SC} - (\dot{Q}_{PT} + \dot{Q}_{VAP}) + \dot{Q}_c$	\dot{m}_{in} is mass flow rate coming into the SA (kg/s)
	h_{in} and h_{out} are enthalpies of \dot{m}_{in} and \dot{m}_{out} (kJ/kg)

$\dot{Q}_{SC} = \dot{m}_{in}(h_{in} - h_s)$ $\dot{Q}_{PT} = (\dot{m}_{out} - \dot{m}_{in})h_s$ $\dot{Q}_{VAP} = \dot{m}_{out}(h_{out} - h_s)$ $\dot{Q}_c = \eta_c \dot{Q}_{sol} = \eta_c AI$ <p><i>Total Input Energy</i> $= IA$ $+ \text{pump work}$</p> $\eta_{sys} = \frac{\dot{Q}_{PT} + \dot{Q}_{VAP} + \dot{Q}_{SC}}{\text{Total Input Energy}}$ $SF = \frac{Q_{Sol}}{Q_U}$	<p>\dot{Q}_c is heat rate to heat transfer fluid in the solar collector (kW)</p> <p>\dot{Q}_{sol} is heat rate from the sun to the solar collector (kW)</p> <p>I is the solar irradiance, A is solar collector area (m²)</p> <p>\dot{Q}_{PT} is the energy required to compensate for any inlet or outlet flow imbalance (kW)</p> <p>\dot{Q}_{VAP} is the energy necessary for heating the required flow rate \dot{m}_{out} from saturated liquid to saturated steam condition (kW)</p> <p>\dot{Q}_{SC} is the heat supply for starting the sub-cooled water thickened coming from the user with a flow rate \dot{m}_{in} up to saturated liquid condition (kW)</p> <p>h_s enthalpy of saturated steam (kJ/kg)</p> <p>η_c and η_{sys} are a collector and system efficiency</p> <p>SF is a solar fraction</p> <p>Q_U is heat load (process demand)</p>
---	--

3.2. Economic considerations

The method of annual saving and payback period are mainly used to check the economic feasibility of systems (S. A. Kalogirou, 2004; TRNSYS 17, 2009; Florides et al., 2002; S. Kalogirou, 1996). The mathematical equations for economic considerations are summarized in Table 3.

Tab. 3: Economic parameters of the system

Mathematical Equation	Remark
$C = C_s + C_o$	C is the total annual cost or a purchase cost at the end of year N
$C_s = C_f + C_a A + C_v V$	C_s is investment costs of the solar system
$P = \frac{F}{(1 + d)^N}$	C_o is the operation cost (maintenance and parasitic costs are considered)
$F = C(1 + i)^{N-1}$	C_f is collector area independent cost
$PW_N = \frac{C(1 + i)^{N-1}}{(1 + d)^N}$	C_a is collector area dependent cost
$FS = 365 \frac{\text{days}}{\text{year}} \left(SF * \frac{Q_U}{\text{day}} * C_{FL} \right)$	A is collector area
$SS = FS + \text{Extra savings}$	C_v is the cost of storage per m ³ of storage volume
$PW_{LCS} = \sum_{N=1}^N \frac{SS}{(1 + d)^N}$	V is a storage volume
	P is the present value of money
	F is cash flow occurring N years from now
	d is a discount rate
	N is occurring years from now

$PP_{year} = \frac{\text{Capital Cost}}{\text{Annual Savings}}$	<p>i is annual inflation rate (the value of money is decreasing over time)</p> <p>PW is total present worth (or discounted cost)</p> <p>FS is fuel saving</p> <p>SF is the solar fraction</p> <p>C_{FL} is the cost rate of conventional fuel</p> <p>SS is solar saving</p> <p>LCS is life cycle saving</p> <p>PP is payback period</p>
---	---

4. Concluding remarks

Solar thermal energy is getting attention for its technical (energy collection efficiency and storage density) and economic advantages. Due to the huge technical potential for solar thermal integration, industrial heating and cooling processes can be considered as the potential application areas for solar thermal energy. There are different system design, configuration, and integration concepts of a solar thermal system for meeting the industrial process heating and cooling demand. The principles of the mathematical models for conceptual design, virtual prototyping, and economic analysis of the system are the key performance indicators. Hence, this paper has reviewed and discussed these aspects to briefly extract a systematic approach and guide to be adopted for industrial solar system development projects given the boundary conditions of solar resource and process demand profiles.

5. Acknowledgments

The authors would like to acknowledge the CoE in REWiSE project at Mekelle University for the fund to the Ph.D. study of the first author.

6. References

- Aidonis, A., Drosou, V., Mueller, T., Staudacher, L., Fernandez-Llebraz, F., Oikonomou, A., Spencer, S., & Sources, C. for R. E. (2005). *PROCESOL II - Solar thermal plants in industrial processes. Design and Maintenance Guidelines*. Retrieved from www.cres.gr
- Anderson, T. N., Duke, M., & Carson, J. K. (2008). Designing a low cost solar collector system for process industry applications. *SCENZ: Is There a Future for Chemical and Process Engineers in New Zealand?* Retrieved from <https://researchcommons.waikato.ac.nz/handle/10289/3626>
- Baer, D., Gordon, J. M., & Zarmi, Y. (1985). Design and optimization of solar steam systems for constant load applications. *Solar Energy*, 35(2), 137–151. doi: 10.1016/0038-092X(85)90004-0
- Baniassadi, A., Momen, M., & Amidpour, M. (2015). A new method for optimization of Solar Heat Integration and solar fraction targeting in low temperature process industries. *Energy*, 90, 1674–1681. doi: 10.1016/J.ENERGY.2015.06.128
- Brown, K. C. (1978). *Applications and Systems Studies for Solar Industrial Process Heat*. Retrieved from <https://www.nrel.gov/docs/legosti/old/481.pdf>
- Brunner, C., Slawitsch, B., Giannakopoulou, K., Schnitzer, H., & Research, J. (2008a). *Industrial Process Indicators and Heat Integration in Industries Institute of Sustainable Techniques and Systems IEA SHC Task 33 and SolarPACES Task IV: Solar Heat for Industrial Processes*. Retrieved from https://www.nachhaltigwirtschaften.at/resources/pdf/ieatask33_4_ipi.pdf

- Brunner, C., Slawitsch, B., Giannakopoulou, K., Schnitzer, H., & Research, J. (2008b). *Industrial Process Indicators and Heat Integration in Industries Institute of Sustainable Techniques and Systems IEA SHC Task 33 and SolarPACES Task IV: Solar Heat for Industrial Processes*. Retrieved from http://www.iea-shc.org/data/sites/1/publications/Process_Integration_Booklet.pdf
- Burckhart, H. J., Audinet, F., Gabassi, M.-L., & Martel, C. (2014). Application of a Novel, Vacuum-insulated Solar Collector for Heating and Cooling. *Energy Procedia*, 48, 790–795. doi: 10.1016/J.EGYPRO.2014.02.091
- Collares-Pereira, M., Gordon, J. M., Rabl, A., & Zarmi, Y. (1984). Design and optimization of solar industrial hot water systems with storage. *Solar Energy*, 32(1), 121–133. doi: 10.1016/0038-092X(84)90055-0
- Collares-Pereira, M., Gordon, J. M., & Zarmi, Y. (1984). Constant sensible heat load applications variable vs constant flow solar systems. *Solar Energy*, 32(1), 135–137. doi: 10.1016/0038-092X(84)90056-2
- Duffie, J. A. and W. A. B. (2013). *Solar Engineering of Thermal Processes* (Fourth Edi). USA: John Wiley & Sons.
- Epp, B., & Oropeza, M. (2017). Industrial Solar Heat Pays Off. *Solrico*, 18. Retrieved from https://www.international-climate-initiative.com/fileadmin/Dokumente/2017/170530_Brochure_EN_Solar_Payback_digital.pdf
- Evans, J. M., & de Schiller, S. (1997). Design of a solar plant for processing honey. *Renewable Energy*, 10(2–3), 225–229. doi: 10.1016/0960-1481(96)00069-9
- Florides, G. ., Kalogirou, S. ., Tassou, S. ., & Wrobel, L. . (2002). Modelling and simulation of an absorption solar cooling system for Cyprus. *Solar Energy*, 72(1), 43–51. doi: 10.1016/S0038-092X(01)00081-0
- Gebreyohannes, Y., Bayray, M., & Lauwaert, J. (2021). A Review on Solar Thermal Utilization for Industrial Heating and Cooling Processes: Global and Ethiopian Perspective. *Momona Ethiopian Journal of Science*, 12(2), 232–256. doi: 10.4314/mejs.v12i2.6
- Global Energy Systems Program. (2020). *Global Energy Storage Database | Energy Storage Systems*. U.S. Department Of Energy - DOE. Retrieved from <https://www.sandia.gov/ess-ssl/global-energy-storage-database-home/>
- Gordon, J. M., & Rabl, A. (1982). Design, analysis and optimization of solar industrial process heat plants without storage. *Solar Energy*, 28(6), 519–530. doi: 10.1016/0038-092X(82)90323-1
- Gupta, M. K., & Kaushik, S. C. (2010). Exergy analysis and investigation for various feed water heaters of direct steam generation solar–thermal power plant. *Renewable Energy*, 35(6), 1228–1235. doi: 10.1016/J.RENENE.2009.09.007
- Hess, S., & Oliva, A. (2010). *Guide to Solar Thermal System Design for Selected Industrial Processes*. Retrieved from www.solar-process-heat.eu
- Justus, D., & Philibert, C. (2005). *International energy technology collaboration and climate change mitigation: synthesis report*. Retrieved from <http://www.oecd.org/env/cc/>
- Kalogirou, S. (1996). Economic analysis of solar energy systems using spreadsheets. *Renewable Energy*, 9(1–4), 1303–1307. doi: 10.1016/0960-1481(96)88516-8
- Kalogirou, S. A. (2004). Solar thermal collectors and applications. *Progress in Energy and Combustion Science*, 30(3), 231–295. doi: 10.1016/J.PECS.2004.02.001
- Klein, S. A., & Beckman, W. A. (1979). A general design method for closed-loop solar energy systems. *Solar Energy*, 22(3), 269–282. doi: 10.1016/0038-092X(79)90142-7
- Klein, S. A., Beckman, W. A., & Duffie, J. A. (1976). A design procedure for solar heating systems. *Solar Energy*, 18(2), 113–127. doi: 10.1016/0038-092X(76)90044-X
- Klein, S. A., Cooper, P. I., Freeman, T. L., Beekman, D. M., Beckman, W. A., & Duffie, J. A. (1975). A method of simulation of solar processes and its application. *Solar Energy*, 17(1), 29–37. doi: 10.1016/0038-092X(75)90014-6

- Kulkarni, G. N., Kedare, S. B., & Bandyopadhyay, S. (2007). Determination of design space and optimization of solar water heating systems. *Solar Energy*, 81(8), 958–968. doi: 10.1016/J.SOLENER.2006.12.003
- Kulkarni, G. N., Kedare, S. B., & Bandyopadhyay, S. (2008). Design of solar thermal systems utilizing pressurized hot water storage for industrial applications. *Solar Energy*, 82(8), 686–699. doi: 10.1016/J.SOLENER.2008.02.011
- Kutscher, C. F. (1983). *A Detailed Design Procedure for Solar Industrial Process Heat Systems: Overview*. Retrieved from <https://www.nrel.gov/docs/legosti/old/1830.pdf>
- Lund, S., & Struckmann, F. (2008). *Analysis of a Flat-plate Solar Collector*. Retrieved from http://www.ht.energy.lth.se/fileadmin/ht/Kurser/MVK160/Project_08/Fabio.pdf
- Manfrida, G., Tempesti, D., Baldini, A., Manfrida, G., & Tempesti, D. (2009). Model of a Solar Collector/Storage System for Industrial Thermal Applications Model of a Solar Collector/Storage System for Industrial Thermal Applications*. *Article in International Journal of Thermodynamics*, 12(2), 83–88. doi: 10.5541/ijot.242
- March, L. (1998). *Introduction to Pinch Technology*. Retrieved from www.linnhoffmarch.com
- Muster, Hassine, Helmke, Heß, Krummenacher, Schmitt, & Schnitzer. (2015). *IEA SHC Task 49 - Solar process heat for production and advanced applications* (Issue February). Retrieved from http://task49.iea-shc.org/Data/Sites/7/150218_iea-task-49_d_b2_integration_guideline-final.pdf
- Penn State University. (n.d.). *EME 811: Solar Thermal Energy for Utilities and Industry*. Retrieved from <https://www.e-education.psu.edu/eme811/node/3>
- Prakash, J. (1994). Transient analysis of a photovoltaic-thermal solar collector for co-generation of electricity and hot air/water. *Energy Conversion and Management*, 35(11), 967–972. doi: 10.1016/0196-8904(94)90027-2
- Santbergen, R., Rindt, C. C. M., Zondag, H. A., & van Zolingen, R. J. C. (2010a). Detailed analysis of the energy yield of systems with covered sheet-and-tube PVT collectors. *Solar Energy*, 84(5), 867–878. doi: 10.1016/J.SOLENER.2010.02.014
- Santbergen, R., Rindt, C. C. M., Zondag, H. A., & van Zolingen, R. J. C. (2010b). Detailed analysis of the energy yield of systems with covered sheet-and-tube PVT collectors. *Solar Energy*, 84(5), 867–878. doi: 10.1016/J.SOLENER.2010.02.014
- Sarhaddi, F., Farahat, S., Ajam, H., & Behzadmehr, A. (2010). Exergetic performance assessment of a solar photovoltaic thermal (PV/T) air collector. *Energy and Buildings*, 42(11), 2184–2199. doi: 10.1016/j.enbuild.2010.07.011
- Sarhaddi, F., Farahat, S., Ajam, H., Behzadmehr, A., & Mahdavi Adeli, M. (2010). An improved thermal and electrical model for a solar photovoltaic thermal (PV/T) air collector. *Applied Energy*, 87(7), 2328–2339. doi: 10.1016/j.apenergy.2010.01.001
- Schmitt, B. (2016). Classification of Industrial Heat Consumers for Integration of Solar Heat. *Energy Procedia*, 91, 650–660. doi: 10.1016/J.EGYPRO.2016.06.225
- Schweiger, H., Mendes, J. F., Carvalho, M. J., Hennecke, K., & Krüger, D. (2015). Solar heat for industrial processes. In *Advances in Solar Energy: An Annual Review of Research and Development in Renewable Energy Technologies* (Vol. 17, pp. 216–260). doi: 10.4324/9781315793221-14
- Shariah, A.M., Rousan, A., Rousan, K. K., & Ahmad, A. A. (1999). Effect of thermal conductivity of absorber plate on the performance of a solar water heater. *Applied Thermal Engineering*, 19(7), 733–741. doi: 10.1016/S1359-4311(98)00086-6
- Shariah, Adnan M., & Ecevit, A. (1995). Effect of hot water load temperature on the performance of a thermosyphon solar water heater with auxiliary electric heater. *Energy Conversion and Management*, 36(5), 289–296. doi: 10.1016/0196-8904(95)98894-S
- Sharma, A. K., Sharma, C., Mullick, S. C., & Kandpal, T. C. (2017). Solar industrial process heating: A review. *Renewable and Sustainable Energy Reviews*, 78, 124–137. doi: 10.1016/J.RSER.2017.04.079

TRNSYS 17. (2009). Retrieved from <http://sel.me.wisc.edu/trnsys>

Uppal, A., & Kesari, J. P. (2015). Solar Industrial Process Heat in Indian Automobile Industry. *International Journal of Latest Technology in Engineering, Management & Applied Science-IJLTEMAS*, 4(10), 117–123. Retrieved from www.ijltemas.in

Wallerand, A. S., Selviaridis, A., Ashouri, A., & Maréchal, F. (2016). Targeting Optimal Design and Operation of Solar Heated Industrial Processes: A MILP Formulation. *Energy Procedia*, 91, 668–680. doi: 10.1016/J.EGYPRO.2016.06.229

Walmsley, T. G., Walmsley, M. R. W., Tarighaleslami, A. H., Atkins, M. J., & Neale, J. R. (2015). Integration options for solar thermal with low temperature industrial heat recovery loops. *Energy*, 90, 113–121. doi: 10.1016/J.ENERGY.2015.05.080

Zondag, H. A. (2008). Flat-plate PV-Thermal collectors and systems: A review. *Renewable and Sustainable Energy Reviews*, 12(4), 891–959. doi: 10.1016/J.RSER.2005.12.012

Zondag, H. A., de Vries, D. W., van Helden, W. G. J., van Zolingen, R. J. C., & van Steenhoven, A. A. (2003). The yield of different combined PV-thermal collector designs. *Solar Energy*, 74(3), 253–269. doi: 10.1016/S0038-092X(03)00121-X

Infinite-NTU Modeling for Studying Charging Cycle of Packed-Bed Solar Thermal Energy Storage

Yacob G. Hiben^{1*}

¹Thermal and Energy Systems Chair, School of Mechanical and Industrial Engineering, Mekelle University, Endayesus Campus, Mekelle, Ethiopia

*yacob.gebreyohannes@mu.edu.et

Abstract

Thermal Energy Storage (TES) is a key component for solar thermal applications to bridge the gap between the demand for thermal energy and the supply of solar energy, whose availability depends on the time of day and season. Thus, cost-effective packed-bed thermal containers filled with a solid storage medium have been proposed for high-temperature sensible heat storage as materials are abundant and relatively cheap. Thus, it is necessary to investigate their performance and temperature profiles during the charge-discharge cycle. Several models are available for this purpose. Typically, the more detailed a model, the greater the computational effort required to solve it, and hence a time-efficient model is needed to prevent excessively long computation times for long-term analysis. At the more basic level, the common Hughes E-NTU model and the less realistic simplified Infinite-NTU model are very important for their less time and computational effort. In this paper, the appropriateness of employing the Infinite-NTU model was evaluated to investigate the performance of a typical and scalable rock-bed TES as a case study. The results presented provide a methodology to quickly test the validity of the model and predict the temperature profile for the case under study. Accordingly, such simple charge-discharge cycle thermal performance predictions are important to plan, design, and rapidly deploy a reliable and economical solar thermal system for the supply of valuable heat to high-temperature demanding applications of power generation and industrial processes as part of a rapid shift towards non-polluting renewable energy.

Keywords: Solar Thermal, TES, Packed-bed, NTU model, Temperature profile

1. Introduction

Basic configurations of solar thermal systems consist of solar thermal collectors, heat transfer fluid, interconnecting pipes, pumps, heat exchangers, and thermal storage and/or auxiliary backup. Storage of solar heat allows buffering mismatches between the heat demand and the availability of the intermittent supply of solar resources. Due to its continuous high-temperature demand, thermal energy storage (TES) is a key component for high-temperature solar thermal applications such as concentrating solar power plants (CSP) and energy-intensive industrial processes. The decision for thermal storage installation depends on the cost/benefit ratio as well as on the control and stagnation concept of a solar system.

TES has a high energy storage density on average up to 10, 000 kW for about 6 hours (Global Energy Systems Program, 2020). TES systems are classified as sensible heat storage, latent heat storage, and thermochemical storage (Kuravi et al., 2013). Traditional and current plants have employed sensible heat systems to store their excess energy. In sensible heat storage, the heat energy is stored as internal energy depending on temperature changes in the storage material. In this scenario, a media (solid or liquid) may store energy by raising its temperature in line with its heat capacity. Among the types of sensible heat storage, hot water (<100 °C) and pressurized water systems (>100 °C) are considered the most common commercial technology, due to the cost, simplicity, and high specific heat of water relative to a majority of other storage media (Furbo, 2015; Kulkarni et al., 2008). The costs of unpressurized hot water storage range on the order of thousands of dollars depending on size, with a 0.5 m³ tank costing roughly \$1300 and a 200 m³ tank \$60,000 (USD in 2002), while costs of pressurized systems are generally higher (Wallerand et al., 2018; Heliodyne. Inc, n.d.).

Although molten salt TES is well-known as the commercial state of the art for high-temperature applications, it is fairly expensive and therefore cost-effective systems are desirable (Kolb et al., 2012). Currently, molten salt two-tank systems limited by operational temperatures (< 600°C) and high costs (> \$35/kWh) are employed. To reduce costs and operate at higher temperatures, two other options have been investigated by (Jacob et al., 2017): a packed bed of rocks and a packed bed of encapsulated phase change material (EPCM). Both of these options have the potential to replace the current two-tank molten salt systems and provide low-cost future storage options.

Packed-bed thermal reservoirs filled with a solid storage medium such as gravel or pebbles are key options for sensible heat storage technologies, as materials are abundant and relatively cheap (McTigue et al., 2018). Packed-beds incorporating air as the heat transfer fluid have been suggested as a more cost-effective approach due to the low-cost of rock and ample availability of air (Zanganeh et al., 2012). Concrete and cast ceramics have also been studied as sensible heat thermal storage materials due to their low-costs, good thermal conductivities, and moderate specific heat capacity. In concrete TES, the high thermal conductivity enhances the heat transfer dynamics in the system and high heat capacity is desirable since it reduces the storage volume. Composite materials such as fiberglass reinforced epoxy concretes have specific heat values close to 1 kJ/kg K (Zhang et al., 2016; Hoivik et al., 2017).

Direct cost estimates of several TES systems were investigated by (Jacob et al., 2017). This comprises the cost of the tank, filler material(s) and heat transfer fluid (HTF), encapsulation (if required), instrumentation and control, and the piping (ductwork) and valves. The investigated systems include traditional two-tank molten salt system (2-Tank), EPCM system utilizing one PCM (1EPCM), cascaded EPCM system utilizing 2 PCMs (2EPCM), quartz/rock thermocline system (ThermoQS), and thermocline system utilizing a geopolymer (ThermoG). The costs of these systems were estimated over a range of temperature differences ($\Delta T=100-500^{\circ}\text{C}$) and a variety of HTFs (molten salt and air). The results of this are presented in Figure 1.

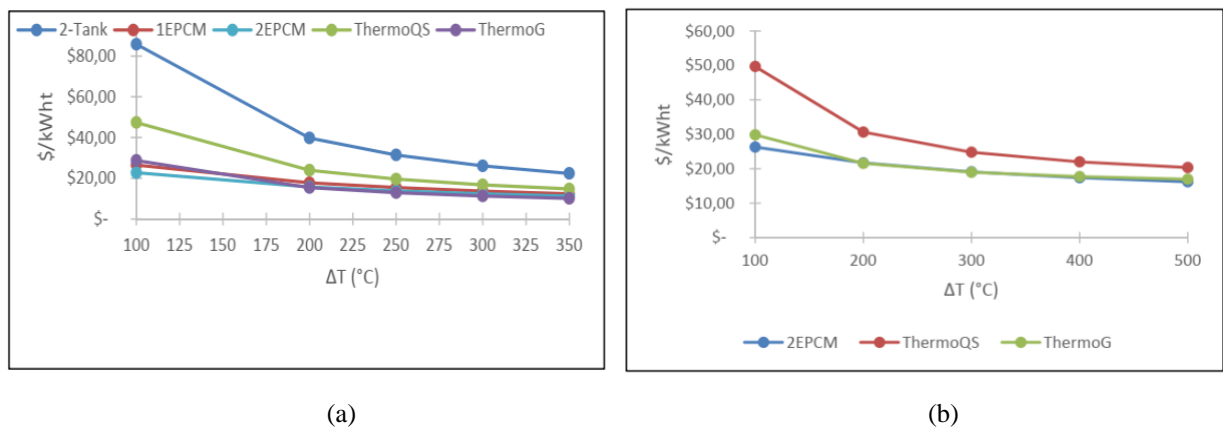


Fig. 1: Comparison of TES costs with (a) Molten Salt HTF, (b) Air HTF

Figure 1(a) shows that all the systems investigated resulted in a lower cost than the traditional two-tank molten salt system for all temperature differences. It can also be seen that for a ΔT of 300 $^{\circ}\text{C}$, the EPCM systems, thermocline system with quartz/rocks, and the thermocline with geopolymer results in 50%, 35%, and 60% savings, respectively. As expected the cascaded system resulted in lower cost estimates than the one PCM system for all temperature differences. Figure 1(b) shows a comparison between the systems with air as the HTF. Initially the cascaded system results in a lower cost but is more expensive when $\Delta T > 200^{\circ}\text{C}$. The thermocline system with quartz/rocks are approximately the same prices as the cascaded EPCM system when $\Delta T > 300^{\circ}\text{C}$. For all temperature differences the geopolymer thermocline system resulted in a lower cost than the quartz/rock system due to the higher heat capacity of the geopolymer filler.

To evaluate the viability of rock-bed TES systems, it is necessary to study their charge-discharge thermal performance and the associated effect on power generation. Essentially, this requires the ability to predict the rock and air temperature profiles through the bed during a charge-discharge cycle. Different models are available for this purpose, including, the more detailed models such as the “Continuous Solid Phase” model whose governing equations account for thermal conduction through the rock and air (Wakao et al., 1979). Usually, the more detailed models require greater computational effort to be solved. This is infrequently problematic for the simulation of a few charge-discharge cycles; however, for long-term analysis such as in the context of annual CSP plant performance simulation, a time-efficient model is needed to avoid excessively long computation times. This is particularly the case when conducting plant-level theoretical design or optimization studies. There are also models at the more basic level such as the popular Hughes E-NTU (Effectiveness – Number of Transfer Units) model and the simplified Infinite-NTU model (Hughes et al., 1976; Duffie, 2013). Unlike the E-NTU model, the Infinite-NTU model assumes an infinite heat transfer coefficient between the solid bed and heat transfer fluid, which implies comparable solid bed and heat transfer fluid temperature profiles.

This paper, therefore, evaluates the accuracy and computational efficiency of the Infinite-NTU model when simulating the performance of a typical and scalable rock-bed TES system as a case study. Based on its

appropriateness, the Infinite-NTU model is employed for the simulation and evaluation of the rock-bed TES system with the given parameters and characteristics. For every hour of operation over charge cycles, the heat transfer fluid (air) and rock-bed temperature profile predictions were achieved for the ten segments of the storage system considered. Thus, such simple charge-discharge cycle thermal performance predictions are found important to quickly plan and design a reliable and economical TES system for a rapid shift towards non-polluting renewable energy systems.

2. Materials and Methods

2.1. Basic Theory

The assumptions underlying the E-NTU model are those of the Schumann model (Schumann, 1929). Flow is assumed to be one dimensional with a uniform axial flow speed, there is no thermal loss from the bed walls, radiant and conductive heat transfer through the bed is negligible, the internal thermal resistance of each solid particle (rock) can be neglected, and the thermal capacitance term of the air can be neglected. These assumptions give rise to the Schumann equations summarized in Table 1.

Tab. 1: The Schumann equations for the fluid and solid phases

The Schumann Equations	Remark
$\frac{\partial T_f}{\partial z} = \frac{h_v A_{cs}}{\dot{m} C_{pf}} (T_s - T_f)$	T_f – Fluid Temperature (air) [$^{\circ}$ C or K]
$h_v = 650 \left(\frac{G_f}{D} \right)^{0.7}$	z – Axial coordinate in the flow direction [m]
$G_f = V_f \rho_f$	h_v – Volumetric heat transfer coefficient [$\text{W}/\text{m}^3\text{-K}$]
$NTU = \frac{h_v A_{cs} L}{\dot{m} C_{pf}} = \frac{h_v L}{G_f C_{pf}}$	A_{cs} – Cross-section area [m^2]
$\frac{\partial T_f}{\partial z} = \frac{NTU}{L} (T_s - T_f)$	m – Mass flow rate [kg/s]
$\frac{\partial T_s}{\partial t} = \frac{h_v}{(1 - \varepsilon) \rho_s C_s} (T_f - T_s)$	C_{pf} – Fluid isobaric specific heat capacity (air) [J/kg-K]
$\tau = \frac{\rho_s (1 - \varepsilon) A_{cs} L C_s}{\dot{m} C_{pf}}$	T_s – Solid Temperature (rock) [$^{\circ}$ C or K]
$\frac{\partial T_s}{\partial t} = \frac{NTU}{\tau} (T_f - T_s)$	h_v – Volumetric heat transfer coefficient [$\text{W}/\text{m}^3\text{-K}$]
	G_f – Fluid mass flux/velocity (air) [kg/s- m^2]
	D – Equivalent particle diameter [m]
	V_f – Fluid velocity [m/s]
	ρ_f – Fluid density [kg/ m^3]
	NTU – Number of Transfer Unit [-]
	L – Bed length [m]
	t – Time [s]
	ε – Bed porosity / Void fraction [-]
	ρ_s – Solid Density [kg/ m^3]
	C_s – Solid specific heat capacity [J/kg-K]
	τ – Thermal time constant [-]

2.2. The E-NTU Model

The Hughes E-NTU model relies on a bed segment temperature approximation to formulate the numerical solution of discretized forms of the Schumann equations for the fluid and solid phases. The rock temperature is assumed to be constant in a given segment, while the air temperature has an exponential profile. One of the different numerical integration approaches may be used to solve the equations in Table 2. Duffie and Beckman make use of Euler-stepping (Hughes et al., 1976; Duffie, 2013).

Tab. 2: The E-NTU equations for the fluid and solid phases

The E-NTU Model	Remark
$T_{fm+1} = T_{fm} - (T_{fm} - T_{sm}) \left(1 - e^{-NTU \left(\frac{\Delta z}{L} \right)} \right)$	T_{fm+1} - The air temperature at the next segment
$\frac{dT_s}{dt} = \frac{L}{\Delta z \tau} (T_{fm} - T_{sm}) \left(1 - e^{-NTU \left(\frac{\Delta z}{L} \right)} \right)$	m – Node number [-]
	Δz – Bed segment length [m]

2.3. The Infinite-NTU Model

The Hughes et al. Infinite-NTU model relies on the assumption that the fluid and solid phases are in local thermal equilibrium all over the packed bed due to the sufficiently high convective heat transfer between the phases. This reduces the model approximation to a single governing equation given in Table 3. The outlet bed temperature is the same as the exit air temperature. The inlet and outlet temperatures of the fluid (air) are considered boundary conditions. Simple discretization and numerical integration of this equation demand significantly lower computational effort in comparison to the E-NTU model (Hughes et al., 1976; Duffie, 2013).

In this regard, Duffie and Beckman state that for the appropriateness of employing the Infinite-NTU model, the Biot number (Bi) is evaluated according to a general correlation in Table 3. The Bi number is recommended to be less than 0.1. They also state that for long-term performance predictions of Infinite-NTU as those obtained by assuming a finite-NTU, values of NTU higher than 25 are recommended. They also noted that even for NTU values as low as 10, the infinite-NTU model should still provide reasonable long-term performance predictions (Hughes et al., 1976; Duffie, 2013).

Tab. 2: The E-NTU equations for the fluid and solid phases

The Infinite NTU Model	Remark
$\frac{dT_b}{dt} = - \frac{\dot{m}C_{pf}}{(1 - \varepsilon)A_{cs}\rho_s C_s} \frac{\partial T}{\partial z}$	T_b – Bed Temperature [⁰ C or K]
$T_{bm\ new} = T_{bm\ prev} - \frac{\Delta\theta L}{2\Delta Z} (T_{bm\ prev} - T_{bm-1\ new})$	$\Delta\theta$ – Dimensionless time [-]
$\Delta\theta = \frac{\Delta t}{\tau}$	Bi – Biot number [-]
$Bi = \frac{hR}{k}$	k – Thermal conductivity [W/m-K]
$h = \frac{h_v}{\text{surface area of pebbles per unit volume}}$	h – Area heat transfer coefficient [W/m ² -K]
$R = \frac{D}{2}$	R – Equivalent radius of pebble [m]

2.4. Case Study Design Specifications and Assumptions

A typical rock-bed TES (Figure 2) characterized by its 1.80 m length in flow direction and 14.8 m² cross-sectional area was evaluated as a case study (Duffie, 2013). The rock-bed TES was modeled considering ten segments at a distance of 0.18 m each.

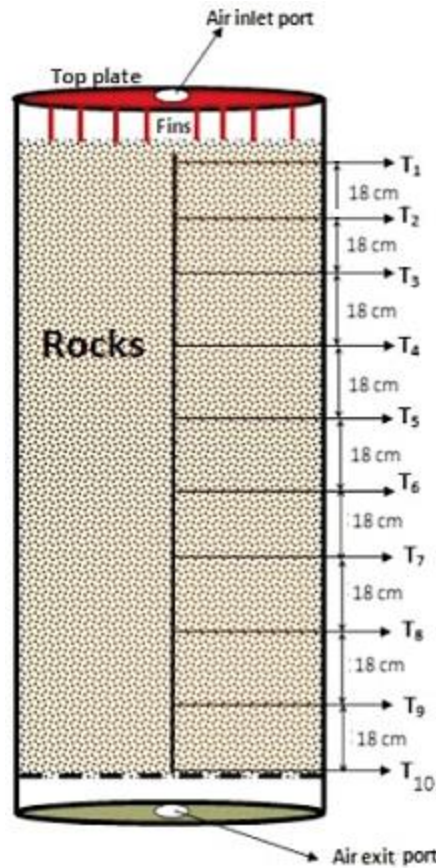


Fig. 2: A schematic of the rock bed system with the top (hot) plate installed, divided into sections for modeling

For the appropriateness and forecast study, properties of air and rock summarized in Table 4 and Table 5 were applied. All properties of air were evaluated at 20°C since using a low temperature to evaluate air properties will be more severe for the evaluation of Bi and NTU criteria than if a high temperature. The bed was considered initially at 25°C and the air inlet temperature is kept constant at 300°C. To maintain a constant air temperature at the bed inlet, the mass flow rate of air through the open volumetric receiver, and hence the bed, must be modulated. In the Infinite-NTU simulations, the beds are treated as being perfectly insulated.

Tab. 4: Properties of Air

Parameter	Value
Velocity	0.053 m/s
Density	1.204 kg/m ³
Heat Capacity	1010 J/kg°C

Tab. 5: Properties of rock

Parameter	Value
The equivalent diameter of the rock	12.5 mm
Density of rock	0.35
Void Fraction	1350 kg/m ³
Specific heat of rock	0.9 kJ/kg K
Thermal conductivity of rock	0.85w/m°C
The surface area of rock per unit volume	255m ² /m ³

A non-zero mass flow rate should be detected when the bed enters charge mode with the charging airflow. Subsequently, the bed should enter discharge mode, with the discharging airflow temperature and mass flow rate. Discharging ceases once the air temperature at the bed outlet falls below the required limit, following which the bed may enter idle mode, remaining there until the next charge cycle begins (Figure 3).

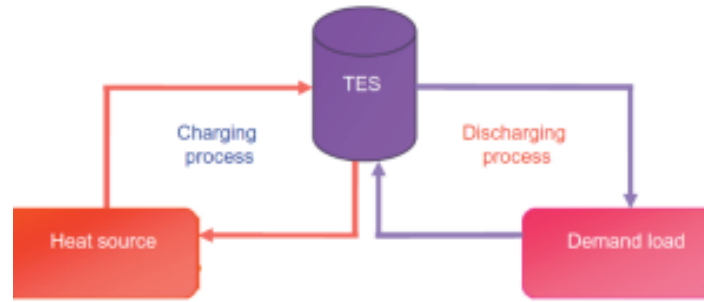


Fig. 3: Schematic of TES integration and operation

2.5. Infinite-NTU Prediction

There is an analytical solution for the Infinite-NTU prediction, but a numerical solution is generally more versatile. In the numerical solution of the Infinite-NTU equation, grid independence in both space and time should be demonstrated for discretization error to be minimized. For the rock-bed TES under consideration, the bed temperature was computed every hour at ten positions 0.18 m each from inlet to outlet. The Infinite-NTU model simulation was undertaken using the computational spreadsheet Excel.

3. Results and Discussion

3.1. The Bi number and NTU

Since the calculated Bi number (0.0587) is less than 0.1, the temperature gradient in the rock is not significant and thus E-NTU is nearly the same as Infinite-NTU. The NTU (68.15) is much larger than 10, this gives the same long-term performance predictions of the Infinite-NTU model essentially as those obtained by assuming a finite-NTU. Therefore, the Infinite-NTU model is found to be appropriate to predict the air outlet temperature and bed temperature at different nodes.

3.2. The Temperature Profiles

The convergence of the Infinite-NTU numerical solution for the charging operation is shown in Figure 4, which displays a very important attribute associated with the Infinite-NTU model. The figure illustrates the bed inlet starts charging in less than one hour. The number of hours that the bed operates in charging mode is around 22 hours.

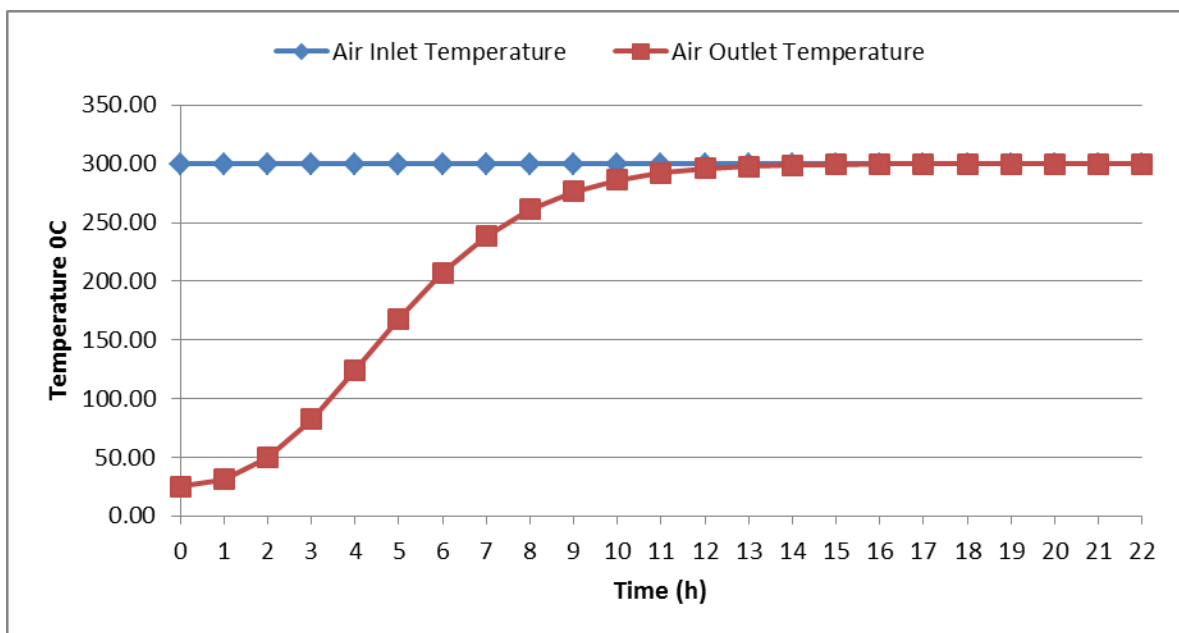


Fig. 4: Inlet and outlet air temperature for every hour operation

Figure 5 illustrates the lag between the bed inlet and outlet during charging operation. The number of hours that the bed lags to fully charge the bed outlet is around 12 hours from the fully charged bed inlet.

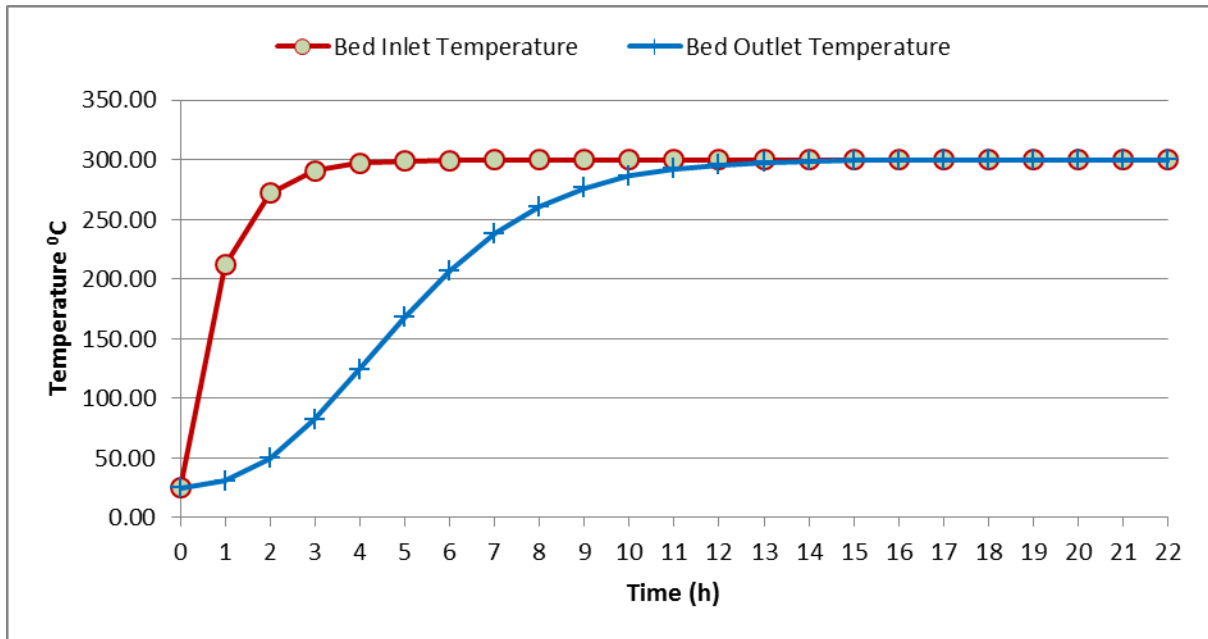


Fig. 5: Inlet and outlet bed temperature for every hour operation

Figure 6 appears to show the ten nodes prediction of the Infinite-NTU numerical solution at every hour. The results also suggest the ten nodes achieve the inlet air temperature in 10, 12, 14, 15, 16, 17, 19, 20, 21, and 22 hours respectively. The charging rate is low when the change in temperature between the supply air and the bed segment becomes smaller.

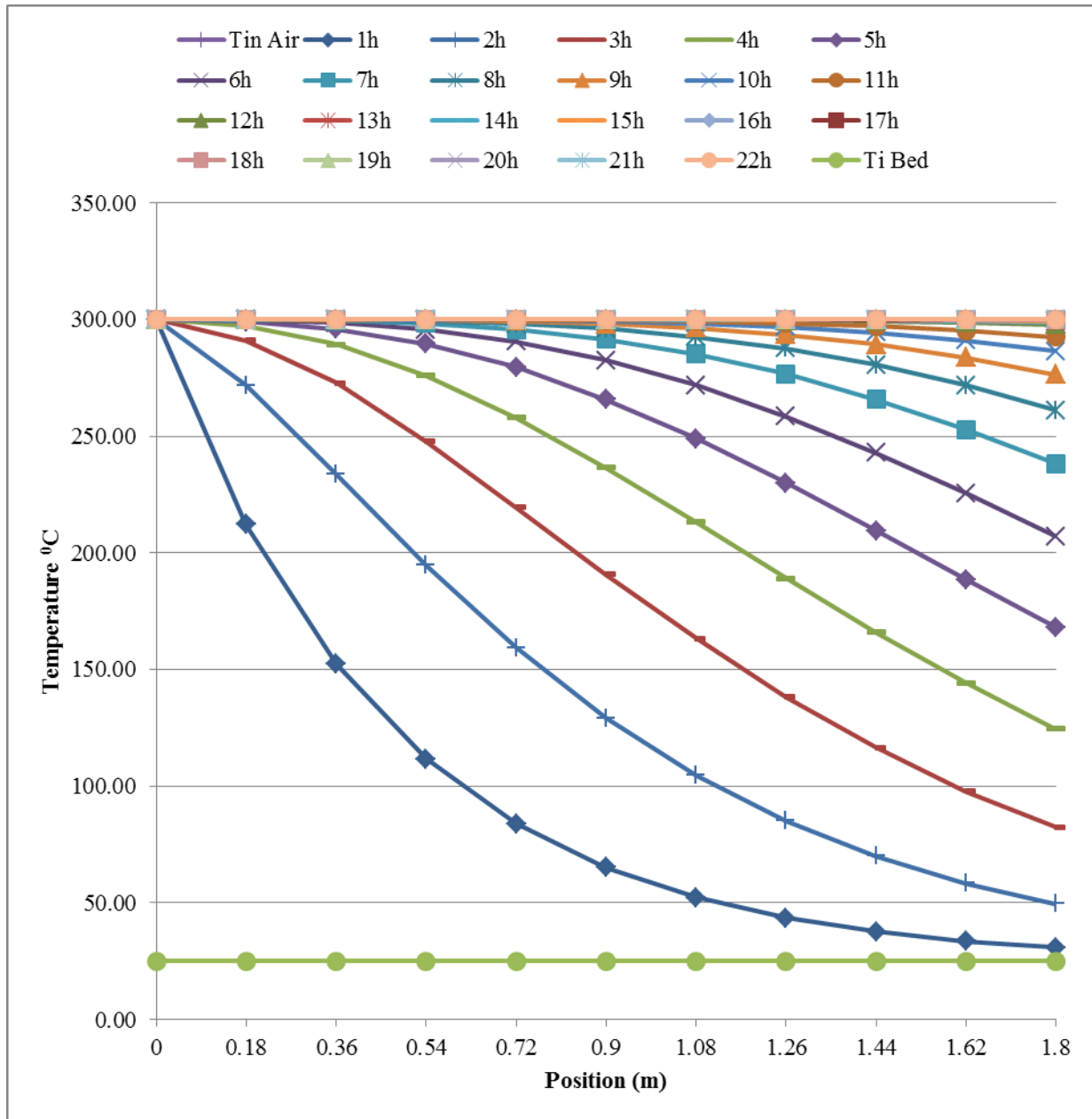


Fig. 6: Bed temperature prediction at the start and end of charging

4. Conclusions

Cost-effective packed-bed thermal containers filled with a solid storage medium have been proposed for sensible heat storage as materials are abundant and relatively cheap. Since it is essentially necessary to assess and predict their temperature profiles during the charge-discharge cycle, a time-efficient and less costly model is necessary. Thus, the simplified Infinite-NTU model is found to be very important. In this paper, the suitability of this less realistic model for a typical and scalable rock-bed TES using air as a charging medium was assessed first for the case study. With the given parameters, numerical solutions to this model were computed to obtain the temperatures of the air and the bed at different times and segments of the bed during charge cycles. The results suggest that the Infinite-NTU model can be appropriate in predicting the air and bed temperatures. The air outlet temperature exponentially reached the inlet temperature during the charging cycle operation. These predictions together with the material properties of the storage medium are very important to determine the design and operational characteristics as well as the performance of the rock-bed thermal energy storage system including the system power capacity, energy storage duration, and energy storage density. Such a reliable knowledge of the TES charge-discharge cycle temperature profile predictions is pre-conditions to plan, design, and rapidly deploy a reliable and economical solar thermal system for high-temperature applications of power generation and supply of valuable heat for high temperature demanding industrial processes like steel, brick, plastic, etc manufacturers. This is also very important to rapidly convert the use of fossil fuels to non-polluting renewable energy sources.

5. Acknowledgments

The author would like to acknowledge funding from CoE in REWiSE project at Mekelle University for the Ph.D. study leading to this article.

6. References

- Duffie, J. A. and W. A. B. (2013). *Solar Engineering of Thermal Processes* (Fourth Edn). USA: John Wiley & Sons.
- Furbo, S. (2015). Using water for heat storage in thermal energy storage (TES) systems. In *Advances in Thermal Energy Storage Systems: Methods and Applications* (pp. 31–47). Elsevier Inc. doi: 10.1533/9781782420965.1.31
- Global Energy Systems Program. (2020). *Global Energy Storage Database | Energy Storage Systems*. U.S. Department Of Energy - DOE. Retrieved from <https://www.sandia.gov/ess-ssl/global-energy-storage-database-home/>
- Heliodyne. Inc. (n.d.). *Heliodyne Commercial - Case Studies PDF Files*. Retrieved from http://www.heliodyne.com/commercial/case_studies/Lucky_Lab_press.pdf
- Hoivik, N., Greiner, C., Tirado, E. B., Barragan, J., Bergan, P., Skeie, G., Blanco, P., & Calvet, N. (2017). Demonstration of EnergyNest thermal energy storage (TES) technology. *AIP Conference Proceedings*, 1850(1), 80011. doi: 10.1063/1.4984432
- Hughes, P. J., Klein, S. A., & Close, D. J. (1976). Packed bed thermal storage models for solar air heating and cooling systems. *ATJHT*, 98, 336–338. Retrieved from <https://ui.adsabs.harvard.edu/abs/1976ATJHT..98..336H/abstract>
- Jacob, R., Saman, W., & Bruno, F. (2017). Capital cost expenditure of high temperature latent and sensible thermal energy storage systems. *AIP Conference Proceedings*, 1850. doi: 10.1063/1.4984433
- Kolb, G. J., Ho, C. K., Mancini, T. R., & Gary, J. A. (2012). Power tower technology roadmap and cost reduction plan. In *Concentrating Solar Power: Data and Directions for an Emerging Solar Technology* (pp. 223–250). Retrieved from <https://www.osti.gov/biblio/1011644>
- Kulkarni, G. N., Kedare, S. B., & Bandyopadhyay, S. (2008). Design of solar thermal systems utilizing pressurized hot water storage for industrial applications. *Solar Energy*, 82(8), 686–699. doi: 10.1016/j.solener.2008.02.011
- Kuravi, S., Trahan, J., Goswami, D. Y., Rahman, M. M., & Stefanakos, E. K. (2013). Thermal energy storage technologies and systems for concentrating solar power plants. In *Progress in Energy and Combustion Science* (Vol. 39, Issue 4, pp. 285–319). Pergamon. doi: 10.1016/j.pecs.2013.02.001
- McTigue, J. D., & White, A. J. (2018). A comparison of radial-flow and axial-flow packed beds for thermal energy storage. *Applied Energy*, 227, 533–541. doi: 10.1016/j.apenergy.2017.08.179
- Schumann, T. E. W. (1929). Heat transfer: A liquid flowing through a porous prism. *Journal of the Franklin Institute*, 208(3), 405–416. doi: 10.1016/S0016-0032(29)91186-8
- Wakao, N., Kaguei, S., & Funazkri, T. (1979). Effect of fluid dispersion coefficients on particle-to-fluid heat transfer coefficients in packed beds. Correlation of nusselt numbers. *Chemical Engineering Science*, 34(3), 325–336. doi: 10.1016/0009-2509(79)85064-2
- Wallerand, A. S., Kermani, M., Voillat, R., Kantor, I., & Maréchal, F. (2018). Optimal design of solar-assisted industrial processes considering heat pumping: Case study of a dairy. *Renewable Energy*, 128, 565–585. doi: 10.1016/j.renene.2017.07.027
- Zanganeh, G., Pedretti, A., Zavattoni, S., Barbato, M., & Steinfeld, A. (2012). Packed-bed thermal storage for concentrated solar power - Pilot-scale demonstration and industrial-scale design. *Solar Energy*, 86(10), 3084–3098. doi: 10.1016/j.solener.2012.07.019
- Zhang, H., Baeyens, J., Cáceres, G., Degrève, J., & Lv, Y. (2016). Thermal energy storage: Recent developments and practical aspects. In *Progress in Energy and Combustion Science* (Vol. 53, pp. 1–40). Elsevier Ltd. doi: 10.1016/j.pecs.2015.10.003

Credit for Reducing Sunshine

Narayanan M. Komerath, Ravi Deepak, Adarsh Deepak

Taksha Institute, Hampton, VA, USA

Abstract

Climate Change is a driver for solar energy and sustainable growth. Since developed nations still dominate anthropogenic heat release and per capita Carbon Footprint, partly for the conveniences of a high standard of living, an exclusive focus on reducing Greenhouse Gases is controversial. It is too slow to stop the temperature and sea level rise and may also trigger unfavorable short-term responses. We propose to expand the concept of Carbon Credits to include other Sustainable Development Goals, specifically including reduction of heat input. Our Glitter Belt architecture comprises swarms of controlled, solar-powered data-gathering reflectors floating in the upper atmosphere worldwide. In the first phase, small swarms of Flying Leaf vehicles serve to reduce uncertainties in system performance, high altitude weather and overall Climate measurements and simulation. Scale-up phases with optimized systems are discussed. With proposed policy support in equating sunlight reflection to Carbon reduction, this is not only affordable but also self-sustaining. Perfect reflectors at the edge of the atmosphere are equivalent to 0.068 Certified Emission Units per square meter. Sunshine credits can be generalized to Nature Credits that recognize many other priorities of nations in a coherent manner, linked to UN Sustainable Goals and Nationally Determined Contributions.

Keywords: Glitter Belt, Sunshine Credits, Nature Credits, Reflection, Anthropogenic Heat Release.

Introduction

We have developed a method called the Glitter Belt (GB) to reduce insolation in a controlled, reversible and non-intrusive manner. It appears to be the best way to combat Climate Change in complete conformance with the recommendations put out by the Intergovernmental Panel on Climate Change (IPCC) and the US National Academy of Sciences (USNAS). Our method offers platforms and networks, to conduct continuous, widespread and well-resolved long-term measurements needed to refine simulation and prediction methods. It is being tested as a way to both build global collaboration, and conduct detailed, continuous measurements. In addition, GB can be used to develop an advanced communications network accessible from remote parts of the world. With advancements in positional certainty and swarm control, GB also offers platforms to observe Space Weather and make some astronomical observations from the edge of the atmosphere.

1.1 Net Radiative Forcing as Metric of Global Warming

In this paper we discuss steps needed to credit reduction of insolation. Reduction of Greenhouse Gas (GHG) emissions is recognized by Certified Emission Units (CEUs), commonly called Carbon Credits, which are Metric Tons of Carbon Dioxide equivalent in potential to absorb Infrared radiation. First a quick glimpse of the opportunity, and a rough equivalency between CEUs and proposed Reduced Insolation Credits (RIC). Net radiative forcing on Earth due to Well-Mixed Greenhouse Gases (WMGHG) exceeds 2.83 W/m^2 of Earth's surface, per Myhre, 2013. We will project this to 3 W/m^2 by 2025. Earth's surface area is $5.11 \times 10^{14} \text{ m}^2$. Total GHG accumulation in the atmosphere from 1990 to 2025 is 154 Gigatons (GT), out of the 806 GT emitted.

1.2 A glimpse of an Insolation Reduction Credit (IRC):

Our control architecture is to use reflectors that float at the edge of the atmosphere and move to keep up with the peak summer sun every day. Solar reflection is taken as 1367 W/m^2 . Under the peak summer sun, 12 hours of bright sunlight, essentially at AM0 (Air Mass Zero, the value in Space at Earth's orbit around the Sun) is a conservative assumption at high altitude. This works out to 2.245 trillion m^2 of reflector area needed. The equivalence then is 0.068 CEUs per square meter of high-altitude reflector. At a nominal market price of \$10 (ten US dollars) per CEU, each square meter of reflector should be creditable at \$0.68. At the expected Kyoto quota value of \$40/CEU, each square meter of reflector is worth \$2.72. However, this may be too low, since the actual Anthropogenic Emission of GHG is closer to 806 Gigatons, of which much has been absorbed into the oceans or land already. CEUs credit reduction of emission, not just removal of net CO₂ present in the atmosphere. In other words, the part of GHG emissions that is absorbed by the oceans or trees, is also credited if reduced at source. Hence, we could demand a fair equivalence of \$14.23/ m^2 of high-altitude sunlight

reflection as Insolation Reduction Credit (IRC). Aluminized Mylar reflective sheets such as those we propose for initial use, achieve 95% reflection, over 98% in the Infrared range, earning \$13.51 per deployed square meter. This should only be earned for staying deployed: a 10-year deployment lifetime amortization may have to be accepted, similarly to what is done for solar PV panels.

This is a starting point to credits for other restorations of Nature. Reflecting sunlight buys time for many other urgent priorities, whose implementation will alleviate or adapt to Climate Change. Many of these have no relation to “carbon reduction” but are listed in the Sustainable Development Goals of the UNO.

1.2 Background: Anthropogenic Global Warming

The increased heat release in the past 300 years comes primarily from waste heat of heat engines. Per Smil (2021), US heat engine efficiency rose from 14% circa 1900 to 50% by 1950 with multi-stage power plants. However, by 2020, efficiency had dropped to 33%, primarily due to proliferation of air conditioning and other electric powered accessories of a high standard of living. Chen et al, 2014, show that Anthropogenic Heat Emission (AHE) worldwide comes mostly from industrial economies of Western Europe and North America.

International campaigns to counter warming have focused instead on reducing release of Infrared-absorbing Greenhouse Gases into the atmosphere. This focus on “Carbon Reduction”, and extreme fears cited regarding moves to counter heat input, must be viewed in the light of the above. The UNFCCC’s Kyoto Protocol (Kyoto, 1998) established a market for tradeable CEUs. Gains in efficiency earned CEUs, either directly or by crediting development of efficient factories and renewable energy plants to replace fossil and wood burning. Industrialized nations accepted quotas to reduce emissions to 1990 levels. Quota deficiencies would incur charges of \$40/MT. As deadlines approached, CEU prices would rise, driving investment in CEU-generating activities, enough to justify the large expense of getting certification from Brussels or Geneva.

Initial enthusiasm about rising prices ended as prices dropped near \$2/CEU with the recession of 2008-2009. It has recovered since, but there is wide price disparity across the world due to a growing array of national and regional regulations. Carbon Market Watch, 2019 cites the main challenges: too many credits available; not enough projects to buy them. A risk of double counting credits. Protecting local stakeholders and the environment, and delivering on sustainable development goals are challenges. The system risks setting up perverse incentives that hamper ambition.

2. Need for Broader Credits

Several reasons point to the need for broader credits than CEUs and a broader market.

2.1 Imbalance in Carbon Footprints

Industrialized nations exhibit Carbon Footprints (average per capita annual emission of GHG) up to 1500 times those of many developing nations. Thus, reducing carbon footprint is a good priority for developed nations, but not justifiable for developing ones seeking to raise standards of living. This is a primary area of conflict.

2.2 Tailored Bilateral/Trilateral Agreements

Nations that refused to sign or ratify the Kyoto Protocol, nevertheless moved in their own ways to counter Climate Change. US entities set up Green Credits. Large wind energy projects in South Dakota, located far from energy markets, were funded by the promise of Green Credits for the electric energy that they would generate. Bilateral and multilateral agreements such as those between the USA and India funded initiatives on Solar Power, simultaneously addressing massive power shortage and capital in India. World Bank initiatives have addressed critical needs to improve ground water quality, particularly in congested communities and mountain glacier watersheds infested with tourists (Neighbor 2020). This translates to major health benefits, a much higher priority than “Carbon Reduction”.

2.3 Near-Term Response to Carbon Segregation

Koch, 2021 show a disturbing result. In the near term, reducing CO₂ concentration in the atmosphere by reforestation may simply cause increased emission from the oceans, which are by far the massive repository of CO₂, frustrating the aim of reducing Net Heat Retention. In 30 to 50 years, the benefits of reforestation will become significant. A sharp increase in tall vegetation over substantial areas will also reduce albedo over now-bare land (increasing heat absorption near the ground), and shift rainfall patterns as the ground cools. Present agricultural investment is based on fairly recent weather. This short-term response is alarming in that extreme expenditures to “reduce Carbon” may leave us with no real answer as sea level rises and climate changes, and

perhaps causes weather shifts. Thus, merely removing anthropogenic GHGs will not suffice unless heating is also countered.

2.4 GHGs to NDCs to SDGs

Discomfort with exclusive focus on CO₂ reduction is evident at the UN. First came Nationally Determined Contributions (NDCs) which enabled ambitious programs at the Paris Accords of 2016. Next came the REDD+ or Reduced Emissions from Deforestation and Land Degradation. This appears to recognize that actions for the common good should be credited, but is hindered by the view that it can be ‘gamed’ to avoid real action. So can Carbon Credits, as experienced in California, per Song, 2021. The third is the establishment of Sustainable Development Goals (SDGs), where Climate Action is 13th out of 17. So, the intent and perceived need have been established for much broader credits.

UNDP, 2021 includes an expanded financing system after the Paris Accords: Nationally Determined Contributions (NDCs) allowed more ambitious mitigation actions. Countries would still be able to use Internationally Transferred Mitigation Outcomes (ITMOs) towards NDCs. The NDCs broaden the system of credits far outside the formal Carbon emission trading system. Recently, a market called REDD+ (Reduced Emissions from Deforestation and Land Degradation) was set up to drive the 17 SDGs developed by UNESCO. Several governments and international funding agencies require new proposals to identify their relevance to the SDGs.

2.5. Rising Urgency

Carbon reductions are not on track to slow down the rise of heat retention. Tougher measures are being put into implementation in several nations, with pressure on others to follow suit. California (2021) discusses plans to cut GHG emissions 15% below 1990 levels by 2020, to 80% below 1990 by 2050, still leaving Carbon footprint of 2MT/person/year. A shift to EVs does little to improve basic heat engine efficiency. The Swedish EPA (2021) describes a program similar to the UN SDGs, but based on Carbon Credits. Bird (2021) describes Norwegian efforts, including road-building in Laos to help meet Norwegian Carbon Reduction goals using CEUs. Finland, 2021 aims to cut GHG by 80% from 1990 levels by 2050, become carbon-neutral by 2035. However, household consumption has increased by 4% since 2015 with rising standard of living. As ordered by their highest court, Germany now aims to hit carbon neutrality by 2045. Wettengell (2021) says the EU has declared climate action its top priority with the Green Deal to become the first carbon-neutral continent by 2050. The US Government has come out with a \$1.6 T plan based on Carbon Reduction

4. Proposals to Directly Counter Global Warming

From the above, we see that effective response to Climate threats must include a broad range of measures that address the real priorities of nations, going far beyond just Carbon Reduction. To buy time, reducing insolation must be considered, to control the heat retention rate. This is controversial. On the one hand, critics express suspicion that this is a way to avoid the difficult measures needed to reduce emissions. On the other hand, they point to the danger of unintended Climate response to drastic measures. The US National Academy of Sciences in a recent report (NAS 2021), has come out with recommendations on how to prepare for measures to reduce insolation. Alternatives include reducing economic activity, curbing air and ground travel, switching to electric propulsion for all transport, switching to a solar-hydrogen economy, and technological installations on vehicles and buildings to make various small improvements in efficiency. There have been many other proposals, radical and otherwise (Table 1). Some involve very intrusive laws. None have shown scalability and controllability, at manageable costs, or an evolutionary growth path accompanied by data acquisition and the ability to swiftly reverse or modulate. Table 2 summarizes the expressed concerns and recommendations of the US National Academy of Sciences (USNAS2021). The NAS approach outlines a spiral development through the phases of Engagement, Research and Research Governance, from initial program design, through assessment and revision, informing decisions through knowledge acquisition, and with several “Exit Ramps”.

Table 1 summarizes prior proposals to counter global warming, classified into 6 approaches.

	Approach	References
1	Reflectors, bubbles or balloons in Space to reflect sunlight.	Early, 1989, Palti, 2008
2	Ground-based reflectors.	Kawai, 2009
3	Chimneys ingesting air and removing GHG	Shankman, 2018
4	Reflective particles in industrial exhaust. Sulfuric acid aerosols.	Chang, 1991, Kunzig, 2008
5	Increasing urban albedo by mandating white paint on roofs and sidewalks. Glass Beads On Arctic Ice Cap.	Akbari et al, 2009, Menon et al, 2010
6	Wind turbines pumping Antarctic sea-water onto the ice cap to compensate for ice cap melting in summer. May be powered by sunlight thus requiring solar PV farms on ice cap.	Moreau 2016, Feldmann, 2019

Table 2: Responses to GeoEngineering concerns

Item	Expressed Concerns	NAS recommendation	Glitter Belt Approach
1	Unauthorized/unilateral actions; Uncontrolled in case of unknown response	Authorization, consultation, notification; Transparency & Trust across nations & generations; Ethical accountability; Research in public interest; Legitimacy and accountability. Fairness & inclusion; Maximized benefits; minimized harm.	Informed collaboration with national & international agencies. Completely monitored test & deployment
2	Impractical or poorly understood	Timely technical availability, respecting ethical and ecological norms; Predictability	Flight tests integrated with measurement & simulation
3	Public awareness & policy-relevant knowledge, inclusion, stakeholder participation	Disciplinary balance, stakeholder engagement; self-organized coalition of state & non-state actors; Coordinate across international entities; Peer Review & transparency. Participation and engagement independent of whether a proposed experiment has any known environmental risks	Seeking tech./ policy collaboration, global interests. Continuous data; International NGO & Consortium. Publication. International Participation
4	Removes urgency; reduce other climate funding;	Funding for geoengineering must be limited to be small relative to expenditures for emission reduction and other proactive measures	Broaden from CEU for global buy-in. Micro credits. No zero-sum approach.
5	Emissions	Test materials should be relatively inert and nontoxic. Individual experiments must not release over 1,000 kg, global less than 10,000 kg/yr.	Zero emissions except electromagnetic signals for data, control and navigation.
6	Temperature Change in Experiment Stage	Induced change in global mean surface temperature under 100 nK (100×10^{-9} C) for a 100-yr time horizon (or 10 μ K normalized to a 1-yr horizon) for individual experiment, 1 μ K (1×10^{-6} C) for 100-yrs/ 100 μ K normalized to 1-yr horizon.	Detectable changes only with massive scaleup when agreed. No concentration: swarms move w/ Summer Sun.

5. The Glitter Belt Project

Without going into other aspects of the Carbon debate, we conclude that all contemplated steps to counter the ill effects of Climate Change, require good, continuous, well-resolved data and ever-more-refined predictive simulations. The first order of business is to reinforce the global capability for such measurements, and from those, to develop reliable predictions with the fine resolution to address local effects.

Present methods of atmospheric and oceanographic data collection use local measurements using ground-based instruments, aerial measurements using balloons, aircraft-based instruments, drop-sondes, ocean buoys, and Space satellites. Aircraft-based measurements have broad reach near land, but have limited range and endurance over the remote stretches of the oceans. Satellites provide global coverage, but it is intermittent and

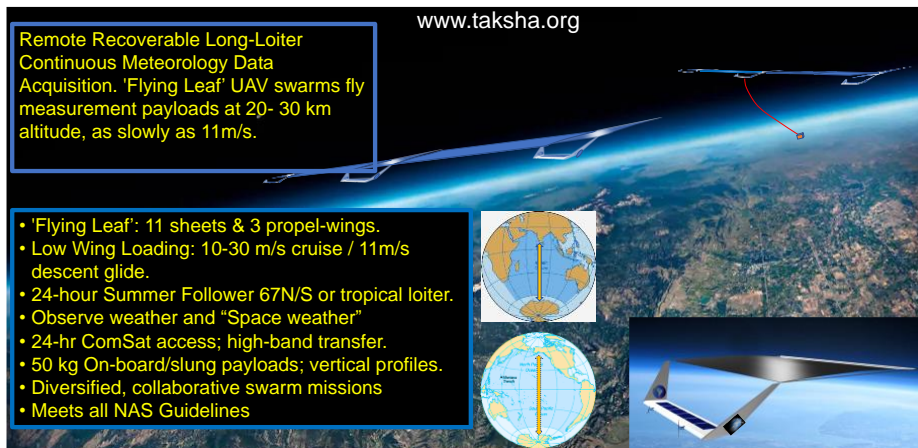


Figure 1: Summary of Flying Leaf Use for Meteorology. From Komerath (2021) by permission

very fast-moving, as well as being 250 to 400 km above the surface.

5.1 Ultralights at 32 km

Our Glitter Belt (GB) project (Figure 2) is developing the technology for swarms of ultralight vehicles flying in the atmosphere

near 32 km altitude. Flying Leaf vehicles are flying wings supporting large thin sheets. The sheets are aluminized on the upper surface and have black lower surfaces. They reflect daytime sunlight back into Space, and absorb night-time radiation from Earth and radiate part of that out. Driven by propellers through motors driven from photovoltaic cells along the wing surface, they cruise at speeds as low as 12 m/s. During the night the very low wing loading enables gliding descent at low speeds. The descent rate is low enough to keep the vehicles far above controlled airspace (18 km) through a 12-hour night. By drifting steadily northward or southward, these vehicles keep up with the Sun as it moves across latitudes through the year. The swarms thus stay with peak summer, year-round. The concept is described in Komerath (2017, 2020, 2021a) and Shukla (2017). Wind tunnel test results were shown in Smith-Pierce (2018).

5.2 Surviving Night-Time Glide

Aerodynamic vehicles have a “speed for minimum drag” which is not zero: it is roughly the speed where the drag that is not associated with lift (such as skin friction, flow separation, interferences) equals the lift-induced drag, which is basically the force associated with energy used in causing flow to spin as in the vortices generated at wing-tips. The latter is minimized by (a) minimizing the lift coefficient by minimizing the Wing Loading (weight or lift supported per unit wing area) and (b) going to as high an Aspect Ratio as possible. In simple terms, putting the wingtips as far away from each other as possible, relative to wing area. The former is minimized by flying slowly enough to keep the boundary layers laminar (avoid turbulence) and having a clean and streamlined design. In this case, also by keeping the sheet from flapping in “flag instability”. With these features, the present design of the Flying Leaf is predicted to have minimum drag at around 11 to 12 m/s at 32 km altitude. The Flying Leaflets, which take off with the sheets rolled up to avoid damage, also have very low takeoff and landing speeds, consistent with launching from playgrounds and beaches rather than airport runways. Once joined up, the Flying Leaf configurations, by virtue of low wing loading (shallow glide angle) and low speed (small vertical velocity component), achieve a very low sink speed. This is low enough to stay well above controlled (Class A) airspace which extends just above 18 km (60,000 feet), through 12 hours of glide. This is why the Summer Follower arrangement is adopted initially: the longest night is 12 hours when crossing the Equator. Other designs of High-Altitude Long Endurance aircraft seen to-date use auxiliary power storage such as batteries or fuel cells to provide power through the night, because they are primarily designed to stay above one temperate-zone region through an entire year. The extremely low Wing Loading of the Flying Leaf makes these unnecessary and thus further reduces weight, or enables carrying measurement payloads or antennae.

5.2 Phase 1: Development and Global Measurement System

Starting with the first test vehicles, these swarms provide an unprecedented opportunity to gather continuous

data, sweeping across remote parts of the world at low speeds. Thus, atmospheric measurements as well as effectiveness measurement are integral to the project. The data collection will also permit better predictions as well as continuous monitoring of regional weather. These aspects were presented in Komerath (2021). We expect that development and flight testing of the Glitter Belt components, including launch facilities, recovery systems, ground stations and communication network to control and monitor the swarms, will be developed through international collaboration and participation during this initial measurement phase. The measurement system and infrastructure are planned as long-term investments, far beyond the phase where any targeted climate intervention is needed.

5.2 Phase 2: Gradual Scale-Up

As concerns are examined and resolved, we project an expansion to massive levels that could indeed reflect enough sunlight to make a difference to net heat retention. This of course will involve a rapid scale-up of manufacturing and launch infrastructure, with a temporary scale-up of system monitoring. If and when such an expansion is approved, funding it becomes an issue. As stated at the beginning, most people may agree that Global Warming is a problem, but do not have any personal incentive to fund its alleviation, beyond government funding through taxes. We show that there are good supplements and alternatives that make sunlight reflection not merely affordable but sustainable through the duration needed to really solve the problem.

5.3 Mature System Scale-Up

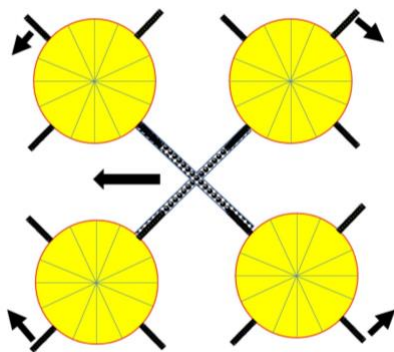


Figure 2: Scale-up concept "Quad-Frisbee" with 4 sheets built up from Flying Leaflet launches, propelled by solar-powered Leaves as rotors.

Initial designs are based on high aspect-ratio aerodynamic flyers described above. If and when scaleup is approved, most of the reflector area added will be optimized for reflection. One concept is shown in Figure 2. This can be built up as a high stratospheric platform using elements similar to the initial Flying Leaflets. The central element is a large sheet structure, with Leaflets attached to the periphery acting as rotor blades. In this case the central quadrotor hub structure may have to be lifted and held for assembly by smaller rotorcraft, until a set of telescoping elements is deployed with rotors to support lift at a moderate altitude. The rest of the structure is conceived as being assembled from modified Leaflet elements, launched with the same existing infrastructure used in the first Phase. Most of the Leaflets in this case will be returned for re-use as the radial sheet structure requires mainly tensile elements. The central support structure of the quad frisbee supports solar cells for power. Once the first set of "blades" is operating, the 4 "rotors" are rotated at a higher speed, progressively slowed down as more and more reflective, lifting sheet is deployed. The assembly operates as a "quadrotor frisbee" to survive night-time glide without power storage other than in the momentum of rotation, and potential energy of altitude. Against the cost and difficulty of initial deployment, each of these vehicles offers 10 times the reflector area per unit weight as the Flying Leaves. Thus, we reason that much of the eventually deployed reflector system will consist of these large ultralight platforms.

5.4 Cost Estimation

Initial system development, we assume, has to be funded by government entities or others who can rationalize expenditures for the public good. Note that the NAS guidelines practically rule out private/ venture capital investments. In this Phase 0, the focus is on reducing uncertainties of all kinds, including engineering, construction, flight performance, high-altitude winds, vehicle longevity, measurement systems, data transmission, numerical analyses and predictive simulations to gauge the safety of control measures, versus the cost of not implementing them. For Phase 1 expansion, our studies show that the proposed system is most

Cost To Reach Global Net Zero Heat Retention

Comparison by weight:

Cheapest Indian automobile: 700 kg, \$3800, incl. 50% markup.

Leaflet: 500kg. →\$1350.

331million Leaflets for Zero Retention → \$447B, + incidentals ~ \$600B.

Mass-produced Leaflet is **much simpler than a car.**



Figure 3: Cost estimate by comparison to automobile manufacturing.

similar to automobile mass manufacturing which is done all over the world. We estimate the cost to reach “Net Zero Heat Retention” by GB Phase 1 Reflectors alone. Figure 3 suggests an upper bound cost of \$600B. The profit portion of automobile cost is removed while including the cost of sales and service infrastructure for a fair comparison. Note that if we go ahead with GB implementation, we will seek to shift to the more optimized Phase 2, bringing a large reduction in costs. However we emphasize that the conversation on controlling Global Warming must be shifted to self-sustainable models. This is discussed in the rest of the paper.

6. Credit for Reflecting Sunlight

6.1 Method 1: Albedo Equivalence

Preventing atmospheric heating is at least as important as reducing the absorption of heat in the atmosphere, to achieve the end objective of preventing continuous climate change. In other words, 1kWh of heat that is stopped from entering the atmosphere should count the same as 1kWh absorbed and retained in the atmosphere, and can be measured using Carbon Credits. This assumption is used explicitly in Akbari (2009) and Menon (2010) from US Federal Labs considering laws to mandate greater albedo in coverings for road surfaces, sidewalks and roofs. Akbari and Menon established a number of 57 Gigatons (GT) of CO₂ as equivalent to an increase in albedo that could be achieved by mandating white-painted roofs, roads and sidewalks in urban areas worldwide. The total cost of implementing such a mandate was not given.

6.2 Method 2: Integrated Anthropogenic GHG vs. Net Heating Rate Difference from 1990

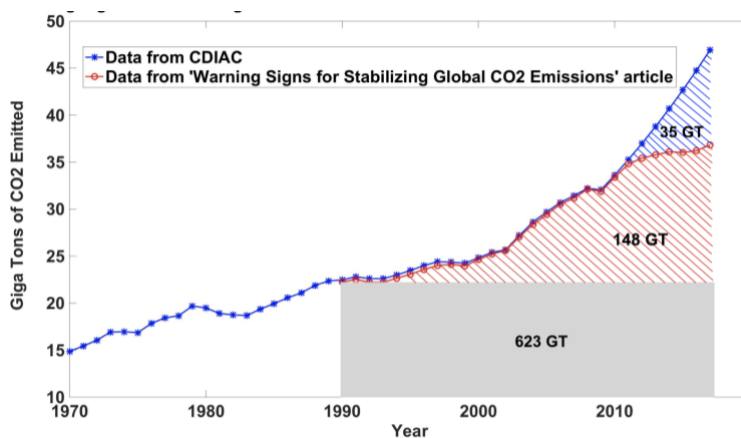


Figure 4: Anthropogenic GHG emission. Smith-Pierce 2018, by permission.

We first limit credit to anthropogenic addition of GHG (A-GHG) since 1990, the Kyoto cutoff date. Summing the annual GHG emission since, equals total creditable A-GHG. The difference between net radiative forcing (NRF) today and in 1990, is equated to this A-GHG. In other words, reducing the difference in NRF to zero is equivalent in immediate effect to removing all of A-GHG since 1990. Figure 4 shows the sharp recent rise in GHGs and the total of 806 GT since 1990. Per Stocker et al, 2013 NRF rose by 1.02

W/m² from 1.9 to 2.92 since 1990. This approach ignores the value in reducing insolation beyond the equivalence to accumulated CO₂ since 1990. A more direct approach would establish a value for reflecting sunlight in terms of the radiation reflected, independent of GHG measures.

The above calculation illustrates that there is a valuation that can be attached to each sheet and its supporting vehicle. The number of years over which the full credit is earned will be a point of contention, but here the argument about addiction and habit change can be turned around: the Glitter Belt buys time and reverses the heating so that damage is controlled, while the global community removes the underlying causes of heat retention. Perhaps in 20 to 30 years the Glitter Belt can be removed without starting a temperature rise again.

6.3 Carbon and Heat Footprint of Glitter Belt Vehicles

The Flying Leaf systems as envisaged, consist of carbon fiber and other composite framework, Aluminized Mylar sheets, photovoltaic panels, motors, propellers, landing gear, control wires and actuators, and

electronics. Each Flying Leaf consists of 11 reflective sheet systems and 3 supporting/propelling wings. Expanded designs will deploy 64m x 60m sheets per reflector module, for a total of 40,000 sqm of reflector. The Carbon Footprint of each 2100 kg Flying Leaf is estimated at 18.6MT. Subtracting from the CEU equivalent, at 0.068 MT per sqm, net credit for a Flying Leaf is 2700 CEUs. Thus, with any reasonable system of credits, Glitter Belt architecture is quite viable and self-sustaining in cost and payoff. Deploying such a system can provide a strong employment base. The Carbon Footprint is dominated by the present petroleum genesis of carbon fiber. Alternatives that use captured, segregated carbon would reverse this by funding carbon segregation from GB credit revenue.

6.4 GB System Levels to Compensate for Specific Heat Emitters

Let us look at system size and accompanying credit sources, to cancel out anthropogenic heat release (AHR) from specific sources. The basic unit is an expanded Flying Leaf vehicle, that carries 11 64m x 60m sheets supported by 3 propelling 64m x 4m wing/tail structures. When fully deployed at altitude, this is 40,000 sqm. of reflector. Aluminized Mylar sheets reflect over 98% of solar Infrared for incidence as shallow as 30 degrees above the horizontal. With the Summer Follower, reflectors catch sunlight for a minimum of 14 hours per day, which we approximate as 12 hours of full-spectrum AM0 reflection, at 95% efficiency. This is 15534 Watt-hours per square meter, giving roughly 60 MWH per day per Leaflet. A Flying Leaf with 11 such Leaflets reflects 658MWH. Following the Summer Sun maintains this value year-round. So each Flying Leaf reflects 240 GWH, or 0.24TWH per year. Table 3 estimates the number of such Flying Leaves to cancel out AHR from various sources:

Table 3: Number of Flying Leaves To Cancel Their Heat Release from Given Anthropogenic Heat Release Sources

AHR Source	TWH/yr AHR @efficiency	Reference	# of Flying Leaves under Summer Sun
Terrestrial Power Generation 26730 TWH	26730 @50%	IEA(2020)	111,375
Aviation: 95B gallons, 3420TWH	1710 @50%	Statistica(2021)	7,125
Transportation 118 Quad. BTU 40% efficient	20749 @40%	EIA(2016):	103,745
Air conditioning: 10% of global electricity	2637@50%	IEA(2018)	11,138
Light vehicles 45Quad BTU extrapolated	15109 (@40%)	TME(2015)	63816

6.5 How Intrusive Is GB?

Floating 111,375 Flying Leaves, all under the zone of peak sunshine, year-round, could cancel out all the heat release from terrestrial power generation. Assuming a uniform distribution, strung out under the peak Summer Sun line, there would be 4.5 per kilometer. If they are spaced over 100 kilometer north-south, there would be 9 per 200 square kilometers, covering under 0.2% of the sunlight area at 32km altitude. From the ground neither vehicles nor shadows will be discernible to the naked eye. But laws of physics still assure the reflected amount. A reasonable expectation is that the Glitter Belt may have to do about 10% of the above at its most mature implementation. Compare this to 93 million road vehicles produced every year.

7. Broader Credits

7.1 Reforestation

Many nations have priorities higher than just Carbon Reduction. These do have strong implications for combating Climate Change. They are better seen as ways of advancing towards the Sustainable Development Goals of the United Nations. Reforestation is a top priority. It can restore some wildlife species and biodiversity. Forests can produce significant commercial crops such as rubber, fruits, medicinal herbs and mushrooms, and controlled harvesting of wood for construction and furniture. Restoring and managing forests takes significant resources. Trees must be planted and provided enough water and protection in the growing years. Denied land usage must be compensated by providing other means of support for local residents.

Reforestation is not without negative effects. California's high-density forests release massive amounts of CO₂, toxins and heat in annual fires. This calls for careful management as well as fast-response fire spotting

and fighting. Investments must go well beyond those creditable with CEUs.

7.2 Vertical Farming, flood-drought control

Major human habitats depend on narrow time windows for arrival of the annual Monsoon rains. Most of their water arrives in heavy downpours over 2 or 3 months, and most of it flows to the sea, often with devastating floods. Vertical Farming, modified from ancient Greenhouse ideas, now uses Space technology to grow plants with artificial LEF lighting reaching multiple tiers, along with metered water, air circulation, temperature and humidity. CO₂ emission can theoretically be directed where needed, such as in mushroom cultivation. Addressing rising sea-levels, and breaking the flood-drought sequences, are top priorities. Increasing demand for indoor plumbing and urbanization, and subsidized electric power for irrigation pumps, have depleted groundwater. This ground water must be replenished.

7.3 Biogas/Biomethanation; Clean Air and Water

Floating-lid (constant pressure) generators are conveniently located in residential backyards and are suitable to digest vegetation. They are eco-friendly and yield enough gas to replace most of a family's needs for (often imported) liquefied petroleum gas for cooking. They reduce the waste disposal problem. The sludge is excellent natural fertilizer. These generators have large value for energy independence, as well as in environmental cleanup and topsoil replenishment. Biomethanation refers to extracting methane from human waste and other sewage, typically in underground, constant-volume facilities. Biomethanation yields enough methane to light up communities, removes hazardous bacteria from soil and ground water, and is thus crucial to health and wellness. Groundwater cleanup removes industrial toxins. Building toilets has significantly reduced outdoor defecation in emerging nations. Pristine areas such as Mt. Everest are being cleaned to remove garbage and sewage left by climbing expeditions. Cleaning up air pollution goes beyond carbon particles and exhaust gases such as sulfur dioxide: soil and metal dust is also a threat.

7.4 Micro Credit Certification

One key to moving ahead on a global scale is to “democratize” the certification of CEUs. Countries in Asia and Africa have taken the lead in transacting most financial transactions through mobile phones. Thus the identity, documentation and responsibility verification aspects are already well in hand. Technical measurements are an essential part of CEU certification, and will need verification protocols. Once again, the process has much in common with that of many present projects, where the proposal, contract, progress monitoring, result transmission and payments and final reporting are all done electronically. This is no more complex than running university sponsored research programs. A template can be set up, permitting projects at small cost levels to be administered and certified reliably. This will open up Micro Credit certification all over the world, to small local community projects, without an expensive and complex pyramid structure.

8. Summary: Equivalence Calculations

Sunlight is a much more general unit for expressing value than a particular gas or set of gases such as CO₂ or GHG. Air purity could be tied to oxygen rather than CO₂, but even this is narrow. Fresh water is a basic resource and easily quantified. Inspired by the Carbon Market, there could be a worldwide valuation metrics for fresh air (Burston & Smith 2020) and water (averaged from international values in OECD, 2021) and land with allowances for urban market spikes. Urban values may be seen differently with reverse migration to rural areas offering better quality of life, equal productivity and access to facilities. Table 4 summarizes results.

Table 4: Suggested Ways and Amounts to Credit Human Priorities

Creditable Activity	Basis for awarding credit	Suggested
GHG vs. reflector area: 32 km altitude	Direct conversion. 0.068 to 0.355CEU/m ² at AM0	\$2.72 to 13.71/sqm
Ground reflector or Albedo Paint	AM1 modified by ground loss	
Solar PV & thermal Power	Heat to work; replacing fossil power	
Reforestation	GHG absorption minus albedo reduction	
Vertical Farming, Clean Manufacturing	Forest area; CH ₄ , water savings	

BioGas & BioMethanation	LPG& CH4 value, ground & water cleanup, amortized energy import rates	\$10/MT to \$800/MT
Air Pollution Removal: Combustion products and chemicals, dust	Fresh Air Credit, Health & water saving.	\$1/MT
Groundwater Replenish & cleanup	Freshwater Credit: average of global costs.	\$1/MT
Flood prevention, Seawalls & land-raising, Drought Alleviation	% of Disruption value saved, Freshwater Credit	\$0.01/MT
Education, Healthcare, telemedicine	Priceless. Determined from National budgets.	
Reverse migration	Travel&time saved; heat and emissions.	

Detailed valuations for Nature Credits will involve extensive policy discussions far beyond the scope of this paper. Value perception is with the particular community and nation rather than global experts. Table 3 shows our present suggestions. Sunlight reflection and albedo increase are direct computation as we showed. Solar PV, solar thermal and reforestation are already valued in equivalent fossil fuels or CO2 credits. Biogas and biomethanation have value beyond the methane capture. Fresh water already has widely varying costs. Clean air, including dust removal by green cover and moisture, can also be assigned credit value, with threshold of purity defined. Curing flood and drought and staving off sea-level rise can be valued by land, infrastructure and water. Health and Wellness, and most of all Education are priceless national and global priorities.

9. Suggested Structure

Given the NAS concerns, international priorities and need to get moving, we suggest a Consortium structure as in Figure 4. Except for national government, there are few entities that have power over others, possibly

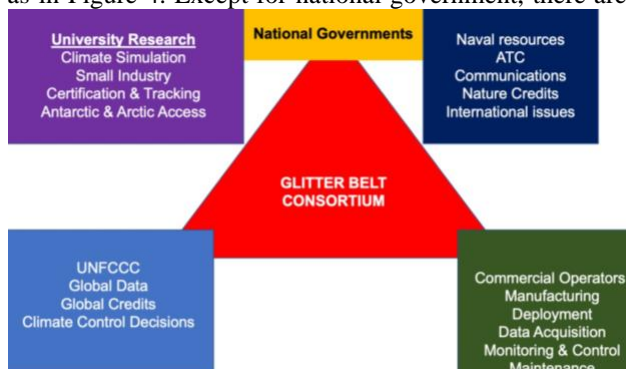


Figure 4: Consortium structure to implement Nature Credits and reverse Global Warming while addressing national priorities.

enabling a focused collaborative effort to slow, stop and reverse Global Warming while moving full speed on what really matters to the people of each nation. The structure is drawn generally from the reasoning in (Komerath et al, 2007) to implement the infrastructure needed for extraterrestrial economic growth. Here urgency to implement plans adds pressure, which must be addressed.

10. Conclusions

- Most Anthropogenic Heat Emission (AHE) patterns and Carbon Footprint are from developed nations.
- Present focus on reducing Greenhouse Gases is controversial and too slow to avert significant damage from temperature and sea level rise.
- Our Glitter Belt (GB) concept of high-atmosphere ultralight aerodynamically-sustained reflectors, promises to achieve needed sunlight reflections to buy time while satisfying scientific, societal and national concerns.
- In the first phase, small numbers of Flying Leaf vehicles of the GB will be used to make continuous, low-speed measurement sweeps over the tropical and temperate zones of the entire planet. This presents an unprecedented opportunity to obtain complete meteorological data to support physics-based predictive simulations, finely resolved enough to predict local phenomena and interactions.
- Once concerns are allayed, GB can be expanded to Phase 1 with Flying Leaf vehicle swarms that follow the Summer Sun for best efficiency in reflecting sunlight into Space.
- In Phase 2, optimized systems will use much larger "Quadrotor Frisbees", offering an order of magnitude more reflector area per unit mass.
- Automobile industry analogues suggest that Net Zero Heat Retention Rate can be achieved under \$600B in cost, even without Phase 2 efficiencies.

- Phase 1 and Phase 2 expansion should be self-sustaining.
- Insolation Reduction Credits (IRC) should earn from 0.068 to 0.356 CEUs per square meter by equivalence to Carbon Credits
- IRCS can be part of broader Nature Credits tied to units of sunshine towards Sustainable Development Goals under Nationally Determined Contributions of the UNFCCC Paris Accords.
- Micro level Nature Credits must be accessible to small entities to enlist mass participation in Restoring Nature. Initial equivalency calculations are presented.
- In conclusion, Insolation Reduction and other Nature Credits mobilize global participation and enthusiasm, while buying time to implement a comprehensive quantum leap in quality of life, and a sustainable future, worldwide.

10. Acknowledgment

The authors gratefully acknowledge partial support from the Taksha Institute. The first author acknowledges support for work leading to the Consortium idea under a Sam Nunn Senior Security Fellowship at the Center for International Security, Technology and Policy.

11. References

- Akbari, H., Menon, S., and Rosenfeld, A., 2009. Global cooling: increasing world-wide urban albedos to offset CO₂," *Climatic Change*, Col. 94, no. 3, pp. 275-286.
- Burston, J. and Newton-Smith, R. Can we put a price on clean air? Yes, we can. World Economic Forum, September 9, 2020. www.weforum.org/agenda/2020/09/we-can-put-a-price-on-clean-air/ Viewed 07/10/21.
- Carbon Market Watch, 2019: Carbon Markets 101: The ultimate guide to global offsetting mechanisms, Carbon Market Watch, Brussels.
- Chang, D. B., Shih, I.-F., 1991: Stratospheric Welsbach seeding for reduction of global warming, US Patent 5003,186.
- Chen B, Dong L, Shi G, Li L.J, Chen L, F., 2014: Anthropogenic heat release: estimation of global distribution and possible climate effect. *J. Meteorological Society of Japan*. Ser. II. 2014;92:157-65.
- Early, J.T., 1989 Space-based solar shield to offset greenhouse effect, *J. British Interplanetary Soc.*, Vol. 42, pp. 567-569.
- Elzen, et al, 2011: M. G. den Elzen, A. F. Hof, A. M. Beltran, G. Grassi, M. Roelfsema, B. van Ruijven, J. van Vliet, and D. P. van Vuuren, "The Copenhagen Accord: abatement costs and carbon prices resulting from the submissions," *Environmental Science & Policy*, vol. 14, no. 1, pp. 28-39.
- Feldmann, J., A. Levermann, and M. Mengel, 2019: Stabilizing the West Antarctic Ice Sheet by surface mass deposition, *Science Advances*, vol. 5, no. 7, p. 4132, 2019.
- Finland: 2021 Annual Climate Report 2021: Emissions in Finland Declined in the Exceptional Year. <https://ym.fi/en/front-page> . Viewed July 3, 2021.
- IEA, 2018: The Future of Cooling: Opportunities for energy-efficient air conditioning. Technology Report, May. International Energy Agency. <https://www.iea.org/reports/the-future-of-cooling>. Viewed July 6, 2021.
- IEA, 2020: Electricity Information: Overview. Statistics report — July 2020. International Energy Agency. <https://www.iea.org/reports/electricity-information-overview>
- Kawai, K., 2009: Solar energy reflection plate for suppressing global warming," US Patent App. 12/918,356.
- Koch, A., Brierley, C. and Lewis, S. L., 2021: Effects of Earth system feedbacks on the potential mitigation of large-scale tropical forest restoration. *Biogeosciences*, 18, 8, April 2021, pp. 2627—2647
- Komerath, N., Nally, J., & Tang, E. Z., 2007: Policy model for space economy infrastructure. *Acta Astronautica*, 61(11-12), 1066-1075.
- Komerath, N. et al, 2017: Hariharan, S., Shukla, D., Patel, S., Rajendran, V., and Hale, E., "The Flying Carpet: Aerodynamic High-Altitude Solar Reflector Design Study," Tech. Rep., SAE Tech. Paper.
- Komerath, N., 2021: Glitter Belt: Atmospheric Reflectors To Reduce Solar Irradiance, US Patent 10,775586, Sep. 15.
- Komerath, N., 2021a Rotationally Stabilized Atmospheric Reflector To Reduce Solar Irradiance. US Patent 10,890,735 B2.

- Komerath, N. and Deepak, A., 2021: Payload Design for Global Continuous Atmospheric Mapping. Virtual Global Monitoring Annual Conference (eGMAC), May 24-28.
<https://gml.noaa.gov/annualconference/abs.php?refnum=34-210424-C> Viewed 7/10/21
- Kunzig, R., 2008: A sunshade for planet Earth, *Sc. Am.*, 299, 5, 46-55.
- Kyoto, 1998: The Kyoto Protocol to the United Nations Framework Convention on Climate Change. UN 20p.
- Mengel, M., Levermann, A., Frieler, K., Robinson, A., Marzeion, B., Winkelmann, R., 2016, Future sea level rise constrained by observations and long-term commitment, *Proc. Nat'l Acad of Sc*, 113, 10, 2597-2602.
- Menon S., et al, 2010: Radiative forcing and temperature response to changes in urban albedos and associated CO₂ offsets, *Env. Res. Letters*, 5, 1, p. 014005.
- Moreau, S. et al, 2016, Assessment of the sea-ice carbon pump: Insights from a three-dimensional ocean-sea-ice biogeochemical model (NEMO-LIM-PISCES), *Elem Sci Anth*, Vol. 4, 2016.
- Myhre, G., D. et al, 2013: Anthropogenic and Natural Radiative Forcing. In: *Climate Change 2013: The Physical Science Basis*. Stocker, T.F., et al, (ed s.). Cambridge U. Press, Cambridge, UK.
- Neighbor, J., 2020: Tidying Up The Top Of The World. *National Geographic*, July 30. Viewed 7/5/21.
<https://www.nationalgeographic.com/science/article/partner-content-bally-cleaning-up-everest>
- OECD, 2021: Water - The right price can encourage efficiency and investment. *Biodiversity, water and natural resource management*. www.oecd.org/env/resources/water-therightpricecanencourageefficiencyandinvestment.htm Viewed 07/10/2021.
- Pachauri, R.K. et al, 2014: *Climate change 2014: Synthesis Report*. Working Groups I, II and II Ipcc.
- Plass, G.N., 1959: Carbon Dioxide and Climate, *Sc. American*, Vol. 201, No. 1, pp. 41-47.
- Palti, Y., 2008: Outer space sun screen for reducing global warming," *US Patent App*. 12/035,886, Feb. 22.
- Shankman, S., 2018: We Can Pull CO₂ From Air, But It's No Silver Bullet For Climate Change, *Scientists Warn*. February.
- Shukla, D., Komerath, N., Hariharan, S., Patel, S., and Hiremath, N., 2017 Tradeoff Study of High Altitude Solar Reflector Concepts, *Tech. rep.*, SAE Technical Paper.
- Smil, V. 2021: Energy conversion efficiency is falling. *IEEE Spectrum* February, 18-19. PDF
- Smith-Pierce. M. et al, 2018: High Altitude Aerodynamic Reflectors To Counter Climate Change. *AIAA Paper*, Applied Aerodynamics Conference, Atlanta, Georgia July.
- Song, L., Temple, J., 2021: The Climate Solution Actually Adding Millions of Tons of CO₂ Into The Atmosphere. *ProPublica*, April 29. <https://www.propublica.org/article/the-climate-solution-actually-adding-millions-of-tons-of-co2-into-the-atmosphere> Viewed July 5, 2021.
- Statistica 2021: Total fuel consumption of airlines worldwide between 2005 and 2021. *Statistica*. <https://www.statista.com/statistics/655057/fuel-consumption-of-airlines-worldwide/> Viewed July 4, 2021.
- Stocker, T.F. et al, 2013: IPCC, 2013: *The Physical Science Basis*. Contribution of Working Group I to the Fifth Assessment Report of the Intergovernmental Panel on Climate Change.
- UNDP, 2021: United Nations, Inter-agency Task Force on Financing for Development, *Financing for Sustainable Development Report 2021*. New York: United Nations, available from: <https://development.un.org/fsdr2021>.
- EIA 2016: *International Energy Outlook 2016. With Projections to 2040*. US Energy Information Administration. May. www.eia.gov/forecasts/ieo
- USNAS, 2021: *Reflecting Sunlight: Recommendations for Solar Geoengineering Research and Research Governance*. Washington, DC: The National Academies Press. <https://doi.org/10.17226/25762>.
- Wettengel, J., 2021: Energy Transition in EU takes centre stage in quest for climate neutrality. June 29. <https://www.cleanenergywire.org/dossiers/energy-transition-eu-takes-centre-stage-quest-climate-neutrality>.

Nonimaging Optics and Constructal Design Towards Optimal Solar Cookers

Eduardo Rincón-Mejía¹, Ana Gabriela Rincón² and Verónica Rincón-Rubio³

¹ School of Engineering/Autonomous University of the State of Mexico, Toluca (Mexico)

² CESMECA/Sciences and Arts University of Chiapas, San Cristóbal de las Casas (Mexico)

³ Ecology Institute/National Autonomous University of Mexico, Mexico City (Mexico)

Abstract

According to the WHO nowadays all over the world millions of people get sick and die each year from inhaling the fumes produced by the combustion of wood and other fuels for cooking, causing much more deaths than the those due to COVID-19! These deaths and illnesses can be significantly reduced by using very efficient, reliable, safe and economical solar cookers with which any type of food could be cooked most of the days of the year. Even though there are today lots of successful designs of solar cookers, we still need such optimised designs that could operate even in frankly cloudy days; the solar cookers presented here meet these strict requirements. Globally, cooking food involves a significant and unavoidable consumption of energy cause more than 7.8 billion people must eat at least three times a day and this cooking is done mostly by burning fossil fuels or firewood, generating a large amount of toxic and greenhouse gases and particles that are very harmful to health and the environment. The massive use of solar cookers would have great benefits, but to guarantee their use for at least 85% of the days of each year it is necessary to have very high-performance solar cookers, keeping ease use and reasonably low manufacturing costs. The use of Nonimaging Optics and the Constructal Design have made possible to create solar cookers with which them is possible to cook any food on almost any day of the year. Details of their design and some operational results are summarised here.

Keywords: Nonimaging Optics, Constructal Design, Solar Cookers

Introduction

According to the World Health Organization (WHO, 2018), the combined effects of ambient (outdoor) and household air pollution -mainly due to fumes produced by the combustion of fuels for cooking- cause about seven million premature deaths every year, mostly as a result of a great mortality from strokes, heart diseases, chronic obstructive pulmonary disease, acute respiratory infections and lung cancer. The WHO also estimates that there are globally 3.8 million deaths per year attributable just to household air pollution. This figure corresponds to nearly double of deaths due to COVID-19 during the first year of the pandemic! The estimate is based on the strength of the evidence, primarily meta-analyses of epidemiologic studies of acceptable scientific quality, although for cardiovascular disease, the evidence is more inferential (Balmes, 2019). As a matter of fact, air pollution poses a major threat to health and climate that causes diseases and mortality all over the world (Kumar and Mehta, 2016; Boogaard et al. 2017; Rosenthal et al. 2018; Conibear et al. 2020).

For millennia humanity based its cooking on the combustion of biomasses. Even nowadays, about a third of the world's population continues to burn firewood because to their poverty they do not have access to fossil gas or electricity. Besides the foregoing, collecting firewood carries risks for women and children, along with a loss of time for living. Furthermore, fuelwood consumption in impoverished regions contributes to deforestation: according to Bailis et al. (2015), "over half of all wood harvested worldwide is used as fuel, supplying ~9% of global primary energy. By depleting stocks of woody biomass, unsustainable harvesting can contribute to forest degradation, deforestation and climate change. Approximately 275 million people live in woodfuel depletion hotspots -concentrated in S. Asia and Africa- where most demand is unsustainable".

On the other hand, in urban areas almost the entire population burn fossil gas or use electricity for cooking. As it is well known, the consume of gas causes much of the indoor air pollution and other hazards, such as burns, explosions and poisonings. Hundreds people annually suffer accidents directly or indirectly related to gas consumption. Besides all that, cooking with gas or firewood favors the production of toxic or carcinogenic substances in food, especially when exposed to high temperatures, which also degrade nutrients and can burn or char them when they are not attended to during cooking.

Our ASES SOLAR2020 Conference is held within the framework of the most serious global pandemic that humanity has suffered in more than a century, which has caused enormous mortality in countries that have populations with high rates of obesity, malnutrition, diabetes, hypertension and other maladies derived mainly from a poor diet based on industrially ultra-processed foods, with a lack of nutrients and an excess of preservatives, flavorings, colorants, sweeteners, and other chemical substances recognized to be addictive, toxic, carcinogenic and favoring obesity and hypertension. In addition to these harmful substances added purposefully to food, there are others that are formed when food is processed using too high temperatures, such as acrylamide and furans amongst many others. The second comorbidity factor that aggravates COVID-19 is chronic respiratory diseases caused by combustion fumes generated in cooking food, internal combustion engines, smoking, fires and other sources of toxic gases. The foregoing shows that, as a priority public health issue, we must change the way we eat as soon as possible, from the production of food, its processing to final consumption. Solar food processing, which includes the essential cooking of some meals to make them edible (such as legumes, tubers, meats, herbs) offers an excellent opportunity to remedy many of the serious problems that we face. In particular, solar cooking of food offers the following great benefits:

- 1.- Reduces exposure to fumes from the combustion of firewood (or LPG, methane or other fuels) that cause respiratory diseases in millions of people.
- 2.- It contributes to achieving food and energy sovereignty, and to reducing poverty (Sun rises for free for everyone!) by dispensing with the need to consume fuel or electricity through inefficient and expensive supply chains.
- 3.- In addition to helping to care for the environment by avoiding deforestation, cooking and pasteurization of water with solar energy reduce the emission of GHG and the formation of dangerous substances that begin to form inside food when the cooking temperature exceeds 120°C.
- 4.- Solar cooking conserves the nutrients quality and offers a much better flavor.
- 5.- Besides all the above, solar cooking contributes significantly to achieving the 17 Sustainable Development Goals (SDGs) of the United Nations 2030 Agenda to face climate change, which today, after COVID-19, it is the second most important issue in the UNO's agenda. As a matter of fact, without solar cooking the SDGs could not ever be achieved.

Solar Cookers

Solar cookers are not a novelty in themselves, they have been working for centuries. However, nowadays they still are a real discovery for many, because of the curiosity they represent and the disbelief about their possibilities. "Except for smoked, there is no culinary process that is not possible with them, nor size that escapes them. However, their use is not generalized, although in the world they are counted by millions" (Lecuona, 2017). They are a great resource in the fight against energy shortages, and although commonly they are not able to satisfy 100% daily needs, on very cloudy or rainy days, conventional means can be used; after all, every good restaurant -and even many dwellings- have several complementary devices to cook any dish at any time! Solar cookers can indeed cleanly supply most of the domestic energy consume in many sunny countries.

There are many types and variants of solar cookers, depending on their application, operating life, cost, size, with the possibility of being built in-situ, etc. (Nandwani, 2004; Lecuona, 2017; Kundapur, 2018). Figure 1 shows the four most successful types, adapted to their use: fast and slow, and the advanced non-imaging type.

All efficient solar cooker has a cavity within which one or more vessels containing the food to be cooked are placed. This cavity is heated by solar radiation, preferentially concentrated by the use of mirrors, that enters it through a transparent cover. The cavity is thermally insulated from the exterior using the most suitable materials. Radiation losses are commonly reduced by using selective coatings.

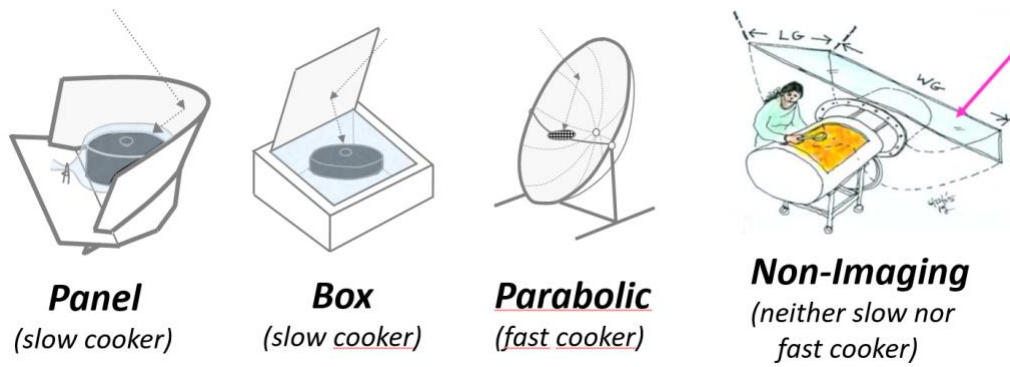


Fig. 1: Four common types of solar cookers (Drawings courtesy of Professor Celestino Ruivo and Architect Joel Goodman)

In order to reach out temperatures high enough to fry and reduce cooking times, solar concentration has often been used, but reaching excessively high temperatures leads to a degradation of nutrients, a generation of toxic products and, due to the increase of thermal losses, to a reduction of its thermal efficiency. That is why it is a key point to design the solar cooker to reach not less, but not much more either, of the required temperature for the adequate cooking process; this is easy to be realised with the aid of nonimaging optics.

Nonimaging Optics

The matter of classical optics has been to resolve problems such as the designing imaging-forming optical systems of a very large aperture. Its applications include devices such as telescopes, microscopes, radiometers, variable focus lenses, etcetera. It is based on theory of electromagnetic waves and includes Snell's law of refraction and the phenomena of diffraction, interference, and even the photoelectric effect (Smith, 1966). By contrast, in nonimaging optics - developed just over half a century ago by Roland Winston, the then Soviet V. K. Baranov and G. K. Melnikov, as well as the German M. Ploke, among others - the underlying idea is, rather than forming images of the light source in a focal zone, it is desired to catch photons in a finite-sized zone, even if the "image" formed there has huge aberrations and is fragmented. For solar concentrators, like the ones used in our nonimaging solar ovens, that is very convenient cause nonimaging solar concentrators are much more efficient than the image-forming concentrators (Winston et al., 2005). Instead of pretending concentrate the sun light in punctual (or linear) focuses, light is conducted through mirrors and/or lenses to a finite region of many possible geometries wrapping the so called "absorber" of the concentrator. However, it must be recalled that: "imaging and nonimaging are not opposite concepts. Only if we restrict ourselves to a finite number of elements can perfect concentrators with plane apertures and axial symmetry not be obtained" (Winston et al., 2021).

3.1 The Compound Parabolic Concentrators

The solar concentrator with a flat absorber was the first to be discovered and were called "Compound Parabolic Concentrator" or CPC because it is formed, for the two-dimensional (2D) case, by two cylindric mirrors of parabolic section, as it is shown in figure 2. Point B is indeed the linear focus of the cylindric-parabolic segment CD, while C is the corresponding linear focus of parabolic segment AB. For mirrors hypothetical perfect, all rays ingressing the aperture area AD with an inclination -with respect to the CPC's axis- lesser than the acceptance half angle θ_0 would be reflected towards the absorber BC after impinging on one of the mirrors; of course, some rays can go directly to the absorber without any reflection. In this case, the non-truncated CPC has a geometric concentration $C_{g\ 2D} = \frac{|AD|}{|BC|} = 1/\sin(\theta_0)$, and for the 3D case, the geometric concentration is $C_{g\ 3D} = [|AD|/|BC|]^2 = 1/\sin^2(\theta_0)$. As the temperature that is possible to reach out with a solar concentrator depends mainly on C_g , the advantage of using a 3D concentration becomes evident.

The foregoing geometry geometry is ideal for applications where the absorber is naturally flat, as in PV systems, but is not quite good for applications like the heating of fluids, where clearly the more adequate geometry for the absorber is a cylinder of circular cross-section. Figure 3 shows a CPC-type 2D concentrator for this kind of absorber. Mirrors AE and FD are no longer parabolic, even though the "CPC" name remains. The Tolokatsin solar ovens takes advantage of this two CPC geometries as it is explained in next sections.

The main disadvantage of CPCs occurs when the acceptance angles are relatively small: the length of the mirrors becomes excessively large and there is a need to truncate them. The optimal truncation is obtained when most of the area of the mirrors is truncated and even so the consequent decrease in concentration does not prevent reaching out the required temperatures and radiative fluxes. However, that optimum condition depends on the variable proportions of diffuse and beam radiation present in a given instant. A criterion for an optimal truncation that is independent of the conditions of radiation is stated in the following section.

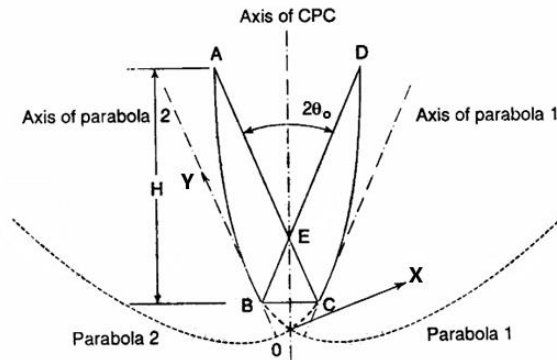


Fig. 2: The Compound Parabolic Concentrator for an flat absorber. It was the first nonimaging concentrator

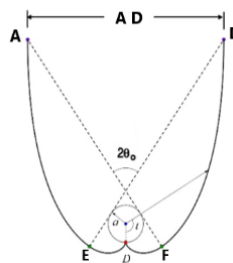


Fig. 3: The Compound Parabolic Concentrator for a circular absorber

3.2 Truncation of CPC mirrors according to Rincón's Criterion

Rincón's criterion states that: "the CPC must be truncated in such a way that rays parallel to the extreme rays (AC and BC in figure 3) are not blocked by the mirrors of the CPC" (Rincón et al., 2009). Observing figure 3, this implies that straight line QT, which is tangent to the parabolic mirror CD at point T, must be parallel to the extreme ray BD. That occurs, independently of the shape of the absorber -assuming that its surface is uniformly convex or plane- when the truncation angle t_t is $t_t = \pi/2 - 3\theta_0$, where $\theta_0 < \pi/6$. With this procedure, the angular window for the acceptance of diffuse irradiance increases from $2\theta_0$ for the non-truncated CPCs, to $6\theta_0$ for the optimally truncated ones. This criterion is used in all the nonimaging concentrators of the Tolokatsin solar cookers.

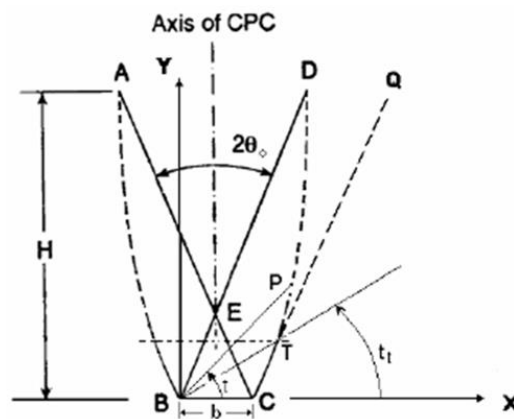


Fig. 4: Truncation of a CPC for a plane absorber according to Rincón's Criterion

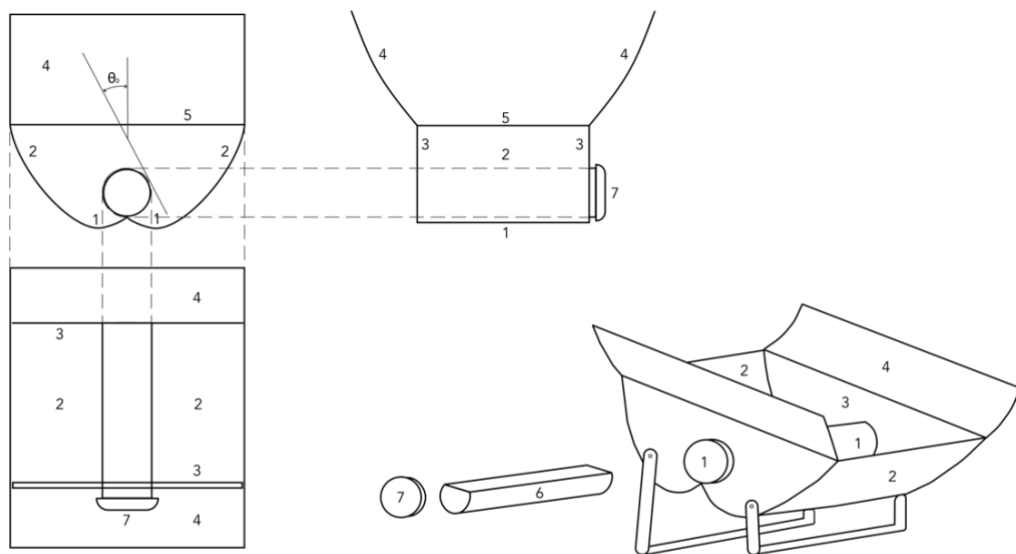
The Tolokatsin Solar Ovens

In 1995 the first “Tolokatsin” solar cooker was designed (Rincón et al., 1997) with which it was possible to cook any food on almost every day of the year. *Tolokatsin* is a Mexica Nahuatl word meaning “dear girl born in Toluca”, cause in that city they were designed for the first time. It was based on anidolic optics, and the original design consisted of a Multi Compound Concentrator (MCC) with exactly eight mirrors, distributed in four pairs, as it is shown in figure 5.

The essential point of these MCCs is that they achieve a 3D concentration from mirrors of simple curvature, truncated according to Rincón's Criterion. This makes them very easy to manufacture, even in locations far from industrial zones. The absorbers of the MCCs are cylindrical containers that can be hermetically closed which are heated by the concentrated sunlight reflected by the mirrors. Inside the cylindrical absorbers, at least one food grade stainless steel tray is placed in which the food is placed as shown in figure 6. Depending on the size of the containers, one, two ore more trays can be placed inside them. No meal can be burn, since the temperature inside the ovens commonly does not exceed 140°C.

With a hermetic closure the ovens work pressurized, but their containers were designed to resist presures one order of magnitude greater than the maximum working pressure attainable with the solar concentrator, so no need of valves nor pressure regulators for a quite safe operation. In more than 25 years of operation of a few thousands of these cookers, no incidents or accidents have been reported.

Thanks to their hermetic closures and that they operate at temperatures at which no bacteria or viruses can survive, as long as the containers are not opened, once the food is cooked they could be kept for days without the need for refrigeration (this is not recommended of course). Food can be placed in the oven even before dawn, and taken out whenever it is desired to eat (noon, afternoon, evening, etcetera). The food will be well cooked, tastier and nutritious than that cooked the conventional way. The time required to cook the food depend on the insolation, the amount of food placed into the oven, the type of food and the thickness of the portions - the thinner, the faster the cooking.



Mirror's pair number	Cross-section's geometry
1	Involute of a circle
2	CPC for a circular absorber
3	Straight line
4	CPC for a flat absorber

1. Container of hermetic closure
2. CPC for a cylindrical absorber
3. Flat mirrors
4. CPC for a flat absorber
5. Transparent cover
6. Stainless steel tray
7. Cap of the container

Fig. 5: Sketch of the *Tolokatsin* Solar Cooker model 1995. It has a 3D Multi Compound Concentrator built up with 8 single-curvature mirrors



Fig. 6: Photographs of two *Tolokatsin* solar cookers model 1995 with their containers opened showing their stainless steel trays with cooked meals inside them

The Constructal Law

Bejan's *Constructal Law* states that “for a finite-sized flow system to persist over time, it must evolve in such a way as to provide ever greater access to the currents that flow through it” (Bejan, 2016). After Bejan's statement, the constructal law has been applied to various engineering systems (Rocha et al., 2012) and more recently in systems of renewable energy by analyzing a solar chimney and an oscillating water column (Dos Santos et al., 2017). In these investigations the configurations that the involved elements should have in order to obtain the most adequate configuration to favor the flows involved were established.

With regard to Multi Compound Solar Concentrators, which clearly belong to devices based on non-imaging optics, the flows are made of concentrated sunlight. Even though the first design of the Tolokatsin furnaces made more than 25 years ago seemed to be optimized in that a 3D solar concentration had been achieved from simple-curvature mirrors which allowed a great performance, according to the constructal theory the design would always be subject to improvement (there is no absolute optimum, cause the optimum evolves in time!). “Every where we look what we see is evolving because it is free to move and morph. Without freedom to change, there is nothing, no design, no evolution, and therefore no future” (Bejan, 2020). In the following lines an account of the evolution of these still-in-evolution-design solar furnaces (used not only as cookers, but sterilizers, ceramic ovens, etc.) is briefly described.

Evolution of the Tolokatsin Ovens

In figure 7 it is summarised the evolution of the Tolokatsin solar ovens. In Fig. 7a it is shown the original design made 25 years ago. That was a very successful one: it got an effective 3D concentration with acceptance angles of $\sim 45^\circ$, which allowed a stationary operation for about 3 hours with no need of adjusting its orientation to follow the Sun, enough time to cook black beans and all kind of foods. There was also no need to take care of the cooking process and the cook could do other tasks without having to expose himself to solar radiation.

The operation temperature beneath irradiances of the order of 700 W/m^2 were around 120°C , so practically all food recipes could be cooked on time. Lots of meals were prepared with this model in the campus of the Autonomous University of Mexico City, where every thursday there were free solar meals opened to every body to demonstrate this simple technology. There still are some videos in the internet from those times.

However, in some cloudy days the elapsed time needed to cook was longer than three hours, and some difficult meals were not possible to cook on a reasonable time. To improve the ovens performance, the pair of parabolic mirrors -which also use to serve as hinged caps clearly visible in Fig. 7a- were substituted for two pairs of parabolic mirrors, as it is shown in the Tolokatsin V model (Fig. 7b), increasing in two the number of mirrors. This change improved the performance of the solar concentrator, but its complexity was increased too.

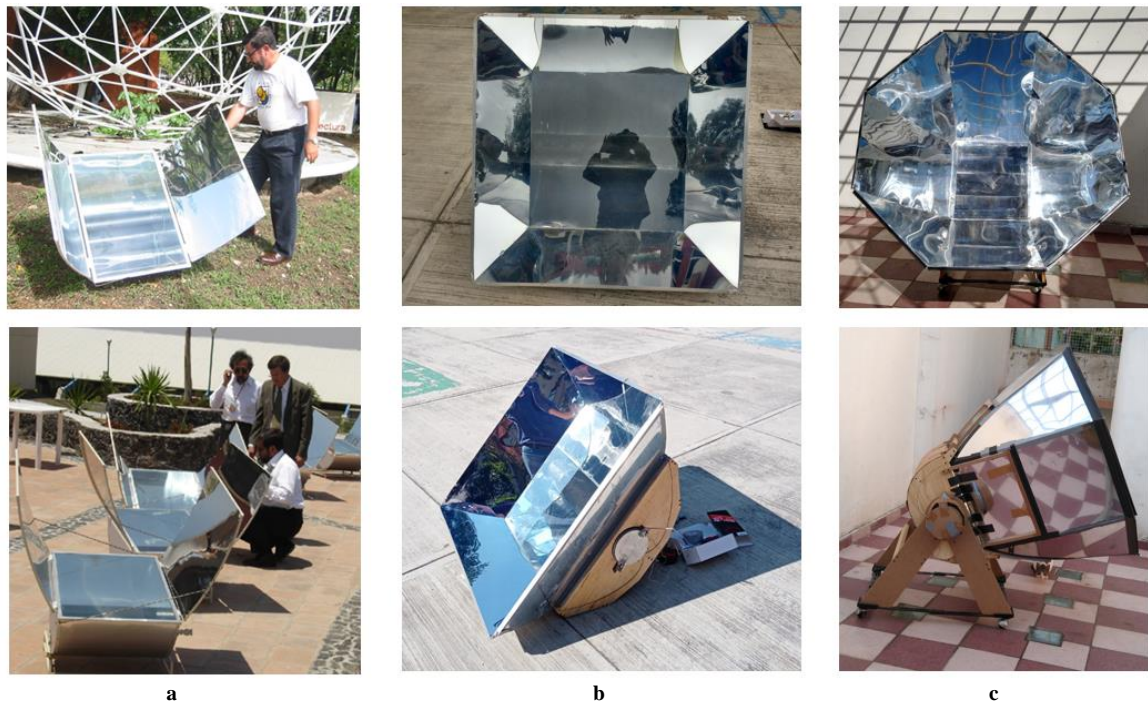


Fig. 7: Constructual evolution of the Tolokatsin solar cookers. a) 1995-model with 8 single-curvature truncated mirrors for a 3D solar concentration; b) Tolokatsin V, with 10 single-curvature truncated mirrors; c) Tolokatsin 2020 with 10 mirrors

Trying to get an even better performance, “to provide ever greater access to the light flow through the MCC” as Constructal Law dictates, the aim was now focused on: a) increasing the optical efficiency of the concentrator by reducing the average number of reflections of rays that imping on the absorber, b) to increase the concentration ratio (and so the stagnation temperature of the absorber), and c) to improve thermal insulation. This procedure led to the Tolokatsin 2020 model wch conceptual design is shown in figure 8. As in the previous design (Tolokatsin V), solar concentration is made in two stages: the first realised by an octagonal arrangement of single-curvature parabolic mirrors optimally truncated, and a second stage (with no contribution to the concentration ratio) consisting in a cavity limited by an involute mirror and two flat ones perpendicular to it, sealed by a double transparent cover, as it is shown in Fig. 8b.

The first stage has a regular octagonal acceptance area of lateral length L , and an exit square area, also with lateral length L . With this construction the geometric concentration ratio is $C_g = 2\sqrt{2} + 3$, with a semiangle of acceptance $\theta_0 = 15.782^\circ$ which allows a stationary operation for more than two hours. Figure 9 shows the meshing of the MCC mirrors used for the ray tracing studies.

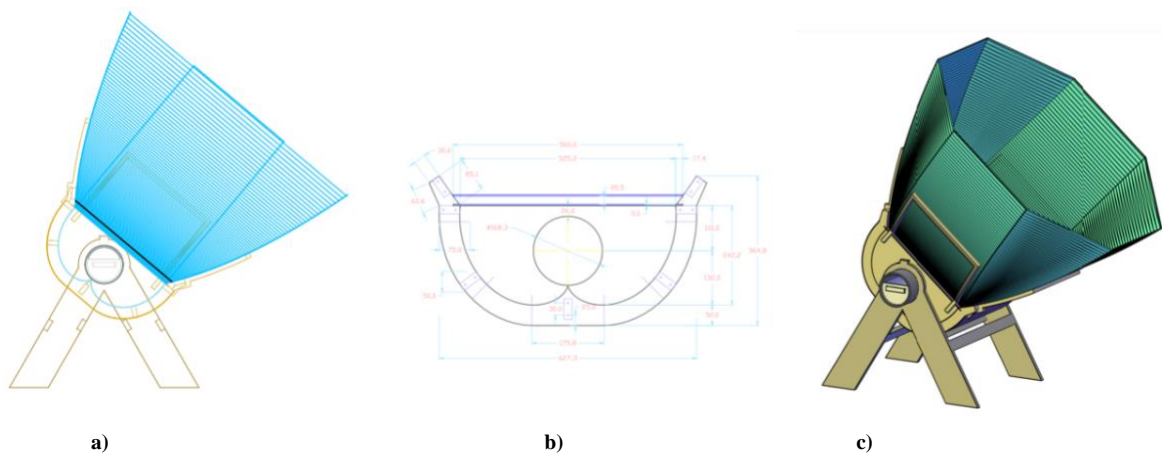


Fig. 8: Conceptual design of the Tolokatsin 2020 solar oven. a) lateral view, b) cavity for the absorber, c) isometric view

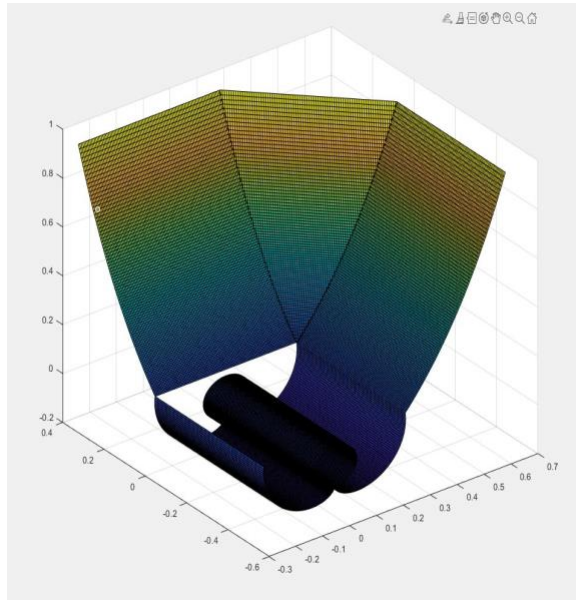


Fig. 9: Preparing the meshing of the MCC mirrors for the ray-tracing studies

6.1 A simple mathematic model

The basic procedure to optimise the design with the aim to get a very efficient operation can be sketched using the following extremely simplified model.

Performing a rough energy balance on the absorber of the solar concentrator, it is obtained that the useful heat power \dot{Q}_u is approximately:

$$\dot{Q}_u \approx A_c G_s \eta_o - A_r [\varepsilon \sigma T_r^4 + (h \Delta T - \kappa \nabla T)] \quad (\text{eq. 1})$$

Here:

A_c is the acceptance area,

G_s is an effective solar irradiance at A_c , $G_s \approx (\cos \beta) G_b + \frac{G_d}{C_g}$ (from Rabl, 1976a), where G_b and G_d are the beam and diffuse irradiances, C_g is the geometric concentration and β is the incidence angle

η_o is the optical efficiency

A_r is the absorber exposed area

ε is the emittance of the exterior surface of the absorber

σ is the Stefan-Boltzmann constant

T_r is the effective mean temperature of the exterior surface of the absorber

h is the mean value of the heat transfer coefficient on the external surface of the absorber

κ is the mean value of the thermal conductivity of the insulation

In turn, the optical efficiency is modeled as:

$$\eta_o = f \alpha \tau \rho^{(N)} \quad (\text{eq. 2})$$

Where:

f is an MCC *interception factor* (Duffie and Beckman, 2013) that takes into account mirror errors

α is the absorptance of the exterior surface of the absorber

τ is the transmittance of the transparent cover

ρ is the reflectance of the mirrors

N is the average number of reflections

The average number of reflections N is evaluated following the pioneering work of Rabl, (1976b, 1977); factors f , τ are strongly dependent on the incidence angle of the rays on the acceptance area of the MMC. The optical analyzes were performed using the US NREL's software *SolTrace* (González-Mora & Rincón-Mejía, 2021).

These ray-tracing studies have some similarity to those performed by Cooper et al. (2013) on compound parabolic concentrators with polygonal apertures. Besides the energy balances, entropy calculations were made up in order to optimise the second-law efficiency inspired on early works on this thema (Petela, 1964 and 2005; Parrott, 1978).

Thus, the thermal efficiency of the MCC is finally given by:

$$\eta_t = \frac{\dot{Q}_u}{A_c G_g} \approx \frac{G_s}{G_g} \eta_o - \frac{1}{c_g G_g} \left[\varepsilon \sigma T_r^4 + (h \Delta T - \kappa \nabla T) \right] \quad (\text{eq. 3})$$

where $G_g = G_b + G_d$ is the global irradiance

Introducing the factors j and g , which compare the thermal losses for convection and conduction with that due to the radiation one (thermal radiation is the main and limiting heat loss in solar concentrators), and the ratio of diffuse to global irradiances:

$$j = \frac{(h \Delta T - \kappa \nabla T)}{\varepsilon \sigma T_r^4} ; g = \frac{G_d}{G_b} \quad (\text{eq. 4})$$

$$\Rightarrow \frac{G_s}{G_g} = \left(\frac{1}{1+g} \right) \left(\frac{(\cos \beta) C_g + g}{c_g} \right) \quad (\text{eq. 5})$$

With two limiting cases: a) $g \rightarrow 0$ (there is no diffuse irradiance), $\Rightarrow \frac{G_s}{G_g} \rightarrow \cos \beta$ (eq. 6)

and b) $g \rightarrow \infty$ (there is no beam irradiance), $\Rightarrow \frac{G_s}{G_g} \rightarrow \frac{1}{c_g}$ (eq. 7)

From eq. 3, the mean temperature of the absorber is approximately:

$$T_r \approx \left[\frac{\left(\frac{G_s}{G_g} \eta_o - \eta_t \right) c_g G_g}{(1+j) \varepsilon \sigma} \right]^{\frac{1}{4}} \quad (\text{eq. 8})$$

According to eq. 8, thermal efficiency is always lesser than the optical one, which is evidently the governing parameter to be optimised. When $\eta_t \rightarrow 0$, the absorber attains its stagnation temperature T_{stg} which maximum and minimum values, corresponding to the no diffuse irradiance and no beam irradiance, are respectively:

$$T_{stg \max} \approx \left[\frac{(\cos \beta) \eta_o c_g G_g}{(1+j) \varepsilon \sigma} \right]^{\frac{1}{4}} = \left[\frac{(\cos \beta) \eta_o c_g G_b}{(1+j) \varepsilon \sigma} \right]^{\frac{1}{4}} \quad \text{and} \quad T_{stg \min} \approx \left[\frac{\eta_o G_d}{(1+j) \varepsilon \sigma} \right]^{\frac{1}{4}} = \left[\frac{\eta_o G_g}{(1+j) \varepsilon \sigma} \right]^{\frac{1}{4}} \quad (\text{eq. 9})$$

Now, defining different functional groups that establish the degrees of freedom of the system that directly affect the thermal power of the MCC, an objective function can be determined. When performing the variation of the geometric parameters, the optimum operating values are determined (González-Mora et al, 2020).

6.2 Artisanal manufacture of the prototype

In spite of the relative complexity of this design, the manufacture of the first prototype of this model was made with easy in a backyard workshop with simple conventional tools, as it is shown in figure 10.

The materials utilised for the manufacture of this prototype were wood for the main structure of the legs and the cavity for the absorber, food grade stainless steel for the trays (this model can use two trays of 5 L each, or one alone of 10 L), a commercial aluminum tube (6 inches of nominal diameter) for the absorber with a self-formulated selective coating on this, two tempered flat glasses for the transparent cover of the cavity, celulosic thermal insulation, and 95% reflective anodized aluminum sheets for solar applications for the ten mirrors of the MCC. The whole apparatus is monted on wheels for an easy manual orientation in two tracking axes.



Fig. 10: Artisanal construction of the first prototype of the Tolokatsin 2020 solar oven

Operational experience

More than 25 years of operation of different models of Tolokatsin solar ovens have proven their high performance, reliability and efficiency. Hundreds of international food recipes have been successfully prepared with them. However, for a more objective assessment of their performance, it is necessary to resort to already existing Technical Standards or to propose new methodologies for this purpose. The existence of very varied types of solar cookers used throughout the world has led to the establishment of standardized methodologies with which the different models can be compared. Amongst the most frequently reported regulations, the American Standard ASAE S580 (2003) and its revision (American Society of Agricultural and Biological Engineers, 2013), which provides a single figure of merit: the normalized heating power, stands out. However, it has the disadvantage of not evaluating the thermal efficiency nor the second-law efficiency of the cookers by seeking only to estimate the heating power normalised with respect to an irradiance of reference of 700 W/m^2 when the cooker temperature is 50°C above the ambient temperature. Short before this standar, Funk (2000), has had proposed a procedure with two merit figures in his pionering proposal. Other authors have proposed especific procedures for their especific solar cookers (Mullik et al., 1996; Sharma et al., 2005; Zhao et al., 2018).

These procedures, although more well designed to be applied in box-type or panel-type solar cookers, generally involve a linear fit of temperature data against insolation times when a certain amount of water is heated, which is reasonable for kitchens that barely reach their boiling temperature, but fail when it comes to characterizing cookers that can widely exceed 100°C , since the losses due to thermal radiation are sensibly non-linear and a linearization of the performance curves is quite inadequate. This leads to proposing new methodologies for the characterization of concentrating solar cookers, among which the Tolokatzin cookers are included. The methodology that will be used in both Mexico and India as soon as the COVID pandemic subsides is that proposed by Khallafa et al. (2020), in which instead of using water, which has a low boiling temperature, it is proposed the use of glycerin as the test load material.

Meanwhile, the tentative application of the Standard ASAE S580 to the Tolokatsin V in a winter day (January 15, 2020) in Mexico City provided the data of Table1 that stand out a normalized heating power above 232 W when 7 kg of water (placed in two trays with 3.5 kg each) increased 50.5°C its temperature. The Tolokatsin 2020 model has more than double of that power, but we are cautiously waiting for newer results.

Tab. 1: Experimental results for the Tolokatsin V solar cooker

	Local hour	G_s (W/m^2)	T_{amb} ($^\circ\text{C}$)	$T_{\text{H}_2\text{O tray 1}}$ ($^\circ\text{C}$)	$T_{\text{H}_2\text{O tray 2}}$ ($^\circ\text{C}$)	$T_{\text{H}_2\text{O}}-T_{\text{amb}}$ ($^\circ\text{C}$)	Adjusted Power (W)
1	10:20	518.6	19	20	30	1	197.62
2	10:40	584.3	20	30	23	6.5	233.86
3	11:00	631.6	21	40	28	13	214.72
4	11:20	696.8	21	51	36	22.5	245.19
5	11:40	699.7	23	61	45	30	244.12
6	12:00	752.8	23	71	56	40.5	272.01
7	12:20	736.0	24	80	69	50.5	232.44
8	12:40	733.3	24	88	82	61	233.21
9	13:00	733.6	25	95	93	69	117.21

Conclusions

It is a big mistake to continue burning fossil fuels or firewood for cooking in the world, when there is such a great solar resource, with which it is possible to cook any food almost any day of the year, using solar cookers of reasonable cost and high performance, self-built or industrialized. The massive use of solar cookers would significantly contribute to reducing greenhouse gas emissions and achieving all the SDGs of the 2030 UNO's Agenda. Solar cookers offer a great potential to fight energy poverty that deserves to be explored in the light of new technologies. They also offer new possibilities for caravans, cabins, hikers, recreation, and rest in areas of great ecological value.

To guarantee and excellent performance and a great reliability, even in unfavorable weather conditions for the use of other solar cookers, it is recommended those designed with the aid of nonimaging optics and the systematic application of the constructal theory, as the Tolokatsin solar ovens are. The main drawbacks of this type of solar cookers are their slightly greater manufacture costs and a rather sophisticated design; but even so, they can be fabricated with easy even in remote small villages of impoverished countries employing locally available inexpensive materials.

Acknowledgments

We deeply thank Dr Alejandro de las Heras and Dr Marina Islas from UAEMex for their collaboration in the manufacture, instrumentation, and testing of the prototype of the Tolokatsin 2020 solar furnace, and MSc Marco Aurelio Díaz Leal for preparing the plans and the manufacture of the prototypes of these solar ovens, to Eduardo Vázquez Valdez for his aid in the manufacture and testing of Tolokatsin V and 2020 prototypes, and to C. Dr Eduardo González-Mora for the 2E (energy and entropy) analyzes of the concentrators and the ray tracings using the US NREL's *SolTrace* software. We also want to thank Prof. Celestino Rodrigues Ruivo of University of Algarve, Portugal, and Architect Joel Goodman for their drawings in Fig. 1.

References

- American Society of Agricultural and Biological Engineers, 2013. Standard ASAE S580. Testing and reporting solar cooker performances, St. Joseph, MI, USA.
- Bailis, R., Drigo, R., Ghilardi, A., Masera, O., 2015. The carbon footprint of traditional woodfuels. *Nature Climate Change*, 5, 266–272.
- Balmes, J. R., 2019. Household air pollution from domestic combustion of solid fuels and health. *J. Allergy Clin. Immunol.*, 143, 1988.
- Bejan, A., 2016. *Advanced Engineering Thermodynamics*, 4th ed. John Wiley & Sons Inc., Hoboken.
- Bejan, A., 2020. *Freedom and evolution*, Springer, Cham.
- Boogaard, H., van Erp, A.M., Walker, K.D., Shaikh, R., 2017. Accountability Studies on Air Pollution and Health: the HEI Experience. *Curr Envir Health Rpt* 4, 514–522.
- Conibear, L. et al., 2020. *Environ. Res. Lett.* **15** 094096.
- Cooper T., Dähler F., Ambrosetti G., Pedretti A., Aldo Steinfeld, A., 2013. Performance of compound parabolic concentrators with polygonal apertures. *Solar Energy*, 97, 308-318.
- Dos Santos, E., Isoldi L., Gomes M., and Rocha L., 2017. The constructal design applied to renewable energy systems, in: Rincón, E.A., de las Heras, A. (Eds.), *Sustainable Energy Technologies*. CRC Press, Boca Raton, pp. 45–59.
- Duffie, J.A., Beckman, W.A., 2013. *Solar Engineering of Thermal Processes*, 4th ed. John Wiley & Sons Inc., Hoboken.
- Funk, P.A., 2000. Evaluating the international standard procedure for testing solar cookers and reporting performance. *Solar Energy* 68 (1), 1–7.
- González-Mora, E., Rincón-Mejía, E., Morillón, D., 2020. Diseño constructal de CPCs y la evolución de los diseños Tolokatsin. *Proc. XVII Congreso Ibérico y XIII Congreso Iberoamericano de Energía Solar* (in

Spanish). Lisboa. <https://doi.org/10.34637/cies2020.1.2013>

González-Mora, E., Rincón-Mejía, E., 2021. Optical evaluation of the Tolokatsin-2020 high-efficiency solar cooker. Proc. ISES SWC 2021, to be held 25-29 Oct. 2021.

Khallafa, A.M., Tawfikb, M.A., El-Sebaic, A.A., Sagade, A.A., 2020. Mathematical modeling and experimental validation of the thermal performance of a novel design solar cooker. *Solar Energy*, 207, 40-50.

Kumar, P., Metha, S., 2016. Poverty, gender, and empowerment in sustained adoption of cleaner cooking systems: Making the case for refined measurement. *Energy Research & Social Science*, 19, 48-52.

Kundapur, A., 2018. A treatise on solar cookers, International Alternate Energy Trust, Udupi.

Lecuona, A., 2017. Cocinas solares. Fundamentos y aplicaciones, Marcombo (in Spanish), Madrid.

Mullick, S.C., Kandpal, T.C., Subodh, K., 1996. Testing of box-type solar cooker: second Figure of merit F2 and its variation with load and number of pots. *Solar Energy* 57 (5), 409-413.

Nandwani, S., 2004. Cocina-horno solar, Editorial Fundación UNA (in Spanish), Heredia, C.R.

Parrott, J.E., 1978. Theoretical upper limit to the conversion efficiency of solar energy. *Solar Energy* 21, 227-229.

Petela, R., 1964. Exergy of Heat Radiation. *J. Heat Transfer* 86, 187-192.

Petela, R., 2005. Exergy analysis of the solar cylindrical-parabolic cooker. *Solar Energy* 79, 221-233.

Rabl, A., 1976a. Comparison of solar concentrators. *Solar Energy*, 18, 93-111.

Rabl, A., 1976b. Optical and thermal properties of compound parabolic concentrators. *Solar Energy*, 18(6), 497-511.

Rabl, A., 1977. Radiation transfer through specular passages - a simple approximation. *Int. Jour. Heat and Mass Transfer* 20 (4), 323-330.

Rincón, E. et al., 1997. Desarrollo de cocinas solares con base en concentradores del tipo CPC. Proceedings XXI National Week of Solar Energy (in Spanish), ANES, Chihuahua.

Rincón, E.A., Durán, M.D., Lentz, A., 2009. New Solar Air Heater Based on NonImaging Optics for High-Temperature Applications, in: ASME 2009 3rd International Conference on Energy Sustainability, Volume 2. pp. 839-844.

Rocha, L.A.O., Lorente, S., and Bejan, A. (Eds.), 2012. Constructal Law and the Unifying Principle of Design. Springer, New York.

Rosenthal, J., Quinn, A., Grieshop, A.P., Pillarisetti, A., Glass, R., 2018. Clean cooking and the SDGs: Integrated analytical approaches to guide energy interventions for health and environment goals. *Energy for Sustainable Development*, 42, 152-159.

Sharma, S.D., Iwata, T., Kitano, H., Sagara, K., 2005. Thermal performance of a solar cooker based on an evacuated tube solar collector with a PCM storage unit. *Sol. Energy* 78, 416-426.

Smith, W.J., 1966. Modern Optical Engineering, McGraw-Hill, New York.

Winston, R., Miñano, J., Benítez, P., 2005. Nonimaging optics, 1st ed. Elsevier, New Jersey.

Winston, R., Jiang, L., Olikier, V., 2021. Nonimaging optics. Solar illumination system methods, design, and performance. CRC Press, Boca Raton.

World Health Organization, 2018. Household air pollution and health: key facts (<https://www.who.int/news-room/fact-sheets/detail/household-air-pollution-and-health>, accessed 14 July 2021).

Zhao, Y., Zheng, H., Sun, B., Li, C., Wu, Y., 2018. Development and performance studies of a novel portable solar cooker using a curved Fresnel lens concentrator. *Sol. Energy* 174, 263-272.

Optimizing the Operational Parameters of an Electrochemical Purification Cell for Corrosion Mitigation in CSP Plants During Operation

Kerry Rippy, Elizabeth Howard, Liam Witteman, and Judith Vidal

National Renewable Energy Laboratory, Golden, Colorado (USA)

Abstract

To make concentrating solar power (CSP) cost-competitive, the next generation of CSP plants will increase efficiency by operating at a higher temperature, which will require a new thermal energy storage material. One option for the thermal energy storage material is a ternary chloride salt that is stable at the temperatures required, but reacts easily with the atmosphere to form MgOHCl , a corrosive impurity. If left unchecked, this impurity will corrode the containment alloys, potentially leading to dangerous spills. We are working to design an electrochemical purification cell to remove MgOHCl from the molten chloride salt during CSP plant operation. In this paper, we use specification of the Gen3 CSP liquid pathway pilot plant to assess the rate at which purification must occur. Additionally, we analyze possible process flow pathways integration of the purification cell into the pilot plant in order to achieve target purification rate. Ultimately, we determine that implementation of a single reactor through which all chloride salts flow is the most efficient design to reduce impurity concentration below 0.1 mol % impurity.

Keywords: Concentrating Solar Power, Chloride Salts, Corrosion Mitigation, Electrochemical Purification

1. Introduction

The U.S. Department of Energy's (DOE) SunShot Initiative includes cost and performance goals for concentrating solar power (CSP) systems (Mehos et al. 2017). CSP is an excellent candidate to replace nonrenewable energy sources because it stores thermal energy to generate electricity on demand. For CSP to meet the goals outlined by the SunShot Initiative, the next generation of CSP plants (Gen3) will need to operate at a higher temperature than the current heat transfer fluid will allow. DOE has supported the development of plans to use the ternary molten chloride salt NaCl-KCl-MgCl_2 as the heat transfer fluid in the Gen3 CSP plants, because it is stable above 800°C and relatively inexpensive (Ding, Gomez-Vidal, et al. 2019; Ding, Shi, et al. 2019).

The primary barrier to using molten chloride salt in a CSP plant is that it is highly corrosive, especially at the high temperatures required (Ding, Gomez-Vidal, et al. 2019). Corrosion in molten chloride salt is driven by oxide and hydroxide impurities (Gomez-Vidal and Tirawat 2016). A procedure using particles of electropositive Mg can purify the salt prior to use in the CSP plant, but the ternary chloride salt is strongly hygroscopic, which leads to corrosive impurity formation during plant operation (Gomez-Vidal and Tirawat 2016). Specifically, any interaction of the molten chloride salt with water in the atmosphere leads to the formation of MgOHCl , which ionizes into corrosive MgOH^+ . The Mg particle purification procedure cannot be used within the CSP plant, because it relies on temperatures above 650°C to melt the Mg particles, and the cold side of the next generation of CSP plant will be at 500°C (Mehos et al. 2017).

To remove impurities that enter the molten salt during CSP plant operation, we are designing an electrochemical cell with Mg anodes to reside in the cold side of the plant. The electrochemical system has been shown to control corrosion at the lab scale. We predicted the rate of moisture ingress into the CSP plant to provide an upper bound on the concentration of MgOH^+ entering the purification cell. Then, we selected and modeled various salt flow pathways to identify ideal process flow.

2. Results and Discussion

2.1. Specifications of the CSP Plants

The modeling in this paper uses the specifications of a conceptualized pilot plant, obtained from the CSP Gen3 Liquid-Phase Pathway to SunShot report.(Turchi et al. 2021)

The pilot plant will utilize a commercial ternary $MgCl_2$ - KCl - $NaCl$ salt. It will have a total salt inventory of 180 MT or 2.15×10^6 mol. Variation of the volumetric flow rate of molten salt through the pilot plant (Q) is expected. In this work, we use $Q = 110$ gpm as the default volumetric flow rate within the reactor. The purification cell will be located on the cold side of the plant, with a temperature of $500^\circ C$.(Turchi et al. 2021)

A continuous sweep of $N_2(g)$ is required to protect pump components from salt vapor deposition and freezing. The expected sweep rate in the pilot plant is approximately 15 scfm ($24 Nm^3/h$). In the high purity $N_2(g)$ will be used, up to 1 ppm H_2O may be present.

2.2. Formation of corrosive impurities in salt

According to Zhao et al.,(Zhao, Klammer, and Vidal 2019) when the corrosive species $MgOH^+$ is present in the ternary salt at 5 wt. %, the yearly corrosion rate of Haynes 230 is greater than $3200 \mu m$ per year. When the concentration of this species is reduced to less than 0.5 wt. %, the yearly corrosion rate of Haynes 230 is reduced to around $40 \mu m$ per year. Thus, it is essential to keep the concentration of $MgOH^+$ low.

However, $MgOHCl$ forms within the ternary salt when exposed to moisture via reaction (1). Based on ongoing work, reaction (1) is fast; mass transport of water vapor through the diffusion boundary layer is the limiting step in this process. Given ullage gas residence times on the order of seconds or more, turbulent ullage gas flow, and high ullage gas flow rate, we assume that all moisture present in the ullage gas will react with the ternary salt.

The resulting $MgOHCl$ then disassociates into its component ions via reaction (2) to form $MgOH^+$. Given the specifications of the pilot plant and $N_2(g)$, this means that up to 1.8×10^{-5} mol H_2O could enter the plant per minute according to equation (3). These results, graphed in Fig. 1, show the potential of accumulation of significant amounts of corrosive $MgOH^+$ over time.

2.3. Mitigation of corrosive impurities in salt

We propose removal of $MgOH^+$ from the ternary salt via an electrochemical purification method, illustrated in Fig. 2. The overall removal of $MgOH^+$ will be accomplished via the net purification reaction (4). To avoid buildup $MgOH^+$ and associated corrosion, rate of this purification process must exceed the rate of impurity formation that was graphed in Fig. 1.

Ongoing laboratory experiments indicate that the electrochemical purification reaction is limited by mass transfer. Specifically, it is limited by diffusion of $MgOH^+$ to the electrode, which is slow. The electrochemical purification reaction at the electrode surface is relatively fast.

Having identified diffusion of $MgOH^+$ as the rate limiting process, we investigated several different geometric configurations for integration of purification unit into the pilot plant to achieve desired purification. First, we considered purification of a small amount of the total flow of molten salt in a loop appended to the main flow, as illustrated in Fig. 3a. Second, we considered use of multiple reactors in parallel, enabling a decrease the volumetric flow rate within each reactor but still purifying all the salt, illustrated in Fig. 3b. Third, we considered use of a single purification cell purifying all the salt, illustrated in Fig 3c.

We evaluated feasibility of each of these approaches by calculation of the electrode surface area required in each case to achieve target purification rate. We selected electrode surface area as a key metric for two reasons: 1) Cost of purification units will scale with electrode surface area. 2) Electrode surface area has previously been identified as a key variable in scaling electrochemical reactors used in industry.(Liu et al. 2014) Thus, the configuration requiring the least surface area will be preferred.

We found that for the pathway depicted in Fig 3a, the flow rate of salt through the purification cell could be lowered, leading to longer residence times. However, since only a fraction of the salt would be purified in this scenario, the purification cell would have to reduce impurity concentration to an extremely low wt. % to achieve

the required purification rate. Our modeling indicated that it would ultimately result in a larger required electrode surface area to purify only part of the salt as compared to purification of all the salt.

For the scenario depicted in Fig. 3b, a lower flow rate is possible in each cell. However, we found that a high Reynolds number and turbulent flow increase mass transport to the electrodes. Thus, for the pilot plant, splitting the salt into multiple parallel purification units adds complexity but does not enhance purification rate.

Ultimately, we found that for the pilot plant, the least surface area would be required for the scenario depicted in Fig. 3c. This also has the advantage of being the simplest design. We note that in a commercial-scale plant with much higher salt flow rate and higher salt volume, similar analysis could yield a different result.

3. Conclusion

Utilizing the specifications of the proposed Gen3 liquid pathway pilot plant, we have calculated a required purification rate for our proposed electrochemical purification method. Furthermore, we have evaluated several different configurations for integration of the purification cell into the pilot plant, and determined that a single purification unit which purifies all of the salt in a single pass is the most viable option for achieving the target purification rate in the Gen3 liquid pathway pilot plant.

4. Tables, figures, equations, and lists

4.1. Figures

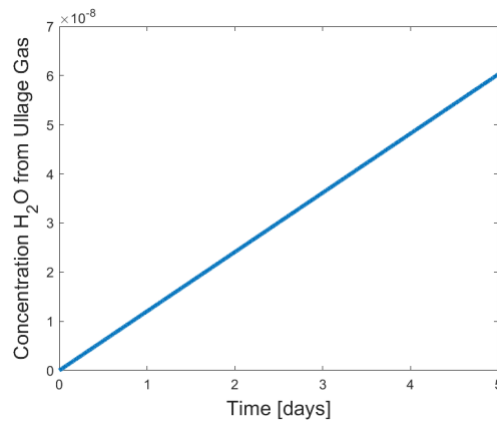


Fig. 1: The concentration of H₂O in the molten salt as it enters from the ullage gas.

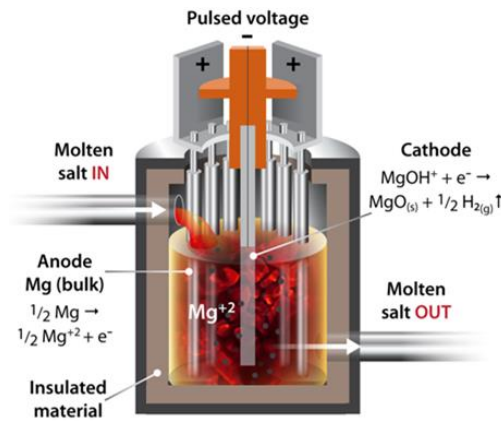


Fig. 2: Illustration of proposed electrochemical purification method. At the cathode, corrosive impurity MgOH^+ is electrochemically converted to MgO , a solid which can be removed from salt via filtration. At the anode, dissolution of Mg^+ balances the removal of the Mg in the MgO , keeping the composition of the ternary salt consistent.

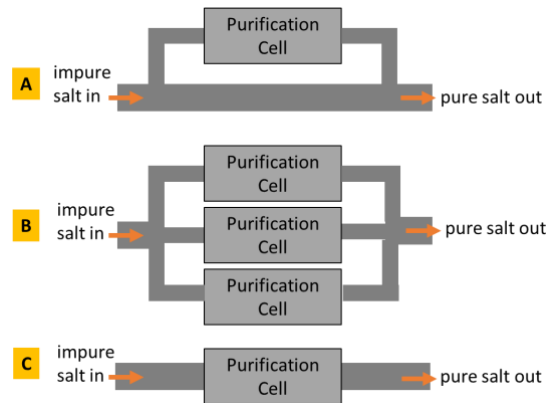
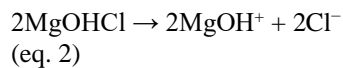
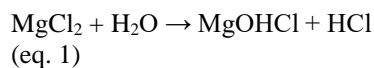
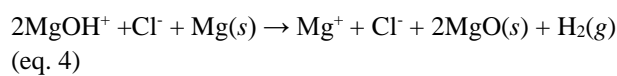


Fig. 3: Possible configuration for molten salt purification using an electrochemical cell. For the pilot plant, our analysis showed that the pathway depicted in 3c required the lowest electrode surface area.

4.2. Equations



$$\frac{15 \text{ scf}}{\text{min}} \cdot \frac{1.20 \text{ mol N}_2}{1 \text{ scf}} \cdot \frac{1 \times 10^{-6} \text{ mol H}_2\text{O}}{1 \text{ mol N}_2} = \frac{1.8 \times 10^{-5} \text{ mols H}_2\text{O}}{\text{min}} \quad (\text{eq. 3})$$



5. Acknowledgements

This work was supported by DOE SETO grant CPS #35931 and the Mines/NREL Advanced Energy Systems Graduate Program. We also thank Sridhar Seetharaman, Matthew Earlam, and Stephen James.

6. References

- Ding, Wenjin, Judith Gomez-Vidal, Alexander Bonk, and Thomas Bauer. 2019. 'Molten chloride salts for next generation CSP plants: Electrolytical salt purification for reducing corrosive impurity level', *Solar Energy Materials and Solar Cells*, 199: 8-15.
- Ding, Wenjin, Hao Shi, Adrian Jianu, Yanlei Xiu, Alexander Bonk, Alfons Weisenburger, and Thomas Bauer. 2019. 'Molten chloride salts for next generation concentrated solar power plants: Mitigation strategies against corrosion of structural materials', *Solar Energy Materials and Solar Cells*, 193: 298-313.
- Gomez-Vidal, Judith C., and Robert Tirawat. 2016. 'Corrosion of alloys in a chloride molten salt (NaCl-LiCl) for solar thermal technologies': *Solar Energy Materials and Solar Cells*, 234-44.
- Liu, Chenglin, Ze Sun, Guimin Lu, Xingfu Song, Yulong Ding, and Jianguo Yu. 2014. 'Scale-up design of a 300 kA magnesium electrolysis cell based on thermo-electric mathematical models', *The Canadian Journal of Chemical Engineering*, 92: 1197-206.
- Mehos, M., Craig Turchi, Judith Vidal, Michael Wagner, Zhiwen Ma, Clifford Ho, William Kolb, Charles Andraka, and Alan Kruiuzenga. 2017. *Concentrating Solar Power Gen3 Demonstration Roadmap*. OSTI 1338899
- Turchi, Craig S., Samuel Gage, Janna Martinek, Sameer Jape, Ken Armijo, Joe Coventry, John Pye, Charles-Alexis Asselineau, Felix Venn, William Logie, Armando Fontalvo, Shuang Wang, Robbie McNaughton, Daniel Potter, Theodore Steinberg, and Geoffrey Will. 2021. "CSP Gen3: Liquid-Phase Pathway to SunShot." OSTI 1807668, United States.
- Zhao, Youyang, Noah Klammer, and Judith Vidal. 2019. 'Purification strategy and effect of impurities on corrosivity of dehydrated carnallite for thermal solar applications', *RSC Advances*, 9: 41664-71.

Reuse of Solar Photovoltaic Systems for Social and Economic Benefit

Rich Stromberg^{1 2 3 4 5}

¹ University of Alaska, Fairbanks (USA)

² Alaska Center for Energy and Power, Fairbanks (USA)

³ Western Colorado University, Gunnison (USA)

⁴ Coldharbour Institute, Gunnison (USA)

⁵ Community Appropriate Sustainable Energy Security (CASES) Partnership, Saskatoon (CA)

Abstract

Photovoltaic modules, inverters and mounting hardware are getting deinstalled as systems age, owners seek to upgrade to more efficient use of rooftop space, buildings undergo major remodeling and other factors. Recycling of modules and other components to recover valued raw materials currently lacks economic processes with the capacity to responsibly deal with the volume of equipment being taken offline. Sending inverters to overseas electronic recycling locations and the modules and mounting systems to landfills has become a default path for many. While incentives for middle- and upper-income buyers have been instrumental in driving lower system costs over the past decades, low- and moderate-income (LMI) households who are most burdened with energy costs have been excluded from this green revolution. Much of this decommissioned equipment still retains many years of energy generation potential and reinstalling these systems to benefit previously excluded populations presents significant opportunity to fill the social equity gap in the triple bottom line of solar energy while delaying ecological impacts until recycling processes can be developed to meet economic and throughput requirements for a sustainable business model. This paper presents the framework for foundational research of the multiple facets of culture, social equity, ecology, policy, technology and sustainable business to create a movement that repurposes high-value equipment away from waste streams and towards a more equitable society.

Keywords: Reuse solar PV, social benefit, ecological benefit, energy burden, policy, sustainable business.

1. Introduction

As solar photovoltaic (PV) systems reach the 20- to 25-year expiration of module warranties, system owners begin to consider replacement using newer technology with significantly higher efficiencies for the same footprint and features not previously available with their original systems. Some PV array owners are upgrading their systems well before the end of their warranty period for similar reasons. Rather than disposing of these legacy systems in a landfill or in raw material reclaim, there is potential for a second life – possibly as long as a second 20 to 25 years.

While federal and state incentives have played a large role in increasing the demand for solar PV systems which, combined with other programs have greatly reduced the per watt installed cost, most incentives have only been available to middle and upper income households and businesses (Heeter *et al.*, 2018). Because low-income households typically lack the income levels or home ownership to participate in tax credit programs, disparities in social equity have increased in the triple bottom line of solar energy. These disparities have created an ever-widening social equity gap that impacts energy-burdened households to a greater extent. (Figure 1)

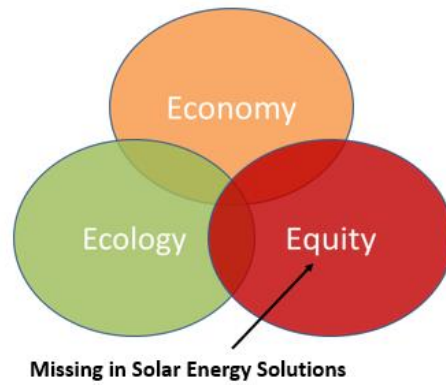


Fig. 1: Social equity gap in commercial and residential PV systems.

Equitable Solar Solutions™ (ESS™) was founded in January 2018 by the author and five undergraduate capstone students at Western Colorado University’s Clark Family School of Environment and Sustainability with the intent to take used solar photovoltaic equipment otherwise destined for the landfill or reclaim and reinstall for the benefit of low-income households. By April 2018, ESS™ had become a key program of Coldharbour Institute, a 501c3 nonprofit that promotes regenerative living practices. Under this business structure, equipment donors receive a tax donation letter that allows for a deduction on their taxable income in addition to any tax credit they may qualify for in purchasing a new PV system.

Two years later, ESS™ has received donations of around 600 PV modules totaling 83 kilowatts of nameplate capacity and more than 55 kilowatts of grid-tie inverters along with various mounting hardware. Age of donated equipment ranges from as old as 20 years in service to systems that have only operated for 12 years, 8 years and one 2-year-old residential system from a home that had been purchased with the intent of tearing it down to build condominiums. Primary focus of the ESS™ program is to ensure that all reinstalled equipment is not only operational but will be reliable over the proposed 20-year lifetime of future projects. This is critical so that recipients are assured of getting PV systems of the highest quality rather than being a disposal site for unwanted waste. The secondary focus encompasses project development by working with partner agencies to identify qualifying households and provide funding for the balance of installation costs.

Projections for volumes of decommissioned solar PV systems can be estimated from historical installed capacity numbers and assumptions of 20- or 25-year system lifetimes. While some commercial and residential system owners may upgrade early, utility-scale generating systems are typically operated under a fixed 20- to 25-year power purchase agreement with less likelihood of early decommissioning. Assuming a 20-year system lifetime and yearly installed capacity in the U.S. (Table 1), as much as 4 megawatts (MW) of solar PV equipment may be retiring at the time of this publication, rising to 10 or 11 MW over the following year.

Tab. 1: U.S. PV Installations, 2000-2012 GTM Research & SEIA (U.S. Solar Market Insight 2012 Year in Review, 2013)).

Installations (MWdc)	2000	2001	2002	2003	2004	2005	2006	2007	2008	2009	2010	2011	2012
Residential	1	5	11	15	24	27	38	58	82	164	246	302	488
Non-Residential	2	3	9	27	32	51	67	93	200	213	336	826	1,043
Utility	0	3	2	3	2	1	0	9	16	58	267	760	1,781
Total Installations	4	11	23	45	58	79	105	160	298	435	848	1,887	3,313

Absent other options, much of the decommissioned PV modules will be sent to landfills with inverters shipped to overseas electronics recyclers. Rails and mounting hardware can easily be sent to regional metal recycling centers. While landfill disposal of silicon-based PV modules comes with low environmental risks, the mounting volumes of waste on the horizon can have a significant impact on municipal landfill capacities causing accelerated need to plan, construct and finance new landfill space. These impacts carry a risk of eroding the solar industry’s social license to operate. In addition to a lack of industry capacity to recycle current volumes of PV modules, the present average processing cost of \$20 per module well exceeds the ~\$2 market value of recoverable raw materials (Sandoval, 2021). Reuse of solar PV systems presently offers the most economic

option until future PV module recycling processes can be developed to extract raw materials at a cost lower than the market value of those materials (Tao *et al.*, 2020).

Two years after inception, the Equitable Solar Solutions™ model has successfully demonstrated proof of concept through installed pilot projects and eagerness of equipment owners and installers to donate equipment with only minimal advertising and solicitation. The challenge moving forward is to understand what barriers exist and which paths provide the most sustainable business models to proliferate solar PV reuse. These factors extend beyond just the technical and financial realm to encompass cultural/social, ecological and political considerations. Included within these primary frameworks exist numerous subfactors that must be understood and addressed to develop successful roadmaps. (Figure 2) Further exploration has revealed that even these subfactors break down more into critical details that inform root cause analysis and solution options. These frameworks comprise the structure being used for doctoral research in reuse of solar PV systems for social and ecological benefit.

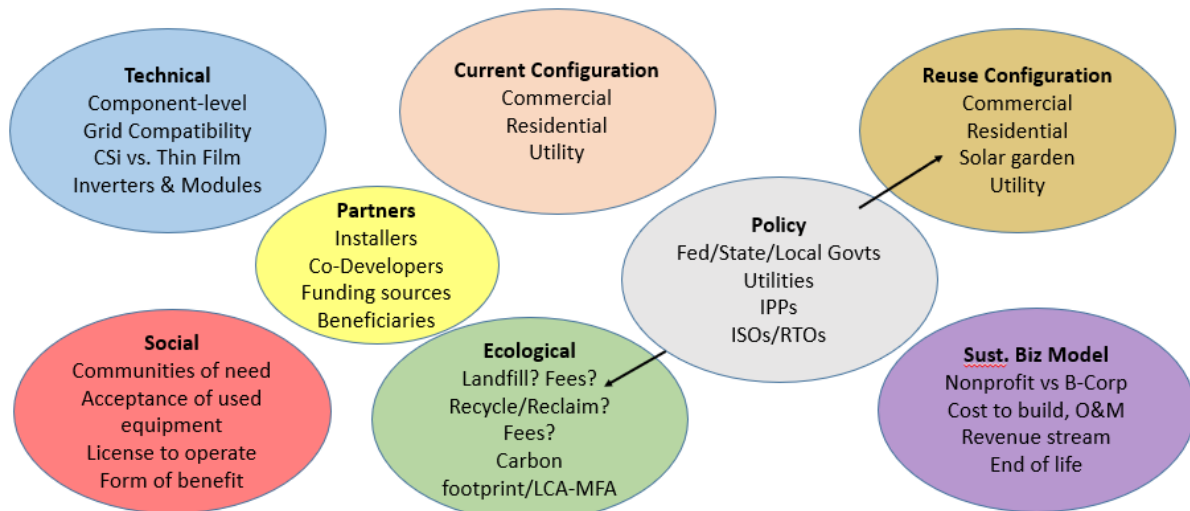


Fig. 2: Primary and secondary focus areas for researching reuse of solar PV equipment for social and ecological benefit.

2. Methods

2.1 Technical

Assessing the quality and degradation of donated equipment is essential to the ESS™ program. The inventory of currently-installed PV systems spans several decades during which components, materials and manufacturing processes have evolved. While not commonplace, product recalls have occurred – most notably certain BP Solar modules manufactured between 1999 and 2007 (www.bpsolarsettlement.com, 2016), all REC modules sold in 2008 (‘REC to Recall All of Its Solar Panels From 2008’, 2009) and one model of Bosch solar modules from 2011 through 2013 (Pickerel, 2017). Manufacturing changes between and within manufacturers can impact degradation rates and failure modes (Jordan and Kurtz, 2013a). Absent a well-documented characterization across all surplus equipment, testing methods must be developed to screen out non-functioning and lower-quality inverters, modules and other system components.

PV modules degrade over time from exposure to UV light, ambient heat and high humidity (Jordan and Kurtz, 2013b). Module power output degradation rates range from near zero to more than 3 percent, but median degradation rates are around 0.5 percent per year and average rates of 0.7 to 0.8 percent per year. It should be noted that thin-film modules have a higher annual degradation rate than silicon technologies (Jordan and Kurtz, 2013a).

Osterwald *et al.* has found an initial rapid degradation rate of PV modules due to oxygen recombination in the bulk crystalline structure. Long-term degradation is dominated by exposure to ultraviolet (UV) light. Encapsulant browning is not thought to result in long-term performance losses (Osterwald *et al.*, 2002). Wohlgemuth and Petersen found that hard failures were commonly caused by corrosion and breaks in the

interconnections between cells (Wohlgemuth and Petersen, 1993).

While manufacturers and laboratories have equipment capable of detailed cell and module characterization, “outdoor field testing has played a vital role in quantifying long-term behavior and lifetime for at least two reasons: it is the typical operating environment for PV systems, and it is the only way to correlate indoor accelerated testing to outdoor results to forecast field performance.” (Jordan and Kurtz, 2013a) Legacy systems still in operation can be assessed for the presence of failed inverters and modules using power analyzers or PV curve tracers such as the Solmetric PVA-1000S. Characterizing performance degradation though can be challenging if all modules are not oriented in the same direction and if access to measuring backside module temperature is impeded. This method produces a useful aggregated result across the entire array or string but backside thermal imaging offers the ability to detect certain failure modes while the PV array is operating (Chattopadhyay *et al.*, 2018). DC optimizers allow for isolation of bad modules while larger systems can be evaluated string by string.

ESS™ personnel adopted a module characterization and test flow consisting of: 1) cleaning any frontside debris/dust; 2) temperature stabilization in the sun of each module for a minimum of 20 minutes; 3) visual inspection of the frame, junction box, cables, frontside (discoloration, metal defects, burn marks, corrosion) and backside film (bubbles, tears, cracks, burn marks, bad vibes); 4) measuring open circuit voltage and short circuit current coincident with backside temperature and plane of array solar irradiance; and 5) thermal imaging of the module backside under short-circuit conditions. (Figure 3) Throughput for full characterization is around six modules per hour for a team of two people. ESS™ has since increased throughput to 35 modules per hour by selecting 10 modules out of each donated batch for complete degradation analysis with the remaining modules receiving a visual inspection, measuring short circuit current independent of module temperature and solar irradiance and backside thermal imaging. ESS™ has plans to build a test array that will provide a platform for testing inverters.

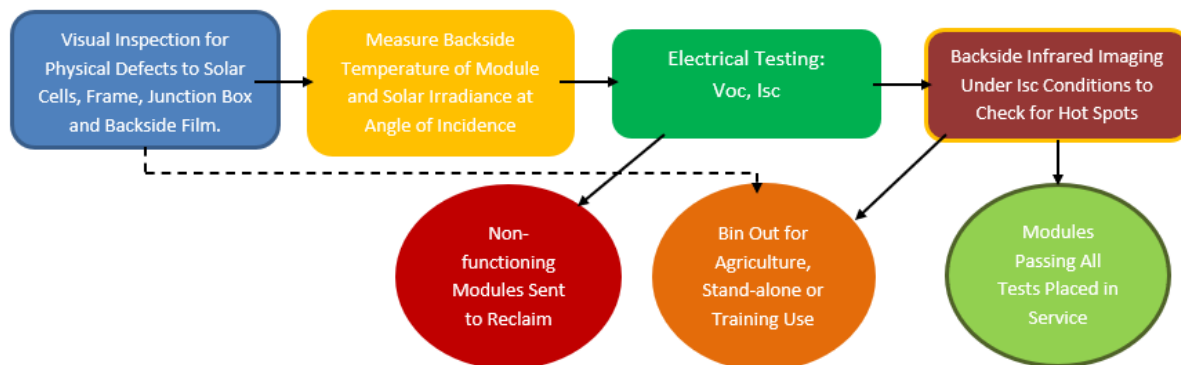


Fig. 3: PV module test flow.

ESS™ has been operating under the assumption that visual defects such as 1) discoloration of the frontside encapsulant, 2) corrosion/delamination within the frontside encapsulant not associated with any burn marks or breach of the backside film or 3) cracks/holes in the backside film not associated with any infrared thermal hot spots should be considered as potential future failure modes rather than merely cosmetic defects (Figures 4a and 4b). Subsequent literature review has caused ESS™ to consider that some of these defects may in fact accelerate year-over-year degradation or cause complete product failure in the future (Jordan and Kurtz, 2013a). ESS™ will be setting up a long-term monitoring configuration in which modules are connected to DC loads to produce maximum power so that specific solar cells representative of various visual defect types can be studied year by year.

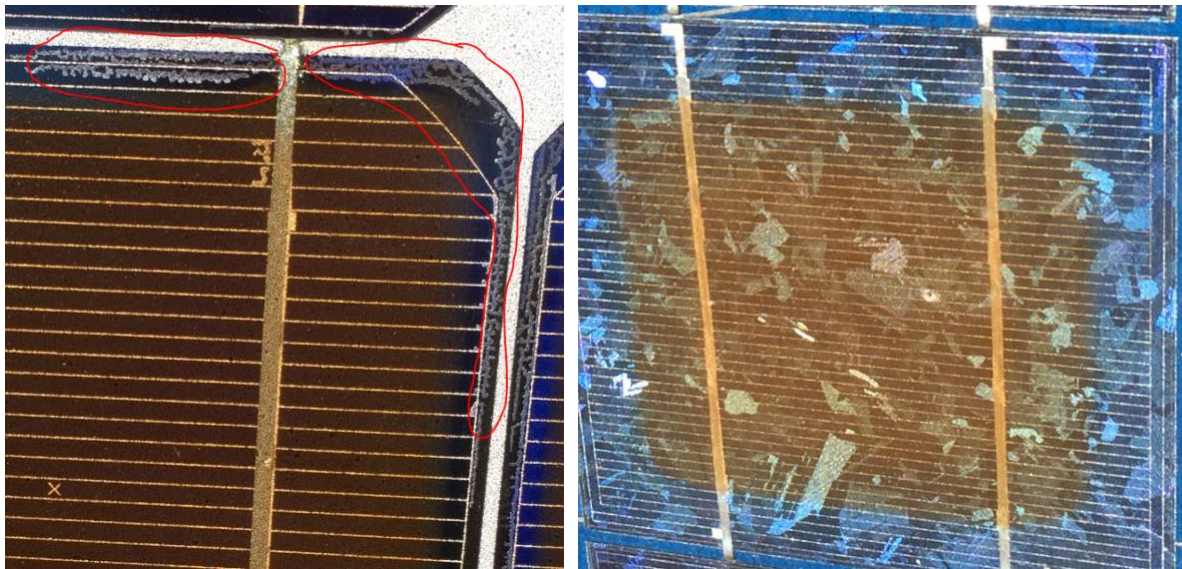


Fig. 4a and 4b: Cell corrosion/delamination and encapsulant browning/discoloration.

All 600 modules acquired by the ESS™ program have been silicon-based technology which has dominated 80 to 95 percent of the PV module market over the past decade. Thin film technologies such as cadmium-telluride (CdTe) rigid modules and copper indium gallium di-selenide (CIGS) flexible modules account for the present remaining five percent of the current work market (Philipps *et al.*, 2021). Any thin film module donations will be considered for evaluation purposes only until sufficient data exists to support a long-term redeployment as the flexible modules are offered with a 5-year limited power warranty versus the 20- to 25-year warranty typical with silicon-based rigid modules (‘SunPower Flexible Solar Panels | SPR-E-Flex-110’, 2018).

DC to AC inverters offer more challenges for reuse than PV modules. Extended warranties are available but most manufacturers offer a standard 10-year product warranty (Svarc, 2021). This reduced warranty may correlate to greater long-term risk for PV array operation. Some inverter suppliers offer replacement circuit boards that can be swapped out by trained personnel but availability of those replacement parts cannot be assured 30 years after the original manufacturing date. Longer-term inverter reliability will be a key focus of this research both in the field and at the planned test array. It may be possible to detect early indicators of inverter failure that could allow for proactive replacement in the field or even screening at the time of donation.

In addition to a focus on inverter reliability, electrical code compliance and grid compatibility will be considered. Once an older inverter is removed from a particular installation, it may no longer meet electrical code requirements for rapid disconnect (NEC 690.12). In some cases, ancillary components may be available to bring the new system up to compliance although the upgrade cost may come close to that of a new inverter. Future code changes could create new challenges with reuse of grid-tie inverters. Larger utility-scale PV arrays and community solar gardens must be compatible with inverter-based resource connectivity/disconnectivity requirements, low voltage ride-through and essential reliability services at time of re-commissioning (Ropp, 2019).

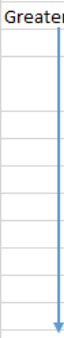
2.2 Cultural and Social

Redeploying equipment that is not capable of operating for an additional 20-year economic life cycle can erode public opinion of the product quality and their perception of the ESS™ model. Testing of all donated equipment is essential to build customer confidence in the product and the service that it offers. If new owners received untested reuse PV systems with early failures, this could create a perception of receiving a lower value asset and others within their community may become resistant to participating in the program. Lower-income communities might rightly claim that they are a dumping ground for society’s electronic waste. Further, deploying substandard systems can erode the social license to operate enjoyed by all renewable energy technologies. Ensuring that customers receive quality and reliable systems is paramount to a reuse business model and social movement.

The vision statement of the ESS™ program is “reusing solar PV systems to create the greatest value for those with the greatest need.” Determining who has greater and lesser need and where the greatest benefit will be

possible is achieved using a defined hierarchy of needs (Table 2) to assess where customers land within that hierarchy. People living without any electricity have the highest need followed closely by those with no available grid connection who must run small gas-powered generators. A 2014 report from RMI points out that 14 percent of homes on tribal lands are not connected to an electric grid (*Native Energy: Rural Electrification on Tribal Lands*, 2014). A major factor driving these households isolated from electrical infrastructure is the existence of disperse homesites on large areas of land that make the cost of extending the local distribution grid to each home prohibitive compared with costs in denser urban and suburban locations. The ESS™ program has discussed potential projects with tribes and there is a unique benefit in partnership that would allow tribal governments to leverage the value of reuse equipment as cost-share on federal grants.

Tab. 2: Hierarchy of needs.

Priority	✓ All That Apply	
Greater Need 	People Living Without Electricity	
	People Struggling to Pay Energy Bills	
	People Living in Low-Efficiency Housing with Inability to Pay for Improvements	
	Underserved/Underrepresented Groups	
	Habitat Homeowners	
	Landlords Serving Lower-Income Populations	
	Educational Opportunities	
	Nonprofits	
	Agricultural Users	
	Government Buildings	
	For-Profit	
	Lesser Need	Other Installations/Homeowners

The U.S. Dept. of Energy defines energy burden as “the percentage of gross household income spent on energy costs.” (*Low-Income Community Energy Solutions*, no date) In the U.S. low-income households can experience as much as three times the energy burden of higher income families. The factors driving this include: greater prevalence of electric heating systems, high air conditioning load and older homes with fewer (if any) energy efficiency features (*Low-Income Household Energy Burden Varies Among States — Efficiency Can Help In All of Them*, 2018). A pilot partnership developed with the Gunnison Valley Regional Housing Authority (GVRHA) uses the energy savings from a reuse solar PV array on a city-owned building and redirects those savings to fund energy efficiency upgrades in low-income households through an already-existing program run by GVRHA. Because of the ongoing benefits of energy efficiency measures, this approach results in more than twice the economic benefit over the lifetime of the project than had the money been spent on monthly energy bill assistance.

Other pilot configurations developed include bundling solar PV arrays with energy efficiency upgrades through the State of Colorado’s Weatherization Assistance Program where previous attempts to install brand new systems were not economical and partnering with Habitat for Humanity builders and homeowners such that system costs can be rolled in with the home financing. The result of the latter is that the total monthly cost of ownership including mortgage payment and utilities is less than building the home without a reuse solar PV array.

One of the more challenging populations in need are low-income rental households because of minimal incentive to upgrade buildings occupied by someone other than the owner. Low-income apartments do not provide an equal distribution of solar-compatible roof space for all units. Even where those rooftops provide good solar gain, agreements must be structured so that the financial benefit goes to the renter rather than merely allowing a landlord to charge higher rent. Apartments that lack individually-metered units also propose challenges with respect to apportionment of any energy savings. In 2017, the Government Accounting Office listed 48 percent of renting households as energy burdened (*Housing Cost Burden for Low-Income Renters Has Increased Significantly in Last Two Decades*, 2020).

One option being explored is the development of community solar gardens dedicated solely to low-income renters. Such a structure would guarantee lower monthly energy bills for the renter and subscription programs can be structured without down payments while meeting the needs of a more transient population (Heeter *et al.*, 2018). Qualification or eligibility can be tied to the Low-Income Home Energy Assistance Program (LIHEAP) or other public assistance programs.

Tenants in HUD housing do not presently have an opportunity to benefit from a reuse solar array or participation in low-income community solar gardens as those tenants are charged a fixed combined monthly rent and utilities payment calculated as 30 percent of their income. Any installed solar array could reduce costs for the HUD program but tenants might expect to see a drop in monthly bills that will not materialize due to this fixed 30-percent calculation. Creating such a false impression could have a negative impact on the ESS™ program.

LIHEAP participants pay a monthly utility bill and thus are a potential beneficiary of reuse solar arrays. Government partnerships similar to the City of Gunnison diverting energy savings from an array on a city building to the GVRHA energy efficiency program could also be structured to divert energy savings to LIHEAP-qualifying households or the LIHEAP program itself. Partnerships with commercial businesses can be structured to share the energy savings between the commercial partner and LIHEAP programs. In the future, transferring ownership of a utility-scale solar PV array for management of the ESS™ program could be used to cover program costs while providing assistance to LIHEAP participants.

Other target populations include small, minority-owned businesses and people with disabilities. ESS™ recently built a prototype mobile solar charging station for a motorized wheelchair user and is building a permanent charging station on the Western Colorado University campus for motorized wheelchairs and E-Bikes.

Historically marginalized communities can be skeptical of new programs, especially in light of past environmental injustices (Masten *et al.*, 2021). There will be significant research focused on building social movements, collaboration with local communities on needs assessments and involving local community members for training, employment and buy-in. ESS™ believes in starting with small pilot projects to lay the groundwork for long-term partnerships based on trust built over time as single-shot large projects have increased risk and can raise suspicions of profiteering. An ancillary concern for these pilot projects will be whether energy savings from subsidized or discounted PV arrays will trigger any energy use rebound effects akin to Jevons Paradox (Jevons, 1865; Foster, Clark and York, 2010).

The agricultural community plays a key role as recipients of second tier equipment that is not suitable for a 20-year rooftop installation. Electrically-functioning equipment with scratches and other visual defects can be placed on farms and ranches at heavily discounted costs where damage from livestock or the environment is less impactful from a financial perspective. Supporting the agricultural community has the added benefit of strengthening food security through lower energy costs.

A key goal of the ESS™ program is to build a social movement to drive awareness and adoption through institutionalized methods such as engaging legislatures, regulatory bodies and industry groups along with noninstitutionalized approaches like partnering with community and grassroots organizations within the target groups of those in need of energy assistance (Staggenborg, 2016). The long-term goal is to develop modular approaches and methods that can be replicated region by region across the country (Tarrow, 2011) to create an increased social license to operate through greater reach and benefit across populations who might have previously had no vested interest.

2.3 Ecological

In quantifying the life cycle carbon intensity of photovoltaic modules, Jean, et al. assume a 20- to 30-year operating life cycle before system decommissioning (Jean *et al.*, 2015). This is consistent with the 20- and 25-year operating warranty offered by most PV module manufacturers that guarantees at least 80-percent of original power output specification at that time. From their analysis of the carbon intensity of electricity in the US and in China, Jean et al. calculate “the median carbon intensity of [crystalline-silicon] PV modules manufactured in the U.S. and deployed in the U.S. [is] 36–65 g CO₂-eq/kWh ... [and] the carbon intensity of PV modules manufactured in China and deployed in the U.S. [is] 61–111 g CO₂-eq/kWh.” This range is representative of the PV modules that are donated to the Equitable Solar Solutions™ program and compares favorably to the much higher carbon intensities of natural gas (~500 g CO₂-eq/kWh) and coal (~1000 g CO₂-eq/kWh) (Trancik and Cross-Call, 2013). Jean et al concludes that “if our goal is to reduce emissions, it is far less important where the PV is made...than where it is used...and most important whether it is used at all.(Jean et al. 2015) Reusing solar equipment for an additional 20 years further reduces the carbon intensity over the lifetime of the modules by 43.78 percent assuming a consistent annual degradation rate or from 36-111 g down to 20–62 g CO₂-eq/kWh depending on where the modules were manufactured.

Some equipment does not meet ESS™' rigorous standards and must be downgraded in the applications for reuse, sent to a capable recycling facility or disposed of in a landfill. Eventually though, the reinstalled equipment has a finite lifetime and responsible end-of-life product management must occur.

While recent research shows that silicon-based PV modules can be safely disposed of in landfills (Sinha et al. 2020) despite the presence of lead solder and other trace materials, such disposal will eventually add significant volumes of material to those landfills. Further, this assumption of safety is based on the continued integrity of each landfill's leachate liner in perpetuity. Any breach of that liner or disposal in non-regulated landfills creates risk to human health and the environment as heavy metals leach into the groundwater and soil (Hernandez et al. 2014). Conversely, the aluminum frames of modules are easily removed/recycled and the silicon cells can be recycled with less energy and lower cost than mining and processing new silicon (Choi and Fthenakis 2010).

Factors driving volumes of PV waste in the U.S. include modules broken in handling, severe weather (high winds, hurricanes, large hail) and residents/businesses upgrading their systems after several decades to newer, more efficient technology. Early failure due to quality and reliability defects are rare in the U.S. In the future, volumes of PV waste are expected to increase dramatically as the first utility-scale solar farms of 1 megawatt and larger in size approach the end of their negotiated 20- and 25-year power purchase agreements (PPAs) with utility or large industrial power off-takers (*U.S. Solar Market Insight 2012 Year in Review*, 2013) The ESS™ model helps to buy time for industry to develop cost-effective recycling processes that can meet future volumes of PV modules as they meet their true end of life.

Current ease and low cost of disposing of solar PV modules in a landfill are a disincentive for system owners to pursue options that divert waste from landfills. Cheap disposal fees create environmental externalities that prevent development of cost-effective module recycling processes and business models (Eshet, Ayalon and Shechter, 2005). Policies that discourage landfill disposal would better incentivize reuse and recycling pathways. Siting of existing fossil fuel infrastructure as well as expanded waste disposal sites disproportionately impacts the public health of low-income and other marginalized communities (US EPA, 2014).

2.4 Policy

Policy and regulations impacting new and reuse solar PV systems exist across federal, state and local jurisdictions as well as within independent system operators (ISOs), utilities and independent power producers (IPPs). National Electrical Code and local government or utility interpretation can affect whether earlier modules and inverters can still be reused once removed from their original installation. They may also specify system modifications to meet new code requirements at the time of re-installation.

Current Colorado, Connecticut, Hawaii, Maryland, and Oregon statutes for participation in solar gardens provide for a small percentage of these cooperative installations to be "carved out" to benefit low-income energy users but some utilities interpret statute to prohibit construction of a solar garden that would target a specific low-income group of subscribers. Xcel Energy requires use of all new PV equipment to participate in their Solar*Rewards® program with involves renewable energy credits and a 20-year contract (*Solar*Rewards / Xcel Energy*, no date) but also offers a basic net-metering plan that would be compatible with used equipment and does not require a long-term contract (*Net Energy Metering / Xcel Energy*, no date),

Generation and Transmission companies often restrict their member electrical cooperatives from generating more than five percent of total community load while some local utilities self-impose limits on renewable energy systems. In 2020, Tri-State Generation and Transmission Association raised this limit for member cooperatives to 10 percent with certain restrictions (*Tri-State members advance greater contract flexibility, starting by increasing member self-generation opportunities by an additional 10% of system demand*, 2020).

Policies will be explored surrounding municipal waste disposal that could provide incentives for reuse or recycling of solar PV system components. These could exist in the form of volume limits or disposal fees that are either fixed or escalating. Incentives could be offered for raw materials such as recycled aluminum and glass that are easier to recover while funding could be appropriated for research and development of more efficient recycling processes and infrastructure. Other forms of incentive could provide municipal solid waste bill credits for system owners who donate old PV systems for reuse instead of disposing.

2.5 Finance and Sustainable Business

Local, state, federal and private grants have been beneficial in funding pilot projects and program development. These will continue to have a critical impact on program development and seeding new initiatives. Other forms of project financing will be needed to meet the expected volumes of decommissioned solar PV equipment in the coming decade.

For individual homeowners and business owners, federal and state tax incentives have been instrumental in increasing market demand that drives down the average costs of solar arrays, these tax credit approaches can only benefit those with high enough incomes to qualify for a \$5,000 or greater credit on their annual income taxes. Low-income households have fewer affordable financing options. Greater use of property-assessed clean energy financing can provide another option beyond home equity loans or other conventional financing. Pay-as-you-go options tied to utility bills that remain with the meter and are transferrable to new residents offer an alternative to loans (Heeter *et al.*, 2018; *Pay-as-you-go models: Innovation Landscape Brief*, 2020)

Alaska Native and Native American tribes can compete for special energy grants, but these programs are underfunded and the most energy-burdened tribes struggle to meet the 50-percent cost match requirements. Partnerships between tribes and ESS™ programs allow for valuation of the donated equipment towards these federal cost match requirements.

Additional grants combining funds from energy and environmental agencies could provide additional sources of funding that address both agencies' goals.

The ESS™ program is exploring split cost and split benefit structures in which a commercial business supports the vision of ESS™ to reuse solar PV systems to create the greatest value for those with the greatest need but also wishes to enjoy the benefits of renewable energy systems. Under such an arrangement, the value of the donated equipment is combined with the remaining cost of installation and the resulting percentage of commercial contribution determines how much of the monthly energy savings is retained by the business owner. The remaining funds are then distributed to a local social benefit program for energy, food, housing or other assistance under a memorandum of understanding (MOU).

As mentioned earlier, solar gardens could be developed specifically to benefit low-income households. In fact, this is ESS™' preferred option for providing energy assistance to renters who make up the largest category of low-income households and are most challenged with housing and energy costs (*Housing Cost Burden for Low-Income Renters Has Increased Significantly in Last Two Decades*, 2020). Funding for these low-income solar gardens could come in the form of targeted grants or could be financed with funding already allocated for assisting these populations. Both California and New York have used portions of their federal LIHEAP funds to finance rooftop solar PV arrays for LMI homes (Heeter *et al.*, 2018). The rationale for this approach is that these are ongoing appropriations and that the impact and payback are more beneficial than simple monthly energy bill assistance. Funding of low-income community solar gardens offers another path for state-managed LIHEAP programs to assist renters at an improved benefit-cost ratio compared with monthly bill assistance. These community solar gardens offer the added benefit to ESS™ of reduced project development time as future equipment donations can be used to expand existing solar garden arrays.

As first-generation utility-scale solar arrays reach the end of their power sales agreements, there may be tax benefits to the current IPPs or investor-owned utilities to donate these assets in place to a nonprofit ESS™ program who will then operate the facility throughout its second life and direct revenues after expenses to social programs. Lastly, various business structures (501c3 vs. benefit corporation vs. other) will be explored to determine which offer optimal use of donated equipment and available funds.

3. Results and Conclusions

From the donated equipment tested to date, nearly two-thirds of PV modules meet Tier 1 testing criteria and are suitable for redeployment on rooftop systems with an expected 20-year future life (Figure 5). Second tier modules have been deployed to ground-based and agriculture uses with third-tier modules being restricted to training purposes or short-term applications. Pilot projects have been completed and monitoring of array outputs

indicate systems are meeting or exceeding projections. As awareness of the ESS™ program grows, donations have increased to more than keep up with the present rate of project development. Additional development of wheelchair charging stations, USB device chargers and eBike charging stations in the public square and golf cart charging allows for other deployments beyond conventional solar arrays.

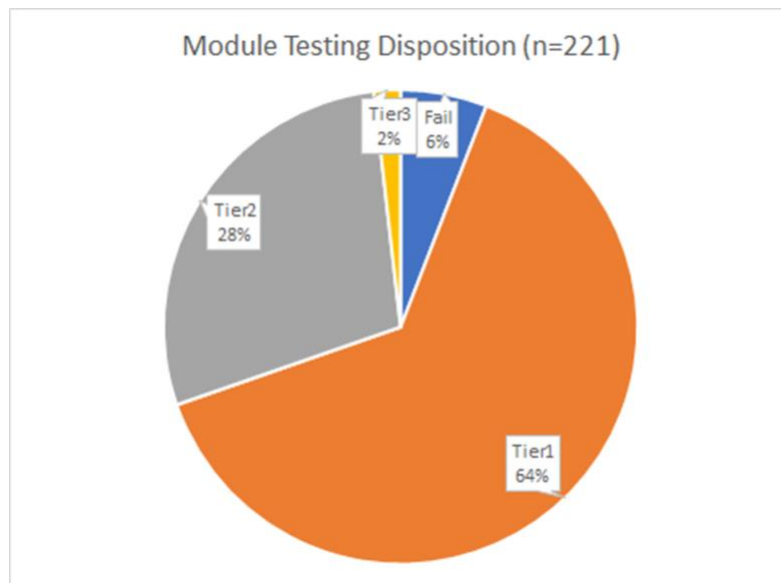


Fig. 5: Testing results from first batch of donated modules. Tier1 modules are approved for all uses.

The scope of this work is larger than a single doctoral degree and the advisory committee will be challenged to set appropriate sidebars on the degree plan that are separate from the longer-term focus of ESS™ program development and research that will continue beyond graduation. Post doctoral degree completion, opportunities exist for partnerships with agencies and industry consortia to further develop methods that divert future volumes of high-value assets from our waste streams to reuse applications that produce greater public benefit.

4. Acknowledgments

Research and activities related to the Equitable Solar Solution™ program takes place on the traditional lands of the Cheyenne, Jicarilla Apache, Nʉmʉnʉʉ (Comanche), and Nʉu-agh-a-tʉvʉ-pʉ (Ute) people. The author wishes to recognize the following people who have been instrumental in support of the Equitable Solar Solutions™ program and ensuing doctoral research. Dr. Richard Wies Jr., chair of my doctoral advisory committee and committee members Dr. Diane Hirshberg, Dr. Daisy Huang, Hon. Patricia Sekaquaptewa, Dr. Meng Tao and Dr. Greg Poelzer. School of Interdisciplinary Studies at University of Alaska Fairbanks. MJ Pickett, executive director at Coldharbour Institute. Dr. Kate Clark, director of the undergraduate ENVIS program at Western Colorado University's School of Environment & Sustainability. WCU student co-founders Maria Agazio, Montgomery Fraser, CJ Gooderham, Riley Moser and Avery Tait . WCU capstone students Travis Artac, Jill Krejci, Heather Reineking, Jack Thomas and Madi White. WCU graduate students Jason MacMillan, Sean Pope and James Cody. WCU student interns Demitra Biddle, Kallie Klein, Asher Lapello, Devin Richardson, Taylor Schultz, Sam Sellen, Austin Shirley and Triston Turner. Academic funding from Gwen Holdmann, executive director at Alaska Center for Energy and Power. Project funding from City of Gunnison and Ryan Harry with the Colorado Energy Office. Equipment donations from Active Solar Energies, Bank of Colorado in Boulder, Bryce and Katie Carter, EcoMark Solar, Sandia National Laboratories, Shaw Solar and Solar Solutions. Technical support from Dr. Abraham Ellis, Jesse Hoff, Nunatak Alternative Energy and Jeff Zirzow. Financial support from Sam Myers, Kelsey Wirth and Community Appropriate Sustainable Energy Security Partnership at University of Saskatchewan. Inspiration from Butch Clark. Kate Collardson with the Colorado Solar and Storage Association.

5. References

Chattopadhyay, S. *et al.* (2018) 'Correlating Infrared Thermography With Electrical Degradation of PV Modules Inspected in All-India Survey of Photovoltaic Module Reliability 2016', *IEEE Journal of Photovoltaics*, 8(6), pp. 1800–1808. doi: 10.1109/JPHOTOV.2018.2859780.

Eshet, T., Ayalon, O. and Shechter, M. (2005) 'A critical review of economic valuation studies of externalities from incineration and landfilling', *Waste Management & Research*, 23(6), pp. 487–504. doi: 10.1177/0734242X05060966.

Foster, J. B., Clark, B. and York, R. (2010) 'Capitalism and the Curse of Energy Efficiency: The Return of the Jevons Paradox', *Monthly Review*, pp. 1–12. doi: 10.14452/MR-062-06-2010-10_1.

Heeter, J. S. *et al.* (2018) *Design and Implementation of Community Solar Programs for Low- and Moderate-Income Customers*. NREL/TP--6A20-71652, 1488510. National Renewable Energy Laboratory, p. NREL/TP--6A20-71652, 1488510. doi: 10.2172/1488510.

Housing Cost Burden for Low-Income Renters Has Increased Significantly in Last Two Decades (2020) *National Low Income Housing Coalition*. Available at: <https://nlihc.org/resource/housing-cost-burden-low-income-renters-has-increased-significantly-last-two-decades> (Accessed: 19 July 2021).

Jean, J. *et al.* (2015) 'Pathways for Solar Photovoltaics', *Energy Environ. Sci.*, 8, p. 1200. doi: 10.1039/C4EE04073B.

Jevons, W. S. (1865) *The Coal Question; An Inquiry Concerning the Progress of the Nation, and the Probable Exhaustion of Our Coal Mines*. London: Macmillan and Co.

Jordan, D. C. and Kurtz, S. R. (2013a) 'Photovoltaic Degradation Rates-an Analytical Review: Photovoltaic degradation rates', *Progress in Photovoltaics: Research and Applications*, 21(1), pp. 12–29. doi: 10.1002/pip.1182.

Jordan, D. C. and Kurtz, S. R. (2013b) *SunPower® Module Degradation Rate*. SunPower Corp. Available at: <https://studylib.net/doc/18789305/sunpower%C2%AE-module-degradation-rate> (Accessed: 5 July 2021).

Low-Income Community Energy Solutions (no date) *Office of Energy Efficiency & Renewable Energy*. Available at: <https://www.energy.gov/eere/slsc/low-income-community-energy-solutions> (Accessed: 15 April 2021).

Low-Income Household Energy Burden Varies Among States — Efficiency Can Help In All of Them (2018) *Office of Energy Efficiency & Renewable Energy*. Available at: https://www.energy.gov/sites/prod/files/2019/01/f58/WIP-Energy-Burden_final.pdf (Accessed: 15 April 2021).

Masten, S. J. *et al.* (2021) 'Global Environmental Engineering for and with Historically Marginalized Communities', *Environmental Engineering Science*, 38(5), pp. 285–287. doi: 10.1089/ees.2021.0103.

Native Energy: Rural Electrification on Tribal Lands (2014) *RMI*. Available at: https://rmi.org/blog_2014_06_24_native_energy_rural_electrification_on_tribal_lands/ (Accessed: 15 April 2021).

Net Energy Metering | Xcel Energy (no date) *Xcel Energy*. Available at: <https://co.my.xcelenergy.com/s/renewable/net-metering> (Accessed: 19 July 2021).

Osterwald, C. R. *et al.* (2002) 'Degradation analysis of weathered crystalline-silicon PV modules', in *Conference Record of the Twenty-Ninth IEEE Photovoltaic Specialists Conference, 2002. Conference Record of the Twenty-Ninth IEEE Photovoltaic Specialists Conference 2002*, New Orleans, LA, USA: IEEE, pp. 1392–1395. doi: 10.1109/PVSC.2002.1190869.

Pay-as-you-go models: Innovation Landscape Brief (2020). International Renewable Energy Agency, p. 22. Available at: https://www.irena.org/-/media/Files/IRENA/Agency/Publication/2020/Jul/IRENA_Pay-as-you-go_models_2020.pdf?la=en&hash=7A2E7A7FF8B5BAB7748670876667628A39DE40D5.

Philipps, S. *et al.* (2021) *Photovoltaics Report*. Freiberg, Germany: Fraunhofer Institute for Solar Energy Systems, p. 48. Available at: <https://www.ise.fraunhofer.de/content/dam/ise/de/documents/publications/studies/Photovoltaics-Report.pdf>.

Pickerel, K. (2017) *Bosch solar panels recalled due to fire hazard*, *Solar Power World*. Available at: <https://www.solarpowerworldonline.com/2017/04/bosch-solar-panels-recalled-due-fire-hazard/> (Accessed: 13 July 2021).

‘REC to Recall All of Its Solar Panels From 2008’ (2009) *Solar Feeds*, 30 June. Available at: <https://www.solarfeeds.com/article/rec-to-recall-all-of-its-solar-panels-from-2008-june-30-2009/> (Accessed: 13 July 2021).

Ropp, M. (2019) *Guide to the IEEE 1547-2018 Standard and Its Impact on Cooperatives*. National Rural Electric Cooperative Association, p. 22. Available at: <https://www.nrel.gov/grid/ieee-standard-1547/assets/pdfs/guide-to-ieee-1547-2018-march-2019.pdf> (Accessed: 18 July 2021).

Sandoval, S. (2021) *Solar Panels Are Recyclable — But They’re Still Ending Up In Landfills*, *KMGH - The Denver Channel*. Available at: <https://www.thedenverchannel.com/expense-hinders-solar-panel-recycling> (Accessed: 1 May 2021).

*Solar*Rewards* | Xcel Energy (no date) Xcel Energy. Available at: <https://co.my.xcelenergy.com/s/renewable/solar-rewards> (Accessed: 19 July 2021).

Staggenborg, S. (2016) *Social movements*. Second edition. New York: Oxford University Press.

‘SunPower Flexible Solar Panels | SPR-E-Flex-110’ (2018). SunPower Corporation. Available at: <https://us.sunpower.com/sites/default/files/110w-flexible-panel-spec-sheet.pdf> (Accessed: 14 July 2021).

Svarc, J. (2021) *Best Solar Inverters 2021*, *CLEAN ENERGY REVIEWS*. Available at: <https://www.cleanenergyreviews.info/blog/best-grid-connect-solar-inverters-sma-fronius-solaredge-abb> (Accessed: 14 July 2021).

Tao, M. *et al.* (2020) ‘Major challenges and opportunities in silicon solar module recycling’, *Progress in Photovoltaics: Research and Applications*, 28(10), pp. 1077–1088. doi: 10.1002/pip.3316.

Tarrow, S. G. (2011) *Power in movement: social movements and contentious politics*. Rev. & updated 3rd ed. Cambridge ; New York: Cambridge University Press (Cambridge studies in comparative politics).

Trancik, J. and Cross-Call, D. (2013) ‘Energy Technologies Evaluated against Climate Targets Using a Cost and Carbon Trade-off Curve | Environmental Science & Technology’, *Environ. Sci. Technol.*, 47(12), pp. 6673–6680.

Tri-State members advance greater contract flexibility, starting by increasing member self-generation opportunities by an additional 10% of system demand (2020) *Tri-State Generation and Transmission Association, Inc.* Available at: <https://tristate.coop/tri-state-members-advance-greater-contract-flexibility-starting-increasing-member-self-generation> (Accessed: 19 July 2021).

US EPA, O. (2014) *Economic Incentives*. Available at: <https://www.epa.gov/environmental-economics/economic-incentives> (Accessed: 18 July 2021).

U.S. Solar Market Insight 2012 Year in Review (2013) *SEIA*. Available at: <https://www.seia.org/research-resources/us-solar-market-insight-2012-year-review> (Accessed: 5 July 2021).

Wohlgemuth, J. H. and Petersen, R. C. (1993) ‘Reliability of EVA modules’, in *Conference Record of the Twenty Third IEEE Photovoltaic Specialists Conference - 1993 (Cat. No.93CH3283-9)*. *Record of the Twenty Third IEEE Photovoltaic Specialists Conference - 1993 (Cat. No.93CH3283-9)*, Louisville, KY, USA: IEEE, pp. 1090–1094. doi: 10.1109/PVSC.1993.346972.

www.bpsolarsettlement.com (2016) *BP Solar Settlement, BP Solar Panel Settlement*. Available at: <https://www.bpsolarsettlement.com/> (Accessed: 13 July 2021).

Influence of Diffuse and Ground-Reflected Irradiance on the Spectral Modeling of Solar Reference Cells

Frank Vignola¹, Josh Peterson¹, Rich Kessler¹, Sean Snider², Peter Gotseff³, Manajit Sengupta³, Aron Habte³, Afshin Andreas³, and Fotis Mavromatakis⁴

¹Material Science Instituted/University of Oregon, Eugene (USA)

²St. Mary's High School, Medford (USA)

³National Renewable Energy Laboratory, Golden (USA)

⁴Department of Electrical and Computer Engineering/Hellenic Mediterranean University, Heraklion (Greece)

a) Corresponding author: Frank Vignola: fev@uoregon.edu

b) Josh Peterson: jpeter4@uoregon.edu

1. Abstract

An enhanced model is introduced to estimate reference cell output on a two-axis tracking surface using measured spectral irradiance and reference cell temperature. The model also uses the reference cell spectral responsivity and the spectral temperature responsivity. Under clear skies in July and December, the model reproduces reference cell measurements with an uncertainty of 0.9% at the 95% level of confidence. Under cloudy conditions during July, the modeled results match the measured data with an uncertainty 4.5% at the 95% level of confidence, and in December, the difference was 5.3%. These uncertainties are over a range of solar zenith angles from 20° to 85°.

Keywords: Reference cell, spectral radiation, modeling

2. Introduction

As larger photovoltaic (PV) systems are installed, it is becoming more important to monitor the system performance and to identify changes in performance to quickly address potential problems as they arise. This can be done using high-quality pyranometers or solar reference cells. Reference cells are similar to miniature solar panels being constructed with the same material as the PV panel and using the same glazing and anti-reflection coating as the panel. The only difference between the reference cell and the PV panel is that the reference cell operates at the short-circuit current and the PV panel in the array operates at the maximum power point. Because the relationship between the short-circuit current and the maximum power point is well understood and characterized, models exist relating reference cell measurements with PV system performance. The relationship between incident radiation, measured by the pyranometer, and the PV system performance is complex because the spectral distribution of the incident radiation and the angle-of-incident (AOI) effects must be considered; therefore, reference cell measurements in the plane-of-array of the PV panels are often used to monitor PV system performance because the reference cells are similarly affected by spectral distribution and AOI effects.

Said another way, reference cells do not make good pyranometers because reference cells exhibit significant spectral and AOI dependencies. These are similar to the dependencies that PV panels exhibit and they must be modeled if pyranometers are used to measure the incident radiation; therefore, comparing reference cell measurements to pyranometer readings requires significant modeling efforts to adjust the reference cell measurements to standard conditions. As used here, *standard conditions* mean a solar zenith angle (SZA) of 45°, a standard irradiance spectral distribution, and a temperature of 25°C. These are conditions that are used to determine the calibration of a pyranometer. A perfect pyranometer does not significantly change its calibration values as the SZA, spectral distribution, and temperature change. All pyranometers do have some dependence on SZA, incident spectral distribution, and temperature, but these systematic biases are only a few percent of the measurement. For reference cells, changes with SZA, temperature, and spectral distribution are significant and, therefore, it is difficult to use reference cell measurements to analyze PV systems at different tilts and orientations. First, a model would be needed to adjust the reference cell measurements to standard conditions, and then a companion model would be needed to adjust the values at standard conditions to the appropriate values at the new tilt, orientation, SZA, spectral distribution, and temperature.

Improved estimates of PV system performance require detailed information on the amount and characteristics of the irradiance on the solar cells. Reference cells provide a controlled basis to characterize the spectral, AOI, and temperature effects on the performance of PV panels and systems. On a two-axis tracking surface during clear periods, a very consistent relationship between spectral irradiance and reference cell performance has been shown using a simplified model (Vignola, et. al. 2017a, 2017b, Vignola, et. al. 2018, Vignola, et. al. 2021, Vignola, et. al., 2020). In the simple model, it was assumed that spectral beam normal irradiance (BNI) and diffuse and ground-reflected irradiance behaved the same under clear skies. Under cloudy skies, for a two-axis tracking surface, the use of this simple model exhibited a 2% to 3% percent shift in the measured output.

3. Simple Reference Cell Spectral Model

The relationship between the measured spectral irradiance (I_λ) and the estimated reference cell measurement (RC_{Model}) is given in eq. 1.

$$RC_{Model} = K \cdot \int R_\lambda \cdot I_\lambda \cdot T_\lambda \cdot (T_{rc} - 25^\circ\text{C}) \cdot F(AOI) \cdot d\lambda \quad (\text{eq. 1})$$

where R_λ and T_λ are the reference cell spectral responsivity and the spectral temperature sensitivity of the reference cell. T_{rc} is the temperature of the reference cell and $F(AOI)$ is the AOI effect of the reference cell. The constant, K , is related to the calibration of the reference cell and is necessary because the reference cell spectral responsivity is obtained from the relative quantum efficiency, and K is only obtained only through measurement or calibration. If all the values in eq. 1 were precisely known, then K would be a constant under all conditions.

A two-axis tracking surface was selected for this study because the incident radiation, during sunny periods, is mostly normal to the surface and AOI effects are minimized. In an earlier study Vignola, et al., (2020), it was assumed that $F(AOI)$ for a two-axis tracking surface from BNI, diffuse, and ground-reflected irradiance was equal to 1 for all wavelengths. For BNI, this is true because normal incident light passes through a glass glazing (Marion, 2017). For diffuse and ground-reflected irradiance this is not true and the transmission depends on the nature of the diffuse and ground-reflected irradiance (Marion, 2017).

This paper builds on previous work (Vignola et al., 2020) but incorporates a realistic $F(AOI)$ for the diffuse and ground-reflected contributions by separating the diffuse irradiance into circumsolar, sky dome, and horizontal brightening components, and by using a transmission model (Marion 2017) to estimate the diffuse and ground-reflected AOI effects. In fact $F(AOI)$ has some wavelength dependencies, but for this analysis, it is assumed to be independent of wavelength.

The main goal of this work is to evaluate the improvement to the simple reference cell model when a realistic $F(AOI)$ for diffuse and ground-reflected irradiance is taken into account. How much does the inclusion of diffuse and ground-reflected irradiance affect the model results under clear and cloudy sky conditions? The model for the diffuse and ground-reflected irradiance comes from Marion (2017), and the separation of the diffuse irradiance into the circumsolar, dome, and horizon brightening comes from Perez et al. (1990).

The data for this study comes from two spectroradiometers and a reference cell mounted on a two-axis tracking surface at the National Renewable Energy Laboratory (NREL) in Golden, Colorado at the Solar Radiation Research Laboratory (SRRL). Only two months will be studied—July 2020 and December 2020—to illustrate the universality of the results and to examine whether the reference cell and enhanced model behave in a similar manner throughout the year. Initially, clear-sky results are evaluated. In the following section, the results during cloudy periods are examined. The results of the comparisons are then discussed, followed by the next steps needed to evaluate the usefulness of this simple model for other fixed and tracking surfaces.

4. Spectral and Reference Cell Data at SRRL

The data used in this study comes from an IMT solar reference cell and two EKO spectroradiometers mounted on a two-axis EKO tracker (See Figure 1). Several other reference cells—Li-Cor 200R, a Kipp & Zonen SP Lite2 pyranometer, and a Kipp & Zonen CMP22 reference pyranometer—also collect data from the same platform. The two spectroradiometers at the SRRL measure spectral radiation from 300 nm–1650 nm. Data from these instruments have been used in earlier studies (Vignola et al. 2017b, Vignola et al., 2018, Vignola

et al., 2021, Vignola et al., 2020) and can provide a test of the enhanced model in the current study when it is applied to diffuse surface orientations and reference cells.

The experimental setup at the SRRL is shown in Figure 1. The two EKO spectroradiometers are shown by the blue arrows. The IMT reference cell highlighted in this study is shown by the red arrow. The other three reference cells are shown by the green arrows.

Data collection on the two-axis tracker started in May 2020 at the SRRL. All data are reported in 1-minute intervals and some instantaneous data are also available. The spectral data takes from 0.1 to 5 seconds to gather and are stored at the top of the minute. All other instruments are scanned once every 3 seconds and the average measurement is recorded at the ending time. To match the time period of the spectral data, sampled data from the reference cells are used in this study. The difference between the averaged and sampled data is small under clear skies, but it can be significant under cloudy skies where irradiance can vary significantly during short intervals.



Fig. 1. Experimental equipment at the SRRL in Golden, Colorado

Although the pyranometers are calibrated at standard operating conditions, the spectroradiometers are calibrated under laboratory conditions with the light source directly overhead. The directional response and spectral response of the pyranometers are well documented. The difference between the responsivity of the pyranometer under standard conditions when the SZA is near 45° and when the sun is directly overhead (0°) is small. The directional response of the spectroradiometers is larger than for the reference pyranometers, and it has been documented in laboratory conditions, but high-quality field evaluation of the directional response of the spectral radiometers are limited. The directional response of the reference cells is considerable and is evaluated in previous studies (Vignola, et al., 2017a, 2017b, Vignola, et. al., 2018, Vignola, et. al., 2021, Vignola, et. al., 2020).

5. Model Assumptions

In Vignola, et al., (2020) the $F(AOI)$ for all irradiance components was assumed to be the $F(AOI)$ for the BNI component and set equal to 1. As an enhancement to this simple model, the $F(AOI)$ for each radiation component was calculated. The $F(AOI)$ for each component was assumed to be independent of the spectral irradiance. This assumption is an approximation and the transmission of light through a glazing is slightly dependent on the wavelength (Marion, 2017). The enhanced model also assumes that the Perez model and the Marion model adequately represent the various irradiance components.

The validity of these assumptions can be tested by comparing the ratio between the measured and the modeled reference cell output at different times of year and under different conditions. A model with little bias would produce a ratio that is independent of time of year and SZA.

6. Evaluations Under Clear Skies

In this section, the reference cell output is modeled under clear-sky conditions using the measured relative spectral response of the reference cell, the spectrally dependent temperature response of the reference cell, the measured temperature of the reference cell, and the spectral irradiance from the spectroradiometers. In the earlier simplified model, all irradiance was assumed to be normal irradiance (Vignola, et al., 2020). The enhanced model separates the incident radiation into its components using the Perez model (Perez, et al., 1990). The incident radiation components are: beam normal irradiance (BNI), ground-reflected irradiance (DTI_{GR}) and diffuse irradiance which are further separated into three components, the circumsolar irradiance (DTI_{CS}), the sky dome irradiance (DTI_{Dome}), and the horizons brightening component ($DTI_{Horizon}$). The modeled DTI (DTI_{calc}) is given in eq. 2.

$$DTI_{calc} = DTI_{CS} + DTI_{Dome} + DTI_{Horizon} + DTI_{GR} \quad (\text{eq. 2})$$

To simplify the terminology in the paper, the sum of the ground-reflected and diffuse components on the surface is referred to as the diffuse tilted irradiance (DTI) which in this study is the diffuse and ground-reflected irradiance on the two-axis tracking surface.

Although the F(AOI) term can be calculated for each component using (Marion, 2017), the spectral distribution of the irradiance that comprises each component is not measured. Although it is theoretically possible to model the spectral contribution of each component, this is complex, depends on high-quality measurements of the atmospheric components, and carries considerable uncertainties. Therefore, to simplify the calculations for the enhanced model, it is assumed that the components have identical spectral distributions equal to the average spectral distribution. This assumption allows one to use the Perez model (Perez et al., 1990) and the Marion model (Marion, 2017) to estimate the average F(AOI) and include the effects of the diffuse and ground-reflected contributions to the overall average F(AOI).

For a two-axis tracking surface, always facing the sun, DTI can be obtained from the global irradiance on the tilted surface (GTI) and BNI.

$$DTI = GTI - BNI \quad (\text{eq. 3})$$

DTI includes both the diffuse and ground-reflected components. DTI obtained using eq. 3 is referred to as DTI_{Meas} . For the two-axis tracking surface the term Global Normal Irradiance (GNI) will be used instead of GTI . The $F(AOI)_{avg}$ used in the enhanced model is given by eq. 4:

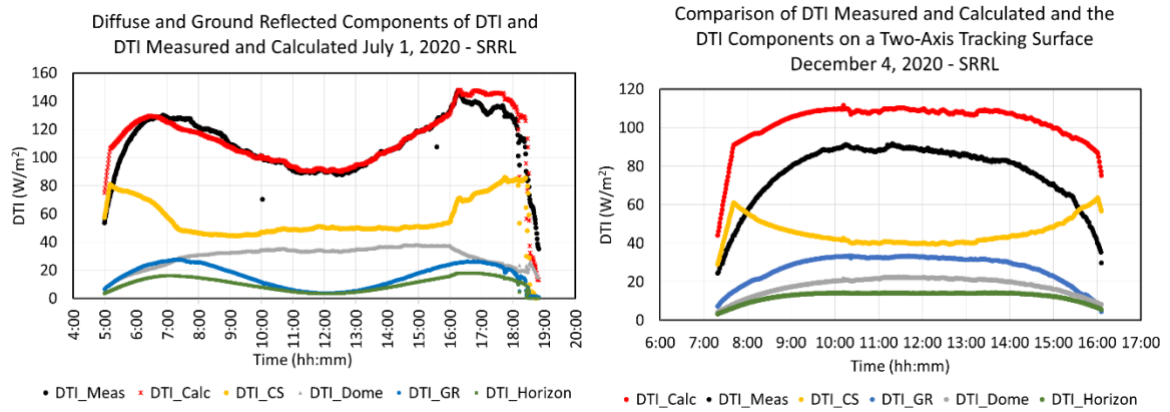
$$F(AOI)_{avg} = \frac{BNI \cdot F(AOI)_{BNI} + DTI_{Meas} \cdot F(AOI)_{DTIavg}}{BNI + DTI_{Meas}} \quad (\text{eq. 4})$$

where $F(AOI)_{BNI}$ for the BNI equals one. $F(AOI)_{DTIavg}$ is given in eq. 5:

$$= \frac{DTI_{CS} \cdot F(AOI)_{CS} + DTI_{Dome} \cdot F(AOI)_{Dome} + DTI_{Horizon} \cdot F(AOI)_{Horizon} + DTI_{GR} \cdot F(AOI)_{GR}}{DTI_{Calc}} \quad (\text{eq. 5})$$

When determining the $F(AOI)_{DTIavg}$ the sum of the DTI components times the appropriate F(AOI) for each component is divided by DTI_{Calc} because the DTI components sum to DTI_{Calc} and not DTI_{Meas} . Therefore DTI_{Calc} is the proper denominator.

Figures 2a compares the DTI obtained from the measured GNI – BNI against the DTI calculated using the Perez model for July 1, 2020, a clear day. Figure 2b compares the measured and modeled DTI on December 4, 2020, another clear day.



Figs: 2a & 2b: The measured DTI, obtained by subtracting BNI from GNI, are the black points. The DTI_Dome are the gray points, DTI_GR are the blue points, the horizon brightening DTI_Horizon are the green points, and the circumsolar DTI_CS are the yellow points. The calculated DTI is the sum of the components and is shown as the red points.

The measured and modeled DTI in July are a close match. This is not the case for the clear day in December, where the modeled DTI_{Calc} is significantly higher than the measured DTI_{Meas} . This comparison was confirmed by Marion (2021) using NREL’s implementation of the Perez model. The DTI components are calculated from measured GHI from a Kipp & Zonen CMP22 pyranometer as well as the measured DHI. Surface albedo was measured using a Kipp & Zonen CM11 pyranometer. No consistent explanation was determined for the difference between the modeled and measured DTI (DTI_{Calc} and DTI_{Meas} respectively); therefore, in order to estimate the average $F_{avg}(AOI)$, the calculated DTI terms were weighted by the DTI_{Calc} and this $F_{avg}(AOI)$ was used with the DTI_{Meas} in the final calculations (see eqs. 4 and 5).

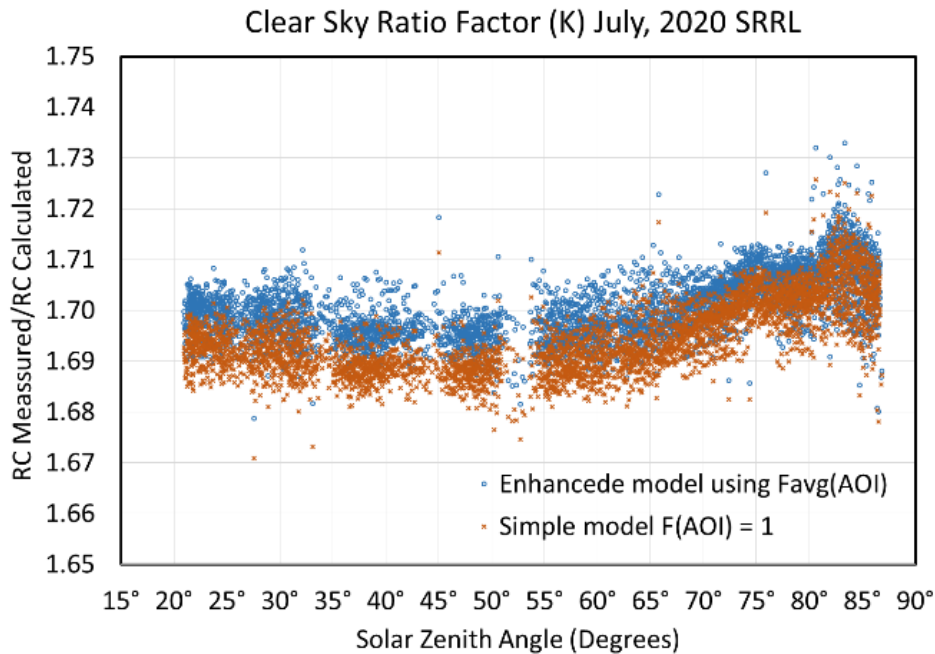


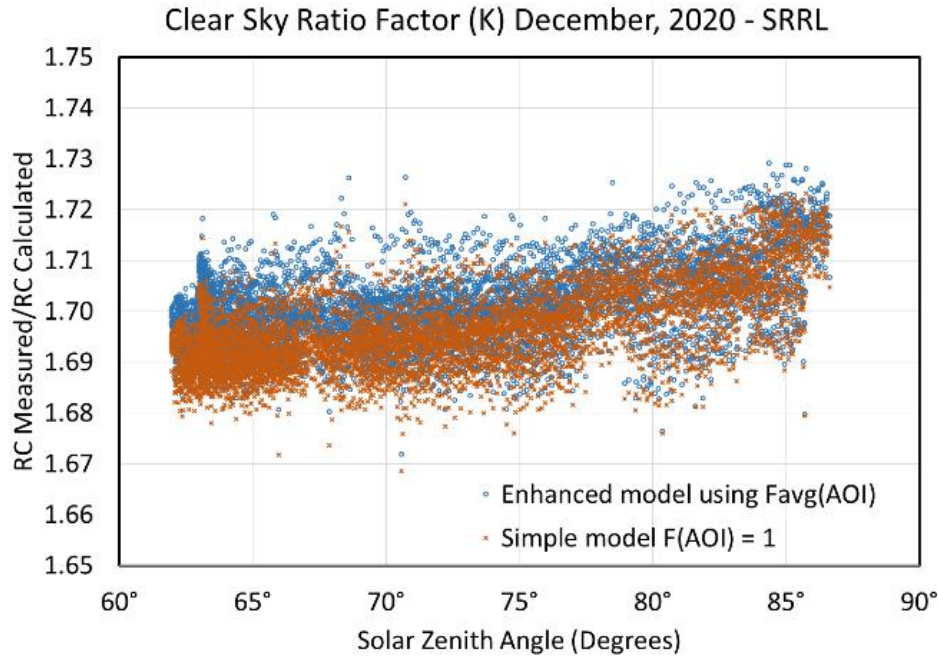
Fig. 3a: Comparison of the ratio factor K the ratio of the reference cell measurements to the calculated reference cell values assuming that the $F(AOI)_{DTI_{AVG}} = 1$ and with modeled $F(AOI)_{DTI_{avg}}$ during sunny periods in July at the SRRL. Periods when the clouds represented less than 15% of the total sky cover were selected as clear skies.

In the simple model under clear skies, the K factor or ratio—the measured reference cell output divided by calculated reference cell output—was determined using the assumption that $F(AOI)$ was always one and $F(AOI)_{avg}$ was used by the enhanced model in calculating the ratio (K’ in the following plots). The $F(AOI)_{avg}$ is always less than one because a portion of any incident radiation not coming at a perpendicular angle to the

surface of the glazing will be reflected or absorbed. This was done for July 2020 and December 2020 (See Figures 3a and 3b).

Fig. 3b: Comparison of the ratio factor K the ratio of the reference cell measurements to the calculated reference cell values assuming that the $F(AOI)_{DTI_{AVG}} = 1$ and with modeled $F(AOI)_{DTI_{avg}}$ during sunny periods in December at the SRRL. Periods when the clouds represented less than 15% of the total sky cover were selected as clear skies.

The summer and winter clear-sky data shown in Figures 3a and 3b were vetted by removing the BNI that



showed significant reductions from the nearby BNI values. In addition, data with negative DTI values were eliminated. Typically, this happens when the GNI sensor is shaded but the BNI sensor is not. With the vetted data, the small increase in the K values at large zenith angles becomes apparent. During July, the average K values was 1.695 with a standard deviation of 0.007 and the average K' value that included the $F(AOI)_{DTI_{avg}}$ was 1.701 with a standard deviation of 0.006. The inclusion of the $F(AOI)_{DTI_{avg}}$ contribution increased the ratio by 0.3%. In the winter, the simple model ratio values (K) were 1.696 with a standard deviation of 0.008 and the ratio values adjusted for the enhance model using $F(AOI)_{DTI_{avg}}$ were 1.701 with a standard deviation of 0.008. Inclusion of the $F(AOI)_{DTI_{avg}}$ contribution increased the ratio by 0.3%.

7. Evaluation Under Cloudy Skies

Under cloudy skies, the inclusion of the $F(AOI)_{DTI_{avg}}$ values is expected to have a larger influence on the $F(AOI)_{avg}$ values because the BNI contribution is significantly reduced and the $F(AOI)_{DTI_{avg}}$ values are less than 1. To show the effect of including the $F(AOI)_{DTI_{avg}}$ values under cloudy conditions, the ratio of the reference cell measurement divided by reference cell's calculated output (K) was compared to the same ratio where the calculated reference cell values were adjusted to include the $F(AOI)_{DTI_{avg}}$ contributions (K'). To examine periods when the sky was most covered with clouds, only data collected when the cloudiness factor was 85% or higher were used. These values are shown in Figures 4a and 4b for July and December 2020 at the SRRL in Golden, Colorado.

For the July data, the unadjusted K value averaged 1.653 with a standard deviation of .039. For the K' value that included the calculation of the $F(AOI)_{DTI_{avg}}$ effect on the average F(AOI), the average K' was 1.699 with a standard deviation of 0.037. The effect of the $F(AOI)_{DTI_{avg}}$ factors reduced the average F(AOI) by

approximately 2.7%. To help ensure that the cloudy periods were examined, only data obtained when BNI was less than 500 Wm^{-2} were used.

Fig. 4a: Comparison of the ratio of measured reference cell output to the calculated reference cell values during cloudy weather when the percentage cloudiness was 85% or greater for July at the SRRL. The plots contain information on the K value obtained with and without including the $F(AOI)_{DTIavg}$ factor.

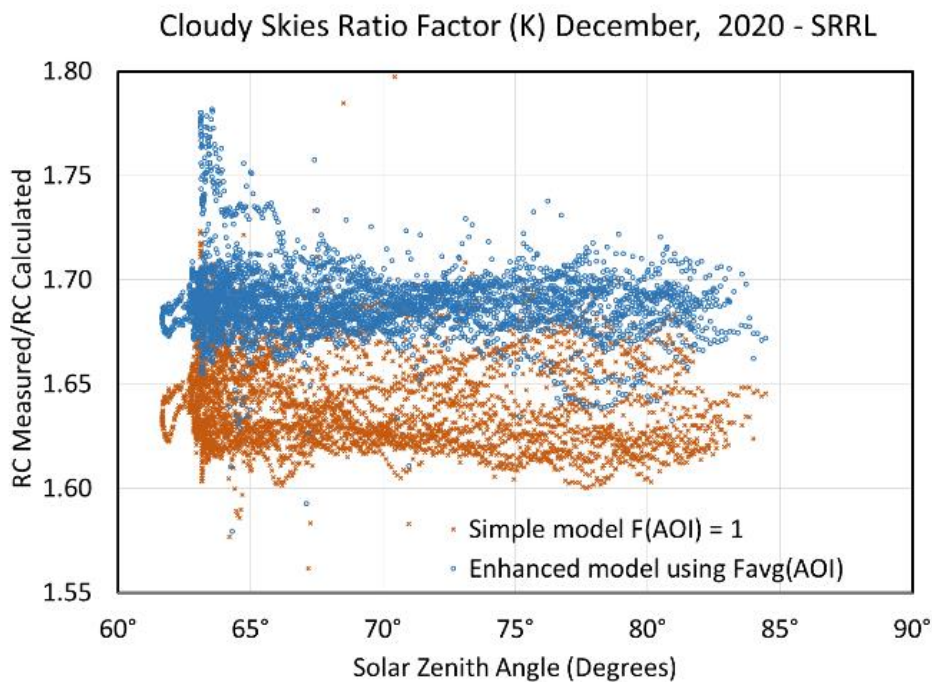
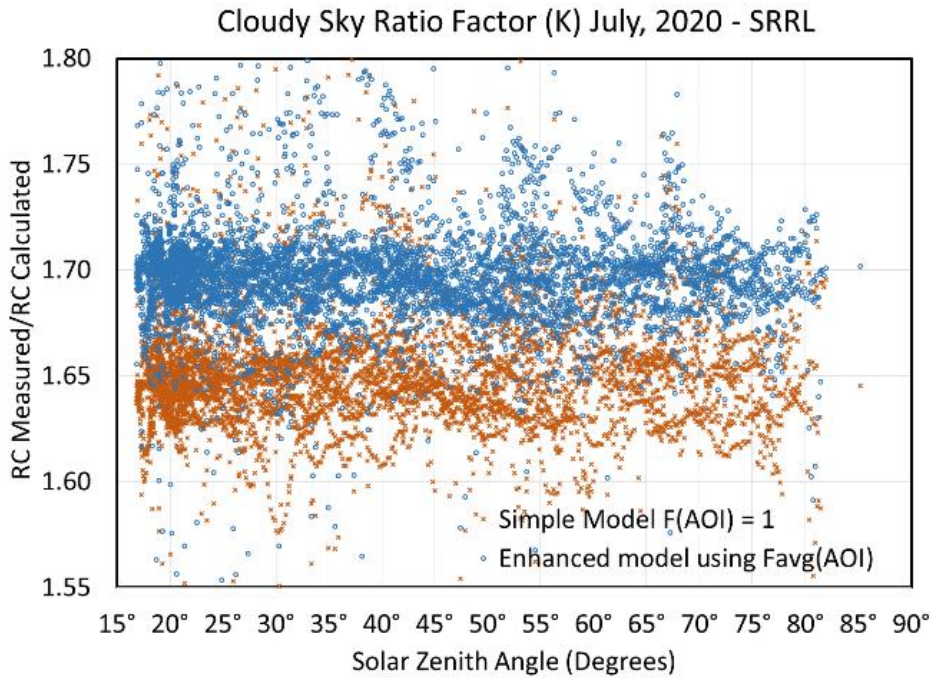


Fig. 4b: Comparison of the ratio of measured reference cell output to the calculated reference cell values during cloudy weather when the percentage cloudiness was 85% or greater for December at the SRRL. The plots contain information on the K value obtained with and without including the $F(AOI)_{DTIavg}$ factor.

During December for cloudiness greater than 85%, the simple model average K ratio was 1.638 with a standard deviation of 0.045 and the enhanced model with the adjusted K' ratio was 1.686 with a standard deviation of 0.042. The inclusion of the $F(AOI)_{DTIavg}$ values increased the ratio by 2.9%. The maximum BNI values under cloudy skies were less than 325 Wm^{-2} . Periods with negative DTI values were not included.

8. Discussion

A simple model for reference cell performance on a **two-axis tracking surface** using spectral irradiance and reference cell temperature measurements is enhanced by including the AOI effects of the diffuse and ground-reflected irradiance values (DTI). Although the $F(\text{AOI})$ value for the BNI irradiance is equal to one (Marion, 2017), the average $F(\text{AOI})$ for DTI irradiance is less than one. Therefore, the average $F(\text{AOI})$ value is slightly less than one under clear skies and is reduced by 2.5% to 3% for totally cloud-covered skies where the DTI term is dominant.

For circumsolar irradiance, the largest contributor to the DTI under clear skies, the $F(\text{AOI})$ was modeled as one. This is an excellent approximation because the transmission of light through the glazing does not change significantly for AOIs less than 30° . For sky dome irradiance, the average transmission of light is approximately 95%. Transmission of light through the glazing from horizon brightening and ground-reflected irradiance depend on the AOI (see Vignola et al., (2020), Marion, (2017) for more detailed information).

The practicality of the enhanced reference cell model depends on how well the calibration constant (K' in this study) of the reference cell remains constant over all circumstances. Of course there will be variation as with any measurements, but if all the systematic biases are appropriately modeled, the ratio between the measured and the calculated reference cell output would be a constant under all circumstances. If assumptions are only partially correct, changes with the average ratio would be observed over different temperature, SZA, or cloud conditions.

Under clear-sky conditions, the inclusion of $F(\text{AOI})$ from the DTI contributions, increased the ratio of the measured to the modeled reference cell output by 0.3% for the IMT reference cell under study. The modeled reference cell output was reduced by the inclusion of the DTI $F(\text{AOI})$ values and hence the ratio of the measured to the modeled was increased. Under clear-sky conditions, the average ratio K' was 1.701 ± 0.012 for July and 1.701 ± 0.016 at the 95% level of confidence. This is very accurate considering this is over a zenith angle ranging from 20° to 85° . There is a slight trend noted with the ratio increased from an average of 1.70 from 20° to 65° to near 1.71 at 85° , or an approximate 0.6% increase over the full SZA range. When the sun is low in the sky, SZA greater than 65° , model assumptions may not be as accurate.

During cloudy or partially cloudy periods there is more variation in the ratios obtained because the instruments see slightly different portions of the sky, and there is difficulty in modeling the DTI components and estimating the $F(\text{AOI})$. The example here used very cloudy skies where the percentage total cloud cover was 85% or higher. Even under heavy cloud cover, the BNI varied from zero to 1000 Wm^{-2} . This represents a wide range of sky conditions. Periods with BNI greater than 500 Wm^{-2} were eliminated to remove periods when the sun shined through a hole in the clouds. Without including the $F(\text{AOI})_{\text{DTIavg}}$, the simple model produced ratios of K' that were 2.5% to 3% lower than the results that included the $F(\text{AOI})_{\text{DTIavg}}$ in the calculations. Including the $F(\text{AOI})_{\text{DTIavg}}$ represents a noticeable improvement in the calculated reference cell measurements; however the uncertainty in the ratio values was approximately 5% at the 95% level of confidence. The difference in the average K' ratio calculated in July during significant cloud cover and under sunny skies was 0.35% at the 95% level of confidence. For the data in December, the difference was 1.6% at the 95% level of confidence. Given the uncertainty of the average K' obtained during cloudy periods from 2.5% to 3%, this is within the uncertainty of the measurements.

One possible source of error in the model estimates likely occurs when the sum of the modeled DTI components were larger than the measured DTI value. To compensate for this difference, the values of all DTI components were adjusted by a constant amount to match the measured DTI value. Because each $F(\text{AOI})_{\text{DTIavg}}$ is different, this method treats all DTI components equally and might have resulted in over- or underestimating some of the $F(\text{AOI})_{\text{DTIavg}}$ contributions. The largest DTI component is the circumsolar component and it has a $F(\text{AOI})_{\text{CS}}$ value equal to 1. Over or underestimating the contribution of DTI_{CS} would certainly affect the $F(\text{AOI})_{\text{avg}}$.

9. Conclusions

Given the uncertainty in the spectral measurements and the other measurements used to obtain the DTI components, these results show a very robust model for estimating the measurements of solar reference cells. These results apply to the IMT reference cell on a two-axis tracking surface, and the data are from one location, the SRRL in Golden, Colorado. At least in principle the simple model works well with $F(\text{AOI})$ equal to one

under clear skies. Under cloudy skies, the enhanced model that includes the calculated $F(AOI)_{DTI_{avg}}$ provides a more consistent ratio K' value. More work is needed examine the results using different reference cells and on different surfaces where the $F(AOI)$ values have a larger variation. For the proposed method to be validated, an improved understanding of reference cells characteristics is needed through enhanced experimental setups.

10. Future Efforts

Four areas of work need to be completed. First, the enhanced method needs to be tested on different reference cells, especially those with a different spectral responsivity. Second, the method needs to be tried at different locations to ensure that the modeling has a universally applicable. Third, the model needs to be tested on different surfaces and orientations. This testing will help examine the $F(AOI)$ modeling that was used. Fourth, modeled spectral data needs to be substituted for the measured spectral data to determine the ability of the model to produce useful results at locations where measured spectral data does not exist. Future plans will incorporate these four analyses.

One surprising result of this study was the overestimate of the DTI components during December. This needs to be examined in more detail to determine the cause of this overestimation. Is the cause a result of the data used in the model or the model itself? Neither prospect is the apparent cause of this difference, and more study is needed. Also, use of other models that determine the DTI components needs to be attempted.

Each DTI component has a different spectral signature, and this signature is dependent on the sky cover. For example, under clear-sky conditions, the irradiance of the diffuse dome component peaks in the blue portion of the spectrum. Under cloudy conditions, the peak of the diffuse dome spectral irradiance has a different distribution. How the different spectral distributions of the diffuse components affect the models estimates has not been studied.

When the final results of this project are completed, one should be able to calculate the accuracy of using modeled spectral data to calculate the reference cell output and even the incident radiation. This uncertainty can be translated directly into the uncertainty to which the production of PV power systems can be estimated using modeled spectral data.

11. Acknowledgements

The University of Oregon Solar Radiation Monitoring Laboratory would like to thank the National Renewable Energy Laboratory as well as the Murdoch Family Trust for funding the project. We also thank the other sponsors of the University of Oregon Solar Radiation Monitoring Laboratory, the Bonneville Power Administration, the Energy Trust of Oregon, and Portland General Electric.

This work was authored in part by Alliance for Sustainable Energy, LLC, the manager and operator of the National Renewable Energy Laboratory for the U.S. Department of Energy (DOE) under Contract No. DE-AC36-08GO28308. Funding provided by U.S. Department of Energy Office of Energy Efficiency and Renewable Energy Solar Energy Technologies Office. The views expressed in the article do not necessarily represent the views of the DOE or the U.S. Government. The U.S. Government retains and the publisher, by accepting the article for publication, acknowledges that the U.S. Government retains a nonexclusive, paid-up, irrevocable, worldwide license to publish or reproduce the published form of this work, or allow others to do so, for U.S. Government purposes.

12. References

1. Vignola, F., Chiu, C., Peterson, J., Dooraghi, M., Sengupta, M., 2017. Comparison and analysis of instruments measuring plane-of array irradiance for one-axis tracking PV systems, IEEE PVSC Conference, Washington D.C., 2017
2. Vignola, F., Peterson, J., Dooraghi, M., Sengupta, M., Mavromatakis, F., 2017. Comparison of Pyranometers and Reference Cells on Fixed and One-Axis Tracking American Solar Energy Society Conference Denver, Colorado October 9–12, 2017
3. Vignola, F., Peterson, J., Kessler, R., Dooraghi, M., Sengupta, M., and Mavromatakis, F., 2018. Evaluation of Photodiode-based Pyranometers and Reference Solar Cells on a Two-Axis Tracking System, World Conference on Photovoltaic Energy Conversion Waikoloa, Hawaii, June 10-15, 2018

4. Vignola, F., Peterson, J., Kessler, R., Sandhu, V., Snider, S., Habte A., Gotseff, P., Andreas, A., Sengupta, M., and Mavromatakis, F., 2021. Improved Field Evaluation of Reference Cell Using Spectral Measurements, *Solar Energy* 215, 482-491, 2021
5. Vignola, F., Peterson, J., Kessler, R., Snider, S., Andreas, A., Habte A., Gotseff, P., Andreas, A., Sengupta, M., and Mavromatakis, F., 2020. Evaluation of Reference Solar Cells on a Two-Axis Tracking Using Spectral Measurements, *SolarPACES*, September 27–October 1, 2020
6. Marion, B., 2017. Numerical method for angle-of-incidence correction factors for diffuse radiation incident photovoltaic modules, *Solar Energy* 147 (2017) 344–348
7. R. Perez, P. Ineichen, R. Seals, J. Michalsky, Modeling daylight availability and irradiance components from direct and global irradiance, *Solar Energy* 44, 271–289 , 1990
8. B. Marion 2021 (private communication)

A Study of Reflector-Enhanced Bifacial PV

Matthew Rueter, Mariam Dobosz, Richard D. Wilk

Mechanical Engineering Department

Union College, Schenectady, NY

Abstract

Bifacial solar PV is a promising technology that can increase the amount of power generated by harvesting power on both sides of a module. Understanding how best to configure the geometry of these bifacial solar collectors is non-trivial as many geometric factors (tilt, ground reflectance (albedo), height above ground, row spacing, module spacing) tend to be interdependent, requiring a case by case analysis in order to optimize the total power output and maintain the frontside incident irradiance while maximizing the backside gain. In addition, as with monofacial modules, use of planar reflectors can be a cost effective way of increasing the incident irradiance, in the case of bifacial modules, on both sides of the module. However, the addition of reflectors adds to the challenge of optimizing the system configuration. The work described here presents an experimental and modeling study of reflector enhanced bifacial modules. Experiments were conducted on bifacial modules with and without reflector augmentation and compared against monofacial PV modules, assessing the effects of specular and diffuse reflectors. A model was developed to calculate the incident and reflected irradiance on the front and back sides of the modules. Beam insolation components were handled with ray tracing and sky and reflected diffuse components were handled with view factors.

Keywords: Bifacial PV, Bifacial Irradiance Model, Reflectors

1. Introduction

Bifacial solar is a promising technology in solar PV with the potential to further reduce the levelized cost of electricity. The concept of collecting and converting sunlight from both sides of a solar collector has been studied for nearly 60 years, including the investigation of solar PV and solar thermal collectors (often referred to as double-exposure collectors). Bifacial solar PV modules are the focus of this study. The transparent back sheet of bifacial PV modules allows them to collect light on the rear surface as well. This increases the power generation of the module per unit area as compared to the traditional monofacial counterpart. This could allow for smaller arrays that occupy less land area while producing the same power and potentially reduce some balance of plant costs. A review of the state of the technology was done by Guerrero-Lemus, et al. (2016).

Various studies of bifacial cells and modules through the years have demonstrated the production of up to about 50% additional energy (Cuevas et al. (1982)) under idealized conditions, but more typically 10-30% under more realistic conditions (Sun et al. (2018)). In the field, getting the most out of a bifacial module requires optimizing the configuration in a way that will maximize the annual energy output. Variables affecting this include the module tilt angle, the surface azimuth angle, the height of the module above the ground, the

reflectance of the ground (albedo) and the spacing between successive rows in the array. The big challenge with bifacial is to maximize the irradiance striking the back side, while maintaining a high level of irradiance to the front side, which is the primary power generating part of the module. The bifacial gain factor BG is used as an indicator of this relationship and is the ratio of the back side power to the frontside power. Many studies, for example Yusufoglu et al. (2014), have studied the effects of these variables on the backside irradiance and on BG. Coming out of this body of work it was clear that there are interdependencies of some of these variables and that nonuniformity of light reaching the backside is an important issue (Kreinin et al. (2010); Yusufoglu, et al. (2015)).

Computational modeling can be applied to cut down on the needed time and expense of optimizing mounting arrangements. However, some experimental data is still required to validate the functionality and performance of the models. Mostly over the last 15 years, predictive models have been developed to accurately predict the rear surface incidence to aid in the system design and to optimize the system configuration. These have been compared with each other and validated with available system data (Pelaez et al. (2019)). To model the rear side irradiance, models use either view factors, ray tracing, a combination of both or simpler geometric relationships (Hansen et al. (2016); Jäger et al. (2020); Durusoy et al. (2020)). View factors are parameters that indicate what fraction of light is reflected onto a surface from nearby surfaces and are computationally less demanding, while ray tracing simulates and follows the directional paths light travels and tends to be better at capturing the non-uniformity.

Although many mountings of bifacial panels are similar to ones for monofacials, some different and novel arrangements have been proposed and analyzed (Joge et al. (2002); Karahara et al. (2003); Guo et al. (2013); Appelbaum (2016); Khan et al. (2017); Sun et al. (2018)) like vertical tilt and east-west facing modules to alter the daily and seasonal power production profile and to fit more collectors into an array.

For a number of years, concentrators and various reflectors have been proposed as a cost-effective way of enhancing the incident irradiance to a collector surface and hence, increasing the power output. This has been the subject of many studies related to thermal collectors and monofacial PV. This concept has also been applied to bifacial modules (Moehlecke et al. (2013); Ooshaksaraei et al. (2013); Jakobsen et al. (2019)). As the bifacial gain is proportional to the amount of light that is reflected onto the back of the panel, the use of reflectors has been investigated as a way to increase the power gain. In this case, additional variables become important like the collector-reflector spacing, height, tilt, size and reflectance of the reflector. With no reflector present, the ground reflected and sky diffuse sunlight behind the collector are normally key in bifacial applications as they are the primary mechanisms by which the rear side of the collector gets irradiated. Therefore, the presence of a reflector would have to complement and not interfere significantly with these other sources. Many possible reflector designs have been proposed, simple ones including mirrors and white paint. More complicated reflectors include the use of light scattering beads or powders, adjustable mirror arrays, and prisms (Lim et al. (2014)).

In this work, a model was developed to determine the front and back incident irradiance on a bifacial solar collector equipped with a rear planar reflector. The model calculates hourly incident irradiance on the front and back sides of a module in most any location for different geometric arrangements. Reflectors can be added to the setup as well and their effect on the incident energy can be calculated as well as potential shading interference. In addition, experiments were set-up and run with surrogate bifacial modules to study some of these variables, and to assess the effects on the rear incident energy of the addition of planar reflective surfaces behind the collector. In addition, the experimental results were compared with the modeling results, to demonstrate the model's ability to predict potential shading interference and to calculate the incident radiant energy striking the front and back sides of a module equipped with a rear reflector. This paper presents some preliminary results from the experiments and modeling cases.

2. The Model

A model for simulating incident energy on solar panels was developed and programmed in the Python coding language. The model used the Numpy and Matplotlib modules in Python. In general, the model is designed to be modular and functions have been written to perform basic calculations. It is intended that this model will serve as an informative collection of functions that can be rearranged for various purposes. The code has the ability to track the sun across the sky, calculate the incident energy on a surface, and model shading and reflected light with ray tracing and view factors.

Tracking the position of the sun was accomplished by calculating the solar altitude angle and solar azimuth angles (Duffie and Beckman (2013)). Solar insolation data was obtained from the National Solar Radiation Database (NSRDB). Hourly data for beam, diffuse, and total insolation on the horizontal surface were obtained and processed to produce average values for hourly insolation in a typical day of each month of the year (monthly average hourly insolation). For a given hour of the day in a given month, the recorded insolation in that hour for every day of the month was averaged, producing a single value for that hour. Functionality was also included to calculate monthly average daily insolation, which was done by summing the total insolation over a month and dividing it by the number of days in the month. Once the insolation data has been processed as desired for one year, the results can be averaged with other years to produce multi-year averages.

The insolation on a tilted surface in a given hour assumes the isotropic sky diffuse model and involves beam, diffuse and ground reflected and is calculated with

$$I_T = (I - I_d) \frac{\cos(\theta)}{\cos(\theta_z)} + I_d \frac{1 + \cos(\beta)}{2} + I\rho \frac{1 - \cos(\beta)}{2} \quad (\text{eq.1})$$

where I_T is hourly insolation on the tilted surface, I is the total hourly insolation on the horizontal, I_d is the hourly diffuse insolation on the horizontal, θ is the incidence angle calculated at the middle of the hour being studied, θ_z is the zenith angle in the middle of the hour, and ρ is the ground reflectance (Duffie and Beckman, 2013).

To move from insolation per square meter to insolation on a surface, the surfaces of collectors and reflectors modeled were described using a grid. The grid breaks the surface into small 2-D square cells that are treated as having the same amount of light shining over their entire surface. In this way the distribution of solar energy across the surface can be broken into discrete elements instead of being modeled as a continuum. A single

parameter defines the side length and grid sizes can be changed by changing this length, allowing coarser or finer grids to be used.

Ray tracing methods were applied to study the effects of reflectors and shading between rows. Rays are assumed to move in a straight line from the sun's location. A specular reflector like a mirror will reflect light from it at an angle equal to the incidence angle and in the same plane normal to the surface at which it struck the panel. This allows reflection to be modeled. Where a collector surface intercepts these rays an extra beam term is added to a list. The total energy of a reflected beam of light is calculated based on the area of the grid element it reflects from on the reflector. All irradiance terms coming from the reflector are multiplied by the collector reflectance, allowing for the modeling of non-ideal reflectors. For shading, the model traces rays of light intercepted by a front row panel back as if the panel was not there to see where they strike the rear panel or reflector. Any parts of a rear row panel or reflector that has its incident rays blocked by the module are considered shaded and no beam irradiance reaches them.

For sky diffuse and reflected diffuse from the ground and reflector, radiation view factors are used. In this work we studied the case of a reflector behind a bifacial collector where both are vertical and aligned (Fig. 1).

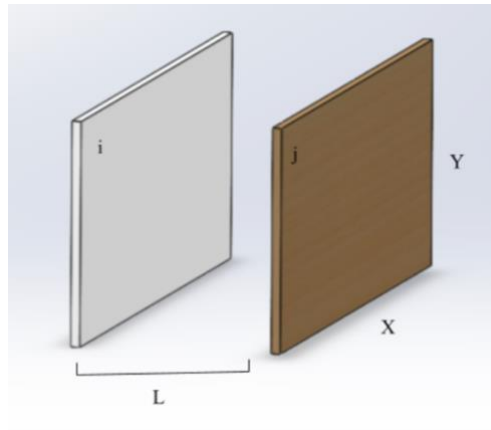


Fig. 1: Geometry for parallel surface view factor where i is the reflector and j is the collector.

In this case a 3-D view factor between the aligned vertical plates is used (Bergman, et al. (2011)).

$$F_{ij} = \frac{2}{\pi xy} \left[\ln \left(\frac{(1+\bar{x}^2)(1+\bar{y}^2)}{1+\bar{x}^2+\bar{y}^2} \right)^{1/2} + \bar{x} \left(y_1 \arctan \frac{\bar{x}}{y_1} \right) + \bar{y} \left(x_1 \arctan \frac{\bar{y}}{x_1} \right) - (\bar{x}) \arctan(\bar{x}) - (\bar{y}) \arctan(\bar{y}) \right] \quad (\text{eq. 2})$$

where:

$$\bar{x} = \frac{x}{L} \quad \bar{y} = \frac{y}{L} \quad x_1 = \sqrt{1 + \bar{x}^2} \quad y_1 = \sqrt{1 + \bar{y}^2}$$

The focus of this study was on the effects of the reflectors, so it was desired to try to isolate this aspect and remove from the computation the effect of ground albedo, which is a contributor to both the front and especially the back side irradiance. Therefore, the ground reflected subroutine was not used in the modeling. In order to match this in the experiments (discussed below) black matte roofing paper was placed all around the collector

and reflector to try to reduce the ground reflected component as much as possible to isolate the irradiance from the reflector and the sky.

3. Experiments

Three separate experimental systems were used to generate experimental data related to bifacial collectors equipped with rear reflectors. The purpose was to understand how some of the key factors that affect the amount of irradiance striking both sides of the collectors and to help validate the model that was developed. The first used simple parallel planar surfaces facing south that were used to validate the accuracy of the shading calculations of the model. This was done by taking photos of the shading patterns on the rear surface (representing the reflector) at different times. The second involved a south-facing collector-reflector pair with the reflector frame set up behind the collector. A bifacial collector was represented in this experiment by a planar panel with the rear side outfitted with six PV cells. These cells were calibrated and used as sensors to measure the irradiance striking the rear side (Fig. 2 a and b) from rear side sources like the sky, ground and rear side reflector. Each of the sensor cells was configured with a 2 ohm resistor and the voltage across the resistor was measured and calibrated over a full range of solar insolation against a Kipp and Zonen Pyranometer.



Fig: 2: a) 3D rendering of the orientation for the second experimental setup and image of b) photovoltaic cells simulating different positions on the rear side of a collector

This set-up allows for the changing of the collector and reflector size and spacing between them, the height from the ground of the collector and reflector, the collector tilt, and azimuth. The cells were placed on the back side of the module used to measure the back side irradiance. The pyranometer was used to measure the front side irradiance and together they were used to determine a measured bifacial gain (BG) factor in terms of a ratio of the back to front irradiances for the given geometric configuration. The rear side reflectance was achieved by placing a reflective surface behind the collector. For this study the reflectors were aligned and parallel to the front panel and they had the same width and height. The set-up allowed the reflectors to be easily changed out in a short time. Two different reflector surfaces were used, reflective Mylar sheet on a substrate and a white diffuse FRP panel. The pyranometer voltage output and the voltages across the calibrated cells were measured and logged using a Measurement Computing data acquisition system.

In the third system, single crystal 50 W monofacial PV modules were placed back-to-back and used to represent bifacial modules. The advantage to this versus using actual bifacial modules is that the power output on the front and back can be measured individually to determine the bifacial gain as a function of a number of

geometric and reflector parameters. Both set ups with the back-to-back monofacial modules were held up by metal frames with reflectors of the same size behind them. Each set-up had a different reflector or no reflector, to compare the effects of different reflectors under the same sun conditions. A third frame with a single monofacial module of the same spec was used to provide a monofacial baseline power output (Fig. 3). Since we were using five of the same monofacial modules in this set-up, we had to ensure that all five modules yielded the same power output. To do this all five modules used were run side by side for several days.



Fig. 3: Experimental Set-Up Using Back-to-Back Monofacial PV Modules

4. Results

To begin, tests were performed to validate the model's capabilities. Figure 4 shows a rendering of how the code previews the correct geometry in three dimensions and demonstrates shading or reflection that occurs during the simulation. The parameters associated with the collector (right surface) and reflector (left surface) geometry, like tilt and surface azimuth angles, height of the modules above the ground, spacing between reflector and collector will be indicated, along with any shading of either surface by the other, and reflected illumination.

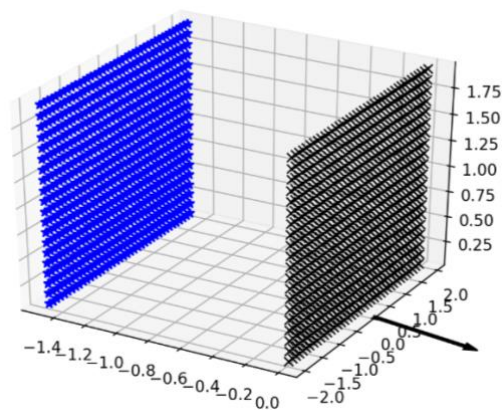


Fig. 4: Geometry for demonstrations of combined shading, reflection, and irradiance analysis. Each of the collector (right) grid points are marked with an X and stars mark the grid points of the reflector (left). The arrow to the right points south.

An experimental verification of the shading model was carried out using a panel representing a collector 0.6096 m high by 1.219 m wide, mounted with a tilt of 45° with a surface azimuth angle of 0° . A reflector of the same

size and tilt was mounted 1.219 m behind the collector. Both the collector and reflector used grid spacings of 0.1 m. The location used was Plymouth Meeting, PA ($\phi=40.14^\circ$) for the date of December 15. A comparison of the experimental and modeled shading achieved in the multi-row shading test is shown in Fig. 5a and b. In general, the agreement between the experimental and simulated results is fairly close, showing that the measured shading matches the calculated shading for this geometry.

Figure 6 shows experimental and modeling results over a day for a collector-reflector system in Schenectady, NY ($\phi=42.8^\circ$) on July 5. The experimental results are from the rooftop system with calibrated cell sensors on the rear of the surrogate bifacial module, measuring the rear irradiance (Fig. 2 a and b). A Kipp and Zonen pyranometer is vertically mounted to the collector and measures the front side irradiance. Bifacial gains are determined from the ratio of the rear and front measured irradiances. For this case a diffuse white FRP panel was used as the rear reflector (reflectance=0.78), mounted 1 m behind and parallel to the collector. Both surfaces were 1.219 m wide and 0.6096 m high, oriented vertically, facing due south and raised 1 m off the ground. As mentioned earlier, black, light absorbing roofing paper was placed horizontally in front of both the collector and the reflector and vertically in the 1 m space below the reflector to greatly reduce any ground reflected irradiance to the rear side of the collector. Data was collected beginning at about 10 am standard time and continued to sunset. Bifacial gains reached 0.37 ± 0.03 in the four hours centered around noon and trended higher as sunset approached, exceeding 1.0 which is consistent with the crossover of the sun back into the northern sky at this time of year, at which point the rear of the module sees direct solar irradiance. This effect is shown in the modeling results on Fig. 6, as well. The calculated BG values from the model spike in the morning and afternoon, but maintain a BG average of 0.38 ± 0.03 around midday, in good agreement with the experiments.

Figure 7 shows the model irradiance results for this case, with the individual components of the front and rear sides plotted over the day. Ground reflected on either side of the collector was not included. The rear side

components (beam and diffuse) each include both incident sky and reflected terms. The rear beam and total show a similar shape to the BG plotted in Fig 6. However, the beam components on the rear side drop to zero during the middle of the day for this case. This is due to the 1 m spacing between the reflector and collector and the large incidence angle of the sun on a vertical surface during the day at this time of year. Any beam reflected from the reflector does not strike the back of the collector.

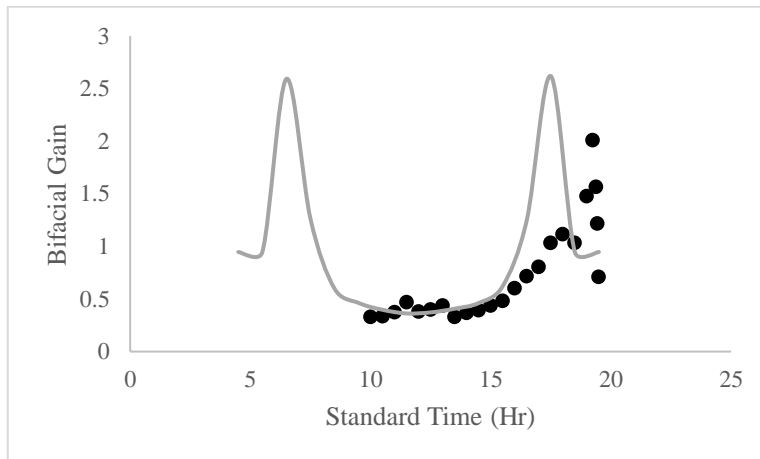


Fig. 6: Overlay of experimental (points) and model predictions (smooth line) for a vertical configuration of collector with a diffuse reflector on July 5, 2021.

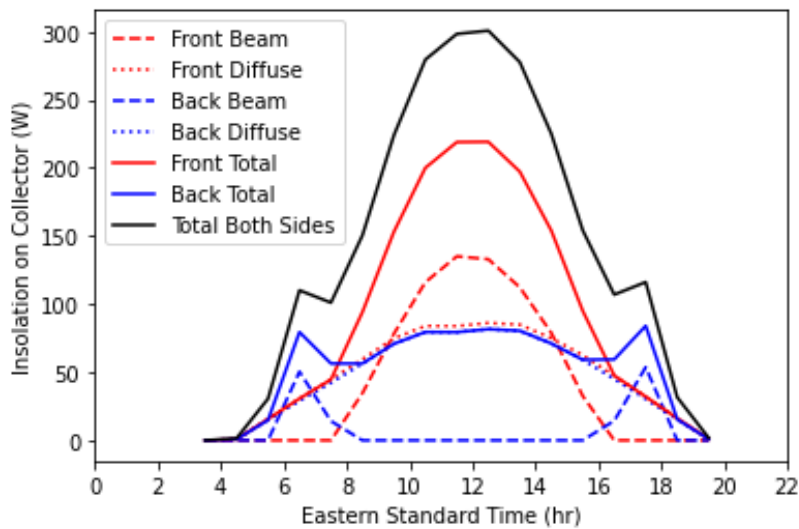


Fig 7: Model output of each sunlight component for a vertical collector and white diffuse collector on July 5, 2021.

For the case shown in Fig. 8, the set-up was maintained and run on a different day where the white diffuse reflector was replaced with a Mylar film reflector (reflectance 0.82). In these experiments, the data is started early in the day to capture the activity near sunrise and during the solar crossover into the southern sky. The model does a decent job at capturing this crossover and the mid-day BG values. There is more scatter in the experimental data on this day due to the variability in the sunlight. The mid-day (10am-2pm) experimental and modeling BG values for this case are 0.64 and 0.43 respectively.

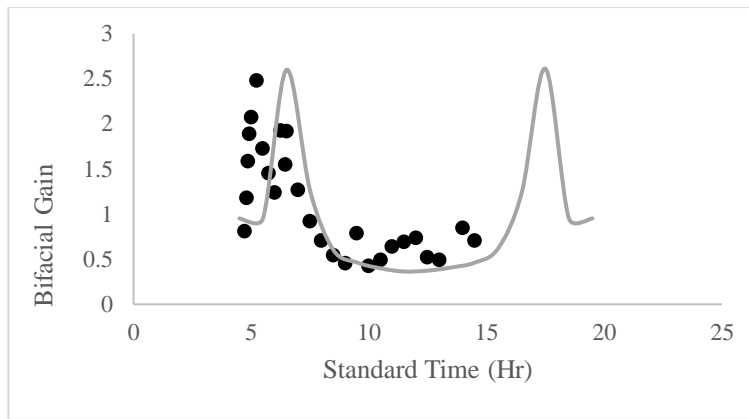


Fig. 8: Overlay of experimental (points) and model prediction (smooth line) for a vertical configuration of a collector and Mylar reflector on July 5, 2021.

Figures 9 and 10 show experimental results from the other roof-top experiment that used twin back-to-back monofacial single crystal 50 W PV modules, along with a single monofacial module for comparison, all under the same sunlight. Each back-to-back system had the option for a rear reflector. For all of the cases described here the collectors and reflectors were south-facing vertical and parallel. The collectors and reflectors were 0.6858 m wide by 0.5334 m high raised up 0.9525 m from the ground and the reflector-collector spacing was 0.5334 m. A calibrated cell, like the ones used in the other experiment, was used here on the front to measure the insolation striking a vertical south-facing surface. As with the other experiment, black absorbing roofing paper was placed all around the set-up to reduce the ground reflected component. In the case of Fig. 9, no reflector was used in the first system and the second system used a white diffuse reflector. The power output was measured from each of the front and rear modules over the central part of a day which allowed the calculation of the BG values shown in Fig. 9. The BG for the no reflector case results just from the rear sky diffuse averaging about 0.16 over the hours tested. The white diffuse reflector showed much better output, averaging a BG of about 0.22, or 35% higher than the no-reflector case. During the hours tested, there was no direct or reflected beam components on the rear side due to the collector-reflector spacing and the high altitude angle of the sun. The front insolation is also plotted on the figure. The BG values tend to rise when the insolation is low and fall when the insolation is high.

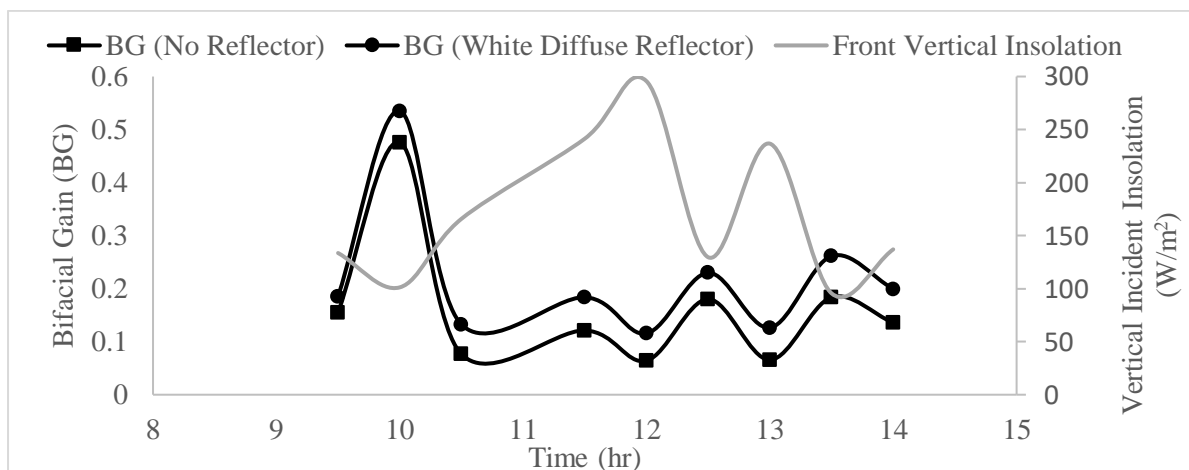


Fig. 9: Experimental data for side by side vertical modules simulating bifacial with no reflector and one enhanced with white diffuse compared to a monofacial panel on July 15, 2021

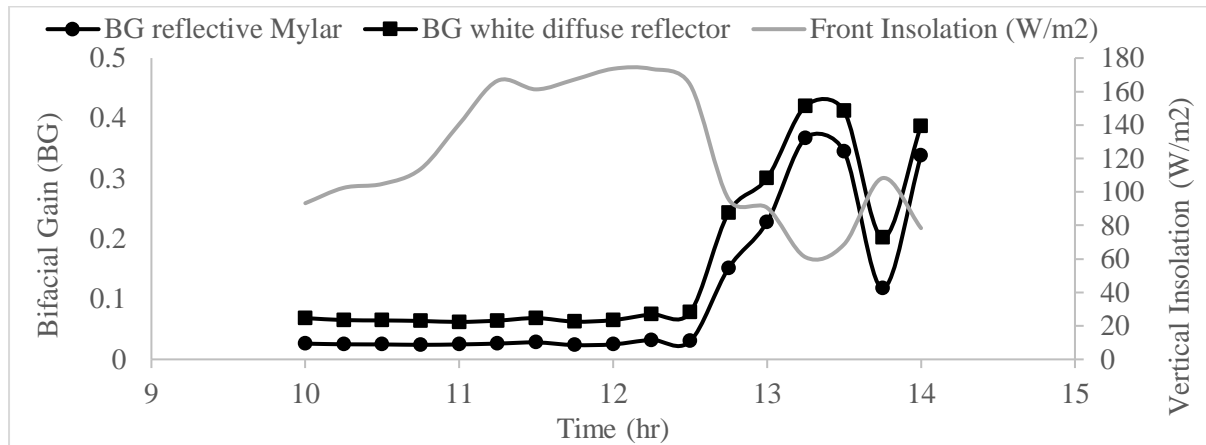


Fig. 10: Experimental data for side by side vertical modules simulating bifacial panels enhanced with a Mylar white diffuse reflectors compared to a monofacial panel on July 9, 2021.

In Figure 10, frames with Mylar and white diffuse reflectors are compared against each other and against a monofacial module. Over the hours tested, the Mylar averaged a BG of 0.11. and the white diffuse averaged 0.16. Overall, from both tests, the white diffuse system yielded about 19% more power than the monofacial module. This could make bifacial panels suitable for roof-tops with white flat or shingle roofs.

5. Conclusions

A model was developed to predict the incident irradiance on the front and rear surface of a bifacial collector equipped with a rear reflector. The model is versatile and can be applied to different locations and for different geometries. It is continuously being improved to capture more and more complex geometry while staying user friendly. Its biggest value may be in defining favorable mounting geometry and configurations in which added reflectors can be complementary to existing ground albedo. The model as it currently stands, only calculates incident irradiance on surfaces. Additional functionality will be needed like module efficiency and temperature dependence to predict the power generated and inform an economic analysis. Experiments were also conducted in this study to provide data to compare to the model and to study the effects of different reflecting surfaces on the bifacial gain. A white diffuse reflector enhanced the bifacial gain over that of the case with no reflector and increased the bifacial gain slightly more than a reflective Mylar film. Bifacial gain is sensitive to time of day and year and to the available beam and diffuse insolation, so its use for informing design must be taken in context. For example, in the summer, due to the large solar altitude angles, reflectors would have to be close to the rear of the collector to capture and reflect beam irradiance, but this could block ground reflectance. In the winter, low solar altitude angles could allow the reflector to be set farther back, not interfering with ground reflected, and reflecting the beam component to the rear of the bifacial module.

6. References

- Appelbaum, J., 2016. Bifacial photovoltaic panels field. *Renewable Energy*. 85, 338-343.
- Bergman, T. L., Lavine, A. S., Incropera, F. P., Dewitt, D. P., 2011. *Introduction to Heat Transfer* 6th Edition, John Wiley and Sons, NJ.
- Cuevas, A., Luque, A., Eguren, J., Del Alamo, J., 1982. 50 Per Cent More Output Power from an Albedo-Collecting Flat Panel Using Bifacial Solar Cells. *Solar Energy*, 29, 419-420.
- Duffie, J.A., Beckman, W.A., 2013. *Solar Engineering of Thermal Processes*, 4th. edition, Wiley, Hoboken, NJ.
- Durusoy, B., Ozden, T., Akinoglu, B. G., 2020. Solar irradiation on the rear surface of bifacial solar modules: a modeling approach. *Scientific Reports* 10, 13300.
- Guerrero-Lemus, R., Vega, R., Kim, T., Kimm, A., and Shephard, L.E., 2016. Bifacial solar photovoltaics – A technology review. *Renewable and Sustainable Energy Reviews*, 60, 1533-1549.
- Hansen, C. W., Stein, J. S., Deline, C., MacAlpine, S., Marion, B., Asgharzadeh, A., Toor, F., 2016. Analysis of Irradiance Models of Bifacial PV Modules. *IEEE*, 978-1-5090-2724-8/16,138-143.
- Jäger, K., Tillmann, P., and Becker, C., 2020. Detailed illumination model for bifacial solar cells. *Optics Express*, 28, 4751-4762.
- Guo, S., Walsh, T.M., Peters, M., 2013. Vertically mounted bifacial photovoltaic modules: A global Analysis. *Energy*. 61, 447-454.
- Jakobsen, M.L., Thorsteinsson, S. Poulsen, P.B., Rodder, P.M., Rodder, K., 2016. Vertical reflector for bifacial PV-panels. *Proceedings of the 43rd IEEE Photovoltaic Specialist Conference*, 2678-2681.
- Joge, T., Eguchi, Y., Imazu, I., Araki, I., Uematsu, T., Matsukuma, K., 2002. Applications and Field Tests of Bifacial Solar Modules. *Proceedings of the 29th IEEE Photovoltaic Specialists Conference*, 1549-1552.
- Khan, M.R., Hanna, A., Sun, X., Alam, M.A., 2017. Vertical bifacial solar farms: Physics, design, and global optimization. *Applied Energy*. 206, 240-248.
- Karahara, N., Yoshioka, K., Saitoh, T., 2003. Performance Evaluation of Bifacial Photovoltaic Modules for Urban Application. *3rd World Conference on Photovoltaic Energy Conversion*, 2455-2458.
- Krein, L., Bordin, N., Karsenty, A., Drori, A., Grobgedl, D., Eisenberg, N., 2010. PV Module Power Gain Due to Bifacial Design, Preliminary Experimental and Simulation Data. *IEEE*, 978-1-4244-5892-9/10, pp. 2171-2175.
- Lim, Y. S., Lo, C. K., Kee, S. Y., Ewe, H. T., Faidz, A. R., 2013. Design and evaluation of passive concentrator and reflector systems for bifacial solar panel on a highly cloudy region – A case study for Malaysia. *Renewable Energy*, 63, 415-425.
- Moehlecke, A., Febras, F.S., Zanesco, I., 2013. Electrical performance analysis of PV modules with bifacial silicon solar cells and white diffuse reflector. *Solar Energy*. 96, 253-262.
- NSRDB: National Solar Radiation Database, last modified 2020, accessed July 29, 2020, nslrdb.nrel.gov
- Pelaez, S.A., Deline, C., MacAlpine, S.M., Marion, B., Stein, J.S., Kostuk, R.K., Comparison of Bifacial Solar Irradiance Model Predictions With Field Validation. 2019. *IEEE J. of Photovoltaics*. 9, 82-88.
- Ooshaksaraei, P., Sopian, K., Zulkifli, R., Alghoul, M.A., Zaidi, S.H., 2013. Characterization of Bifacial Photovoltaic Panel Integrated with External Diffuse and Semimirror Type Reflectors. *Intl. J. of Photoenergy*. 2013, 465837.

Sun, X., Khan, M. R., Deline, C., Alam, M. A., 2017. Optimization and performance of bifacial solar modules: A global perspective. *Applied Energy*. 212, 1601-1610.

Yusufoglu,U.A. Lee, T.H., Pletzer, T.M., Halm, A., Koduvelikulathu, L.J., Comparotto, C., Kopecek, R. Kurz, H., 2014. Simulation of energy production by bifacial modules with revision of ground reflection. *Energy Procedia* 55, 385-395.

Yusufoglu,U.A.. Pletzer, T.M., Halm, A., Koduvelikulathu, L.J., Comparotto, C., Kopecek, R. Kurz, H., 2015. Analysis of the Annual Performance of Bifacial Modules and Optimization Methods. *IEEE J. of Photovoltaics*. 5, 320-328.

A

Andreas, A.

Influence of Diffuse and Ground-Reflected Irradiance on the Spectral Modeling of... 93

C

Clemens, J.

True Sustainability With Low Embodied Energy..... 7

D

Deepak, A.

Credit for Reducing Sunshine..... 52

Deepak, R.

Credit for Reducing Sunshine..... 52

Dobosz, M.

A Study of Reflector-Enhanced Bifacial PV..... 103

F

Fazli, F.

Community Solar Food Drying in Afghanistan..... 19

Foster, R.

Community Solar Food Drying in Afghanistan..... 19

G

Gotseff, P.

Influence of Diffuse and Ground-Reflected Irradiance on the Spectral Modeling of... 93

H

Habte, A.

Influence of Diffuse and Ground-Reflected Irradiance on the Spectral Modeling of... 93

Hiben, Y.

A review on Solar Thermal System Design, Integration, and Techno-economic Modeling... 31

Infinite-NTU Modeling for Studying Charging Cycle of Packed-Bed Solar Thermal Energy... 43

Howard, E.

Optimizing the Operational Parameters of an Electrochemical Purification Cell for... 76

K

Kahsay, M.B.

A review on Solar Thermal System Design, Integration, and Techno-economic Modeling... 31

Kessler, R.

Influence of Diffuse and Ground-Reflected Irradiance on the Spectral Modeling of... 93

Komerath, N.M.	
<i>Credit for Reducing Sunshine</i>	52

L

Lauwaert, J.	
<i>A review on Solar Thermal System Design, Integration, and Techno-economic Modeling</i>	31

M

Mavromatakis, F.	
<i>Influence of Diffuse and Ground-Reflected Irradiance on the Spectral Modeling of</i>	93

Miller, D.	
<i>Introduction</i>	1

P

Peterson, J.	
<i>Influence of Diffuse and Ground-Reflected Irradiance on the Spectral Modeling of</i>	93

R

Rincón, A.G.	
<i>Nonimaging Optics and Constructal Design Towards Optimal Solar Cookers</i>	64

Rincón-Mejía, E.	
<i>Nonimaging Optics and Constructal Design Towards Optimal Solar Cookers</i>	64

Rincón-Rubio, V.	
<i>Nonimaging Optics and Constructal Design Towards Optimal Solar Cookers</i>	64

Rippy, K.	
<i>Optimizing the Operational Parameters of an Electrochemical Purification Cell for</i>	76

Rueter, M.	
<i>A Study of Reflector-Enhanced Bifacial PV</i>	103

S

Sengupta, M.	
<i>Influence of Diffuse and Ground-Reflected Irradiance on the Spectral Modeling of</i>	93

Snider, S.	
<i>Influence of Diffuse and Ground-Reflected Irradiance on the Spectral Modeling of</i>	93

Stromberg, R.	
<i>Reuse of Solar Photovoltaic Systems for Social and Economic Benefit</i>	81

V

Vidal, J.

Optimizing the Operational Parameters of an Electrochemical Purification Cell for... 76

Vignola, F.

Influence of Diffuse and Ground-Reflected Irradiance on the Spectral Modeling of... 93

W

Wilk, R.

A Study of Reflector-Enhanced Bifacial PV... 103

Witteaman, L.

Optimizing the Operational Parameters of an Electrochemical Purification Cell for... 76

